A New Constitutive and Numerical Model for Arching of Cohesive Powders in Hoppers

Carmen Jiawen Su

A thesis submitted in partial fulfilment of the
requirements of the University of Greenwich
for the Degree of Doctor of Philosophy

2017

DECLARATION

I certify that this work has not been accepted in substance for any degree, and is not concurrently being submitted for any degree other than that of Doctor of Philosophy being studied at the University of Greenwich. I also declare that this work is the result of my own investigations except where otherwise identified by references and that I have not plagiarised the work of others.

....
Carmen Jiawen Su (PhD Student)

Date:

....
Professor Mike Bradley (Supervisor)

Date:

....
Professor Koulis Pericleous (Supervisor)

Date:

ACKNOWLEDGEMENTS

ABSTRACT

Deaths and casualties caused by silo collapses have happened across the industry over the world, especially in production plants which store and handle fine powder. The collapses not only cost financially to settle for compensation, also cost companies' reputation and credibility for partnership. Industry experts believe that the high frequency of silo failures are mainly due to "shortcomings in one or more of four categories: design, construction, usage, and maintenance". However, there is one category has been overlooked by industry, it is the technology in storage, flow and handling of fine powder.

This thesis studies the technology within the area of flow and handling of find powder. Whether or not a cohesive powder would freely discharge through a given orifice is a question at the centre of numerous bulk solids handling issues encountered in industry. The work in this thesis contributes towards answering the question by using a combination of empirical powder property determination and numerical simulation.

Cohesive arching at the outlet is a formation of an arch of cohesive powder (usually fine powder) at the smallest cross-section of a flow channel in a silo (usually the outlet). If it builds up the material inside of the silo, it can potentially cause the failure of the silo by material overload.

The aim of the research is to establish a precise and cost-effective constitutive model that is able to predict the cohesive arching and stress condition in a silo.

The numerical simulation is conducted under Finite Element (FE) approach developed and coded in a numerical solver PHYSICA, new concepts and variables to address the discrepancy between the field of powder mechanics and numerical simulation.

DEDICATION

To

my mum,
Anna Jieping Wong

and

my beloved boyfriend,
Andrew Wong

CONTENTS

Glossary

α	Hopper half angle
β	Interface momentum transfer coefficient in multiflow
δ	Effective angle of internal friction of powder
δ	Overlap distance between two adjacent particles
ϵ	Strain
$\frac{du}{dy}$	Rate of shear strain
$\frac{d}{dt}$	Time derivative
γ	Viscous damping coefficient
κ	Slope of the unloading-reloading line in the Cam-Clay model
λ	Slope of the virgin compression line in the Cam-Clay model
μ	Friction coefficient
μ	Viscocity
ν	Passion Ratio
ω	Angular velocity
ρ	Density
ρ_b	Bulk Density of Powder
σ	Stress

σ_0	Unconfined reaction stress
σ_1	Pre-consolidating stress
σ_2	Horizontal reaction stress
σ_c	Unconfined failure stress
σ_m	Mean stress
σ_h	Global Horizontal Stress
σ_{lh}	Elemental Local Horizontal Stress
σ_{ls}	Elemental Local Shear Stress
σ_{lv}	Elemental Local Vertical Stress
σ_v	Global Vertical Stress
σ_{xx}	Normal stress in x-direction
σ_x	Axial stress
σ_{yy}	Normal stress in y-direction
σ_y	Transverse stress
σ_{zz}	Normal stress in z-direction
τ	Shear strength
τ_{xy}	Shear stress
τ_{yx}	Shear stress
θ	Angle of Rotation for Principle Stress
φ	Effective angle of wall friction
ϑ	Angle of Rotation for Stress Transformation
$\vec{f_i}$	Contact force increment
$\vec{u}$	Velocity

g	Subscript of indicating gas phase in multiflow
n	Subscript for normal direction
s	Subscript of indicating solid phase in multiflow
t	Subscript for tangential direction
A	Area
c	Cohesion of powder
D	Compliance matrix
E	Young's Modulus
f	Phase fraction in multiflow
F_N	Vertical applied force to the ring in Jenike shear tester
F_S	Horizontal applied force to the ring in Jenike shear tester
FF	Flow Function in powder characterisation
ff	flow factor in powder characterisation
G	Shear modulus
g	Gravity
I	Moment
K	K ratio of powder
k	Spring stiffness coefficient
L	Original height of the confined cylinder filled with powder in the confined uniaxial compression test
M	Slope of the critical state line in the Cam-Clay model
m	Gradient of yield locus
m_i	Mass increment
p	Thermodynamics pressure

$p\prime$	Normal effective stress
q	Deviatoric stress
R	Vector or rotational relative radius
r_i	Radius for particle i
r_j	Radius for particle j
T	Torque
u	Travel distance of the lid in the confined uniaxial compression test
u	Velocity in multiflow
V	Volumne
v	Specific volume
v	Velocity
v_κ	Intercept of the virgin compression line in the Cam-Clay model
v_λ	Intercept of the virgin compression line in the Cam-Clay model
x	Distance measured from the bottom of the hopper
z	Depth measured from the top of the hopper

Chapter 1

INTRODUCTION

This chapter lays out the flow of the thesis, the problems industry faces while handling powders, the goal of the research project and the fundamental principle of the arching problem which this project is solving.

1.1 Outline of the Thesis

The research and findings of this PhD are reported in the following order:

(a) Chapter 1 Introduction explains the background and the history prior to this research which leads to the aim of this research.

(b) Chapter 2 and Chapter 3 Literature Review details the background of this research and existing technology associated with the research topic.

(c) Chapter 4 Preliminary Study outlines the findings in preliminary simulations, however the conclusion from these findings suggest that the preliminary simulations were all failed attempts, which reason leads to Chapter 5 and Chapter 6.

(d) Chapter 5 Theory contains the structure of the developed model and both empirical theories and numerical theories behind it.

(e) Chapter 6 Implementation consists of i) the tests to obtain input parameters for the numerical model, and ii) coding developments which address the software shortfalls.

(f) Chapter 7 Results and Discussion discuss the results and finding on study cases.

(g) Chapter 8 Conclusions and Future Work critically reviews the developed model and suggests further improvements.

1.2   Research Rationale

Manufacturing continues to be an important part of both developed and developing economies, and a large proportion of its industries will deal with powders either as finished products or during intermediary processing steps. This applies to agriculture, construction, energy, materials, chemicals, foods and pharmaceuticals to name a few. Process engineers are well accustomed to dealing with fluids, which are made to flow reliably from one vessel to the next at a predictable velocity. However, the behaviour of powders is not as easy as fluid to predict.

During storage, powders are subjected to compressive forces which are subsequently retained as a residual cohesive strength. This means there is no guarantee that any of the powder will flow out of the opening when the valve is released. The detrimental effect of this upon an overall production process is self-evident. It is not a surprise that drug and food powders are particularly susceptible, because they tend to deal with finer particles and smaller equipment.

This PhD research project arose from and has been guided by a particular limitation of an earlier project which simulated powder behaviour. The previous project is

documented as the QPM project [1; 2; 3; 4; 5; 6], the QPM project was a cooperation between the Centre for Numerical Modelling and Process Analysis, University of Greenwich, The Wolfson Centre, University of Greenwich and Department of Chemical and Process Engineering, University of Surrey. The project simulated Granular Material in Large-Scale Engineering Processes, using a Computational Fluid Dynamics (CFD) continuum approach [7; 8]. The model successfully simulated processes at an industrial scale; which included hopper filling, hopper emptying, pneumatic conveying etc. However incipient flow of the powders was assumed to occur automatically at the beginning of the discharge requiring no criterion to determine "failure" [1]. Further research was required in the numerical modelling of the simulation of initial discharge of a hopper.

Pharmaceutical and agricultural industries often encounter aching problems in the silos or hoppers while handling fine powders within their production plants. The installed system is inadequate in relation to the powder being handled, this usually occurs because of the lack of understanding of the behaviour of the powder by the system designer [9; 10]. There are two types of arching: mechanical arching and cohesive arching. The former is often associated with coarse bulk materials and the latter is often associated with fine powders. This research project deals only with the latter.

Cohesive arching is the formation of an arch of cohesive powder normally at the smallest cross-section of a flow channel (usually the outlet of the hopper). Figure 1.1 shows a typical cohesive arching problem in a half cylinder hopper , the hopper is constructed in half from perspex plastic for observation. The figure also shows the typical case where the cohesive powder can support itself in a shape of an arch near the outlet.

---

[1] "Failure" in this content is understood to mean the initiation of collapse in a body of powder, leading to flow
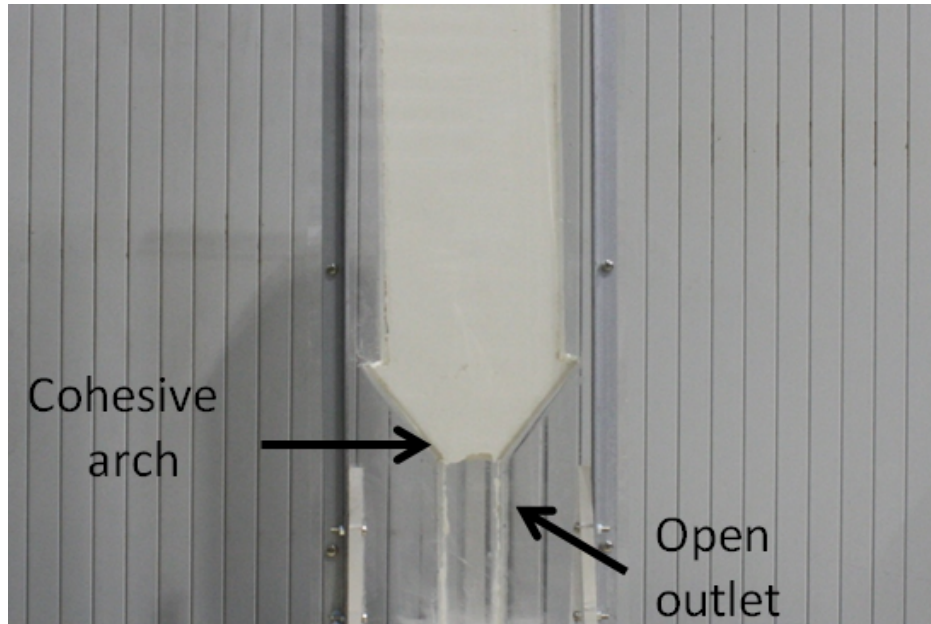
Figure 1.1: Cohesive arching of a cohesive powder in a perspex hopper with an open outlet.

The hoper is built with diameter of $170mm$, height of $600mm$ and the opening of $30mm$. The hopper has been filled with wheat flour while the valve was closed, then the valve was released.

1.3   Aim of Research

The aim of this research project was to establish a precise and cost-effective constitutive model that predicts the arching and stress conditions in a wedge hopper, starting from the stage where a closed hopper is filled with cohesive powder to the stage where the outlet is opened and the hopper starts to empty. Most hopper consist of two section: a straight section and a convergent section. A wedge hopper has rectangular prism straight section and a wedged in convergent section. A cylindrical hopper has a cylindrical straight section and a cone-shaped convergent section. The reasons of

conducting this research will be explained in State of the Art in Industry in Chapter 2, in which the chapter also includes the reviews on currently existing numerical models and their shortfalls when it comes to the prediction of arching.

The model in this research is designed to be employed in industry that deals with any types of cohesive powder, which are very fine and under stress in general. Due to the small size of particles and relevantly large size of the hoppers in production plants, an enormous number of particles are involved. For a 10 tonnes silo filled which cement[1] would easily contain 4.5×10^{23} particles. The numerical continuum approach is more viable than the discretised approach to simulate such situations. The powder is a large number of particles, and the compatibility of the numerical continuum approach aligns with the numerical assumption which the powder is treated as a continuous material with properties that change smoothly with position.

The currently established numerical continuum models predict the stress and strain conditions in powder compaction, however the failure criteria were not developed from the powder principle. The experimental models which predict the failure of the powder only take account of the simultaneous stress conditions, but they lack of the ability to accommodate the stress history in powder compaction which accounts for the simultaneous stress conditions. The simulation model developed in this study is the combination of numerical and experimental models which provides stress predictions throughout the filling and the emptying of a hopper.

1.4   Structure of the Research Programmne

This section details the workflow in this research programme and its development.

At the beginning of the research programme, the author firstly has familiarised herself with both background theory of Powder Mechanics and numerical modelling. In order

---

[1]A typical cement particle usually has a diameter of $30\nu m$ and a bulk density of $1600 kg/m^3$

to obtain the knowledge in both fields, in addition to literature review, the author has attended short courses held by the Wolfson Centre for Bulk Solids Handling, University of Greenwich, and the master's course run by Department of Mathematical Sciences, University of Greenwich.

Secondly, the author attempted to simulate the powder behaviours with both Computational Fluid Dynamics (CFD) and Finite Element Method (FEM) approaches, in order to to select the most suitable model to develop.

Thirdly, the author designed and conducted empirical testing on the powder material to obtain input parameters for simulations.

Fourthly, source codes were re-developed and implemented with the complex constitutive relationship of the powder and the parameters from empirical testing.

Lastly, the author has conducted parametric studies with the model to test the range within which the model would functional coding.

Chapter 2

LITERATURE REVIEW ON POWDER MECHANICS THEORY

This chapter is to review the existing numerical models on powder mechanics and discuss their capabilities for this research, which is aimed to predict the stress and arching condition inside a hopper.

Powder Mechanics has not been one of the most traditional subjects, because, in the history of research, it first appeared in early 1900's as micromeritics [11; 12; 13; 14]. Then researchers found various aspects of powder mechanics are similar, or even the same as Soil Mechanics. Soil Mechanics since then has a huge influence for the development in Powder Mechanics for their similarities on cohesiveness and compressibility, until Jenike in 1960's introduced the flowability concept specifically for powder to contribute to better hopper and silo design [15; 16].

2.1   State of the Art

Merrow [17] conducted a study in 1981 on the cost of growth and performance across industrial production plants. His findings suggested that a typical medium to large-sized production plant could cost between half a billion to over one billion US dollars for its design and construction, in additional other several millions for annual operation cost. For production plants that handle powder and bulk solids, they might consist of a mixing system, transport system and storage system. If any problem arises in one of the systems, the whole plant would fall short from its normal production rate, or even at worst, come to a stop.

This project's scope falls in the range of the issue arise in the design and the operation of storage system.

In regards of designing a mass flow hopper to achieve a smooth operation in the production plants, the industry has been employing the Jenike's analytic model to predict the minimum width of the hopper outlet with given hopper geometry, powder characteristics, hopper material and the stress history of the powder.

The Jenike's analytic model has proved its reliability over the last four decades for standard hopper shapes: circular hoppers; square hoppers; and cynical hopper with rectangular outlets. However, hoppers with non-standard shapes have been used in the production plants for different reasons, such as to maximise hopper capacity or to have multiple outlets for higher production rate. In those situations, the Jenike's method for flow problems has been inadequate[18]. Therefore powder mechanics researchers have focused their efforts towards more general computational strategies which may be adaptable and flexible over the traditional Jenike's method.

2.2 Flow patterns in hoppers

There are four basic phenomena that occur in hoppers and silos, they are: a) mass flow, b) core flow (sometimes regarded as funnel flow), c) arching and d) rat-holing. The former two are flow patterns (Figure 2.1 suggested by Khambekar [19])that are associated with flow occurring in the hopper. The latter two lead to a no-flow situation (Figure 2.2 presented by the Wolfson Centre [20]).
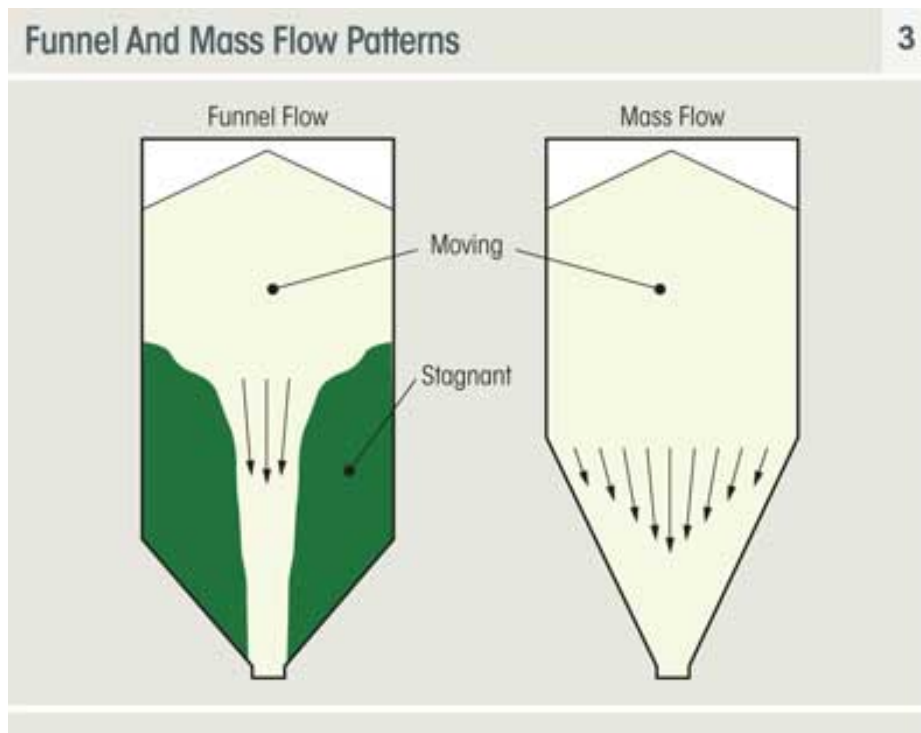
Figure 2.1: Flow patterns of Core Flow (left) and Mass Flow (right).
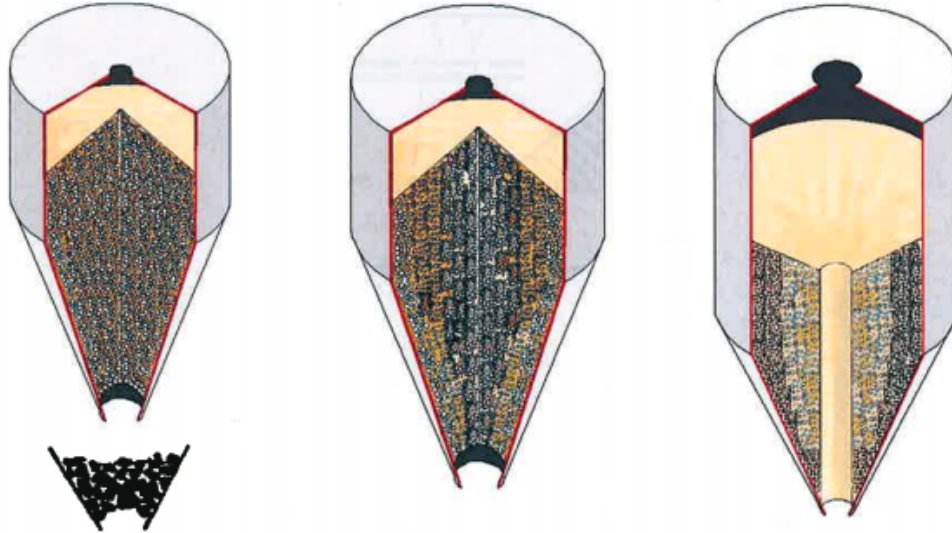
Figure 2.2: Obstructions to flow: Mechanical arch(left), Cohesive arch(middle) and Rat-holing (right).

2.3 Cohesive Arching and Cohesion

A hopper filled with cohesive powder can be discretised as in Figure 2.3. Figure 2.4 represents the element in the layer of arching at the outlet with a free body force diagram. Each layer of arch supports its own weight, the lowest layer does not receive any forces from the layer above it. Cohesive arching occurs when the powder's internal strength forming inside the arch is larger than the current stresses acting upon it, known as arching condition. If the current stresses acting upon the arch exceed the arch strength, incipient flow will occur; this phenomenon is called the Failure of the Arch.
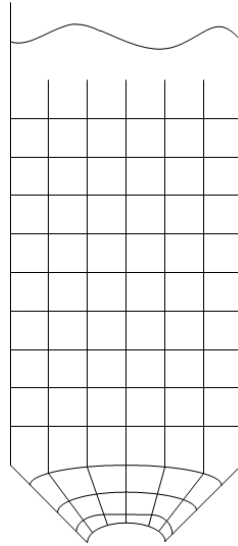
Figure 2.3: Discretised hopper.
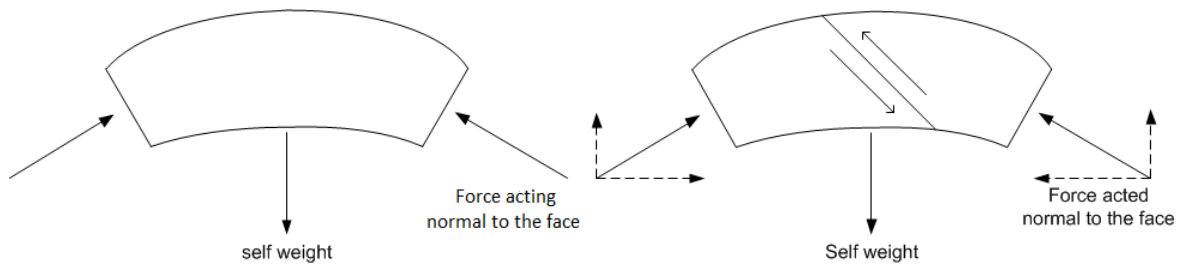
Figure 2.4: Free Body Diagram of the element in the layer of arching at the outlet with: a) Arching Condition, b) Failure Condition.

A Coulomb material is a brittle material, whose shear failure envelop is defined by the Mohr-Coulomb mathematical model. The shear strength in powder mechanics describes the magnitude of the shear stress that a powder can sustain. The shear resistance of powder is a result of friction and interlocking of particles at particle contacts. A cluster of compressed cohesive powder is a Coulomb material that has the ability to retain the shear strength after the external compressive load is removed. As seen in Figure 2.5, cohesive powder maintains a shear strength within the powder

11

itself, τ, when the external applied stress, σ, is zero. The magnitude of the remaining strength is called the cohesion of the material, c. The relationship between the shear strength and the stress is shown in following figure. The Yield Locus can be represented mathematically by:

$$\tau = m\sigma + c \qquad (2.1)$$
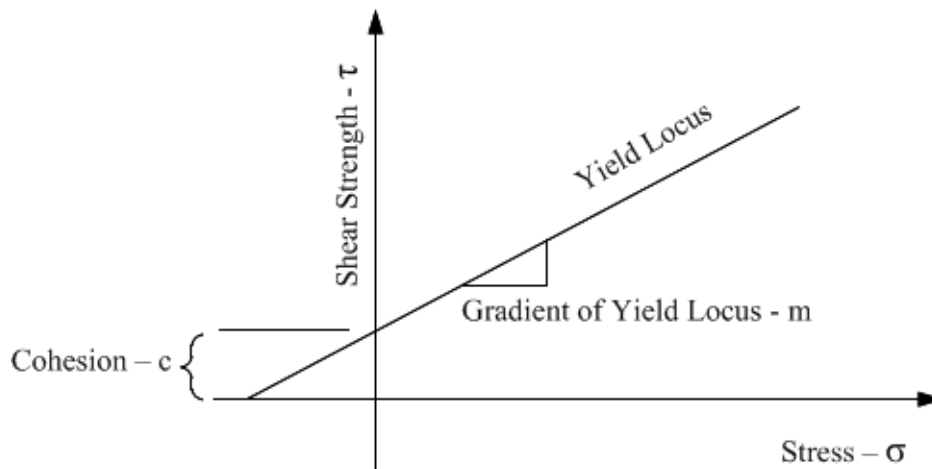
Figure 2.5: Yield Locus of a typical cohesive material after compaction to a certain density

where m is the shape of the shear strength to normal stress curve.

The cohesion of the powder is influenced by both ambient conditions and intrinsic powder characteristics, these include:

- stress history that has acted upon the powder

- temperature

- particles size distribution

- particle shape

- chemical composition

- moisture content

Due to the high volume of knowledge involved in each aspect, only stress history is selected to be considered in this research project. This research project is only interested in the filling and the opening of a hopper, in other word the time frame of the procedure is too short for any other parameters listed above to change, therefore parameters apart from stress history listed above will be assumed to be constant though out the project.

For a normal hopper, the normal stress profile at the wall will typically look in Figure 2.6
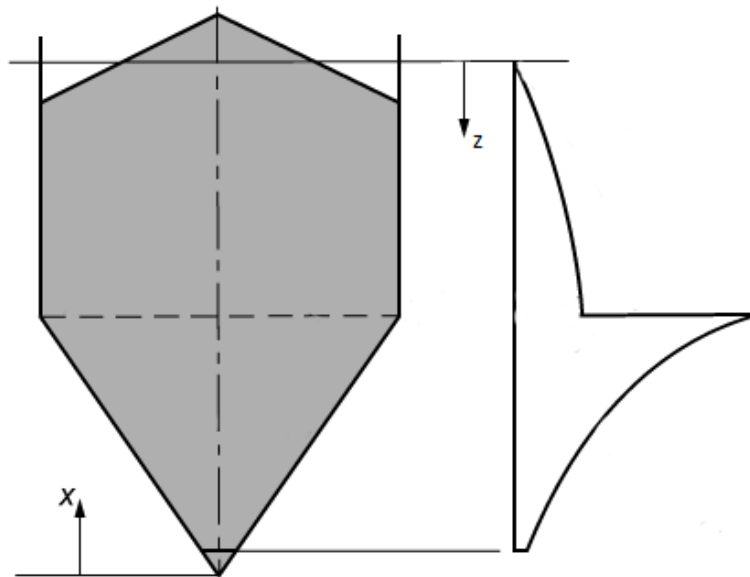
Figure 2.6: A typical normal stress distribution at the wall

The cohesion of the powder will be affected by the stress, therefore the cohesion of the powder is changing throughout inside of the hopper. One of the problems to solve in the numerical simulation is to correlate the cohesion with the stress history. This is an essential prerequisite to predict the arching condition in any given hopper.

2.4 Analytical Approaches for Predicting Arching

2.4.1 Unconfined Uniaxial Failure and its operational test

As previously mentioned in Figure 2.3, Figure 2.4 and Figure 2.5, the discrete element in the arching section is Coulob material which is subjected to compressive loads. If the element in the layer orientated vertical-horizontal, it can be approximately represented as a powder specimen undergoing uni-axial compression until it fails under compression.

The unconfined failure test was developed in the 60's to measure the failure condition. The test measure the shear strength of the material and it is used as one of the parameters to determine flow properties and predict the arching condition in hopper [21].

The test consists of two stages: a) the Pre-consolidation stage, b) the failure stage.

Powder is filled into a cylindrical confinement and the redundant powder at top is scraped off to give an even surface. A flat lid (red in Figure 2.7) is placed onto the powder. The cylinder is then securely positioned under a Texture Analyser which applies and measures the load onto the lid to consolidate the powder.
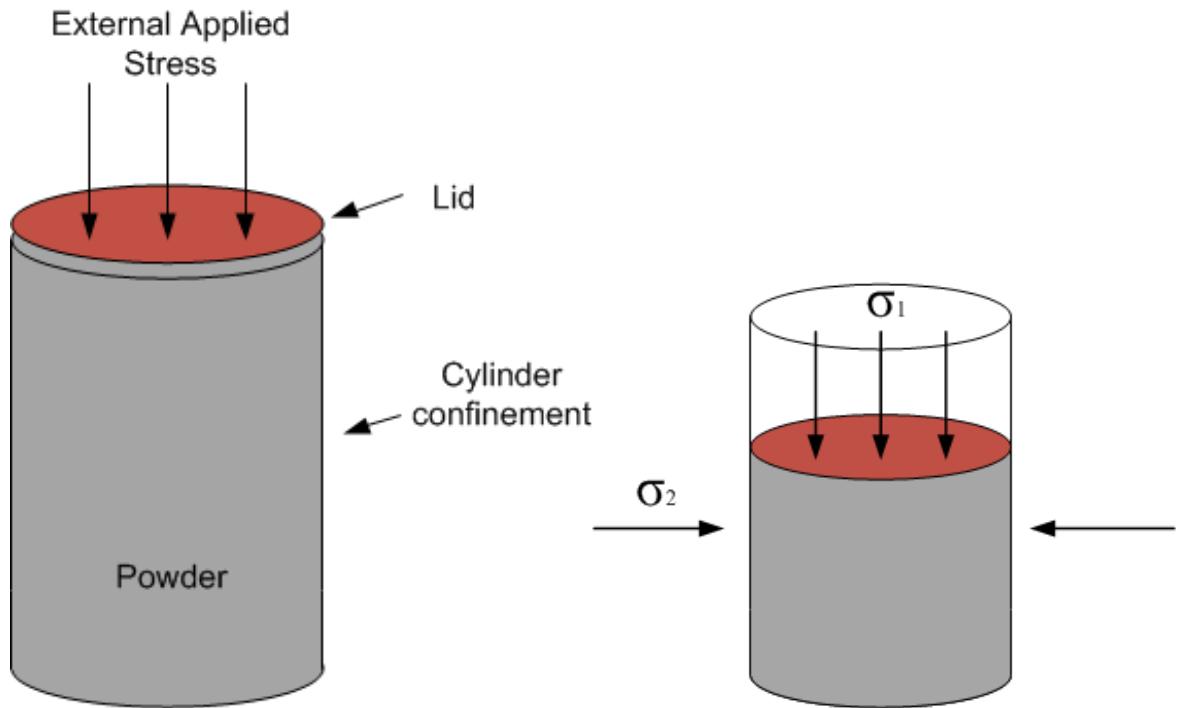
Figure 2.7: Powder specimen inside a cylinder confinement at the start of consolidation (left) and at the end of consolidation (right).

The wall of the cylindrical confinement will generate a horizontal reaction stress, σ_2, onto the powder as the powder is subjected to a vertical consolidation stress, σ_1. These two stresses will generate a half Mohr's circle as shown in Figure 2.8

Figure 2.8: Mohr's Circle stress analysis during consolidation stage.

After the powder is consolidated, the external stress is temporarily removed and the cylinder confinement is also removed. The powder is then subjected to vertical incremental stress until the breakage of powder occurs, the stress is then recorded as unconfined failure stress of the consolidated powder, σ_c. During the unconfined failure stage, there is zero horizontal stress, σ_0 (Figure 2.9), acting onto the powder as the powder is unconfined. σ_c and σ_0 are added onto Figure 2.10 to create a Yield Locus for the powder under a specific consolidation stress, σ_c. The tangent points of the two semi Mohr's Circles are connected with a straight line [22]. It is also because the powder is a Coulomb material. The extended line is said to be the Yield Locs of the material under a certain consolidate stress, σ_1.
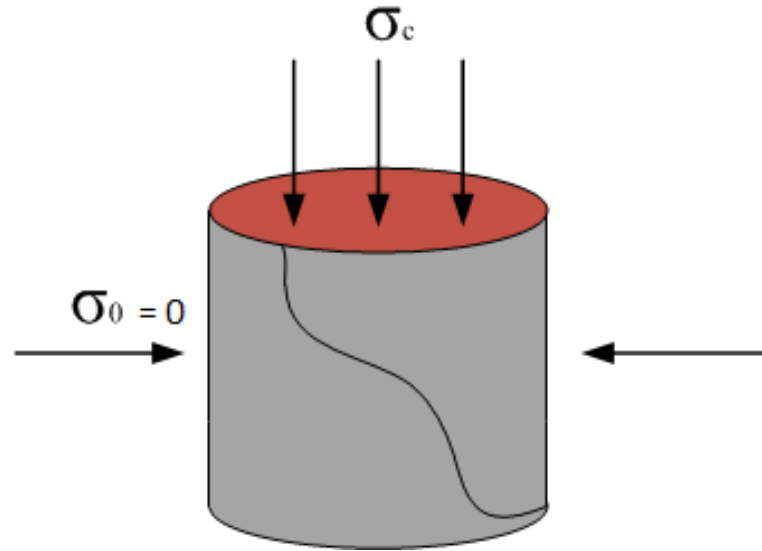
Figure 2.9: Unconfined Failure stage.
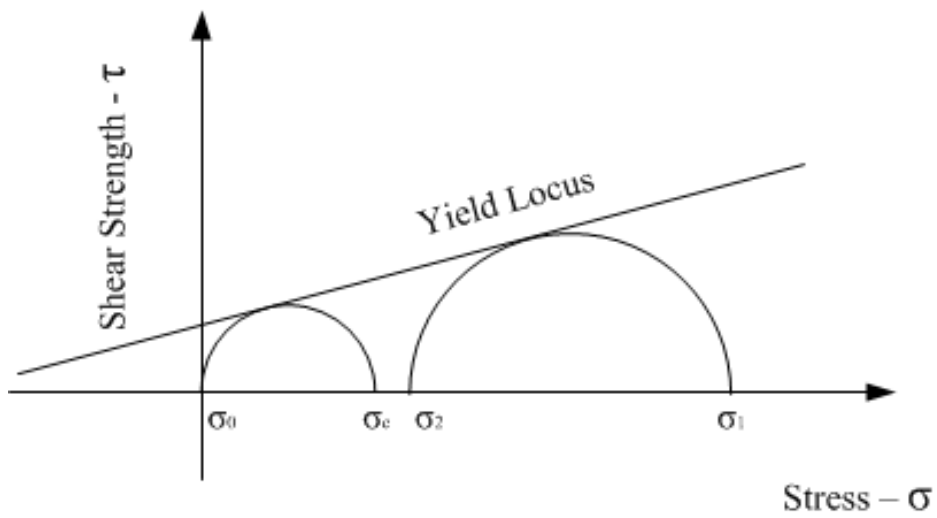
Figure 2.10: Mohr's Circle stress analysis during unconfined failure stage.

The same test procedure is then repeated with a series of different initial consolidation stresses (Figure 2.11).
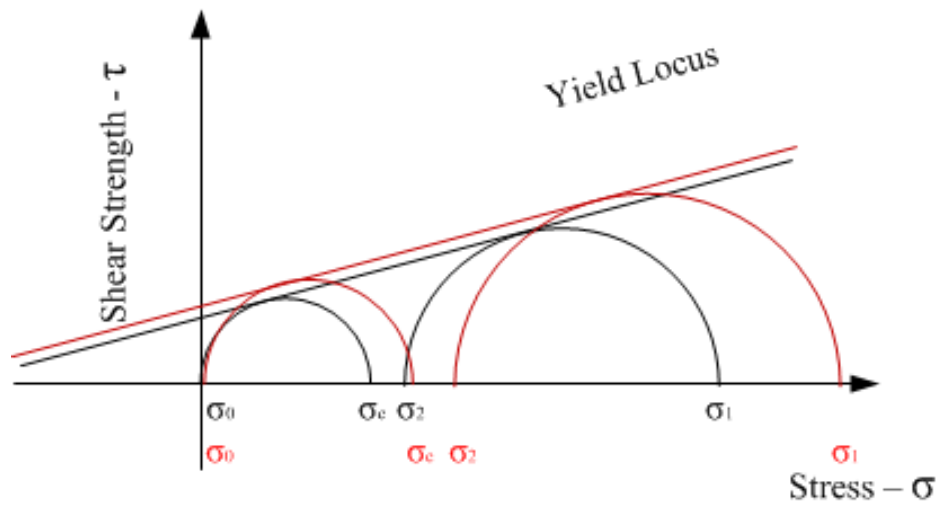
Figure 2.11: Yield Loci generated with a series of tests with different consolidate stresses.

For each Yield Locus, a pair of a consolidation stress, σ_1, and an unconfined failure stress, σ_c, can be found and they are plotted in σ_1 - σ_c plane to form a Failure Function (FF), as shown in Figure 2.12. For most powders, σ_1 and σ_c seemingly have a linear proportional relationship.
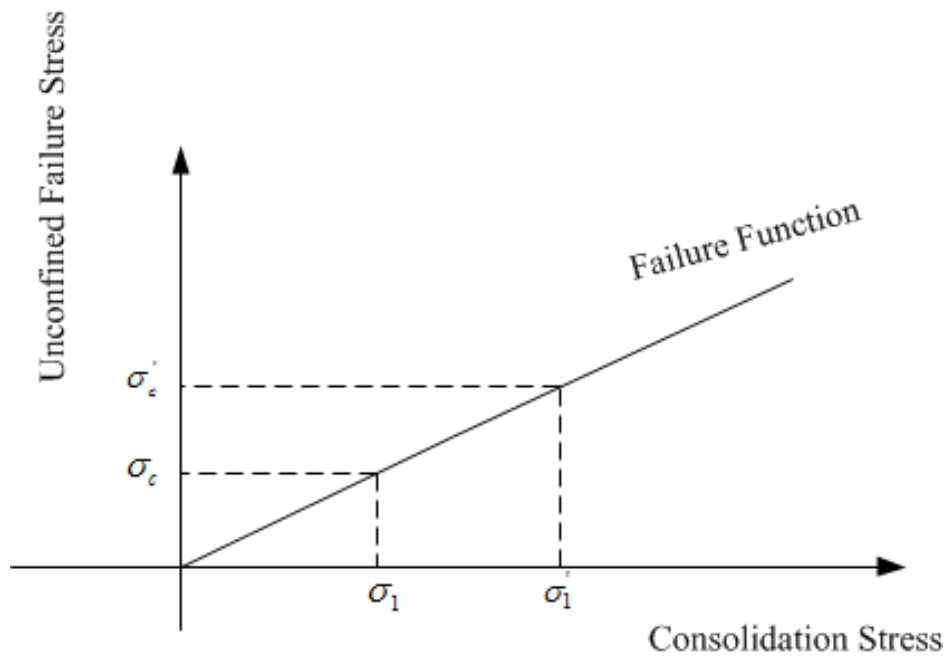
Figure 2.12: Failure Function.

"Failure Function" or "Flow Function" is a crucial measurement for powder flowability; the steeper the gradient, the more more difficult for the material to flow, which is called cohesive material, and vice versa for more free flowing material (Figure 2.13).
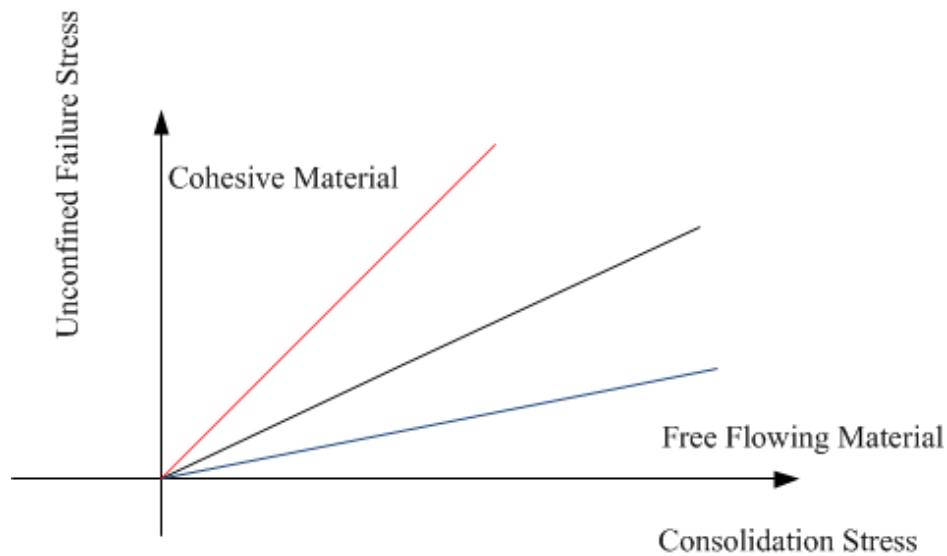
Figure 2.13: Cohesive Materiel v.s Free Flowing Material.

2.4.2 Shear Failure and its Operational testers

As mentioned before, the powder characterisation and its interaction with the hopper are important factors to determine the flow of powder in any given hopper or silo. There are several shear testers which are designed to measure the flowability of any given powder. They based on the Jenike and Walker shear testers. The incipient flow of any granular material or powder occurs at its steady-state(also refereed as critical-state) condition. Under this condition, the powder will start shearing at its critical applied stress and critical density. There are a few testers built with the consideration to measure the parameters at critical state.

The Jenike shear tester (Figure 2.14) was introduced in the 1960's [15; 21], it was the first tester designed to measure the flowability of any given powder.
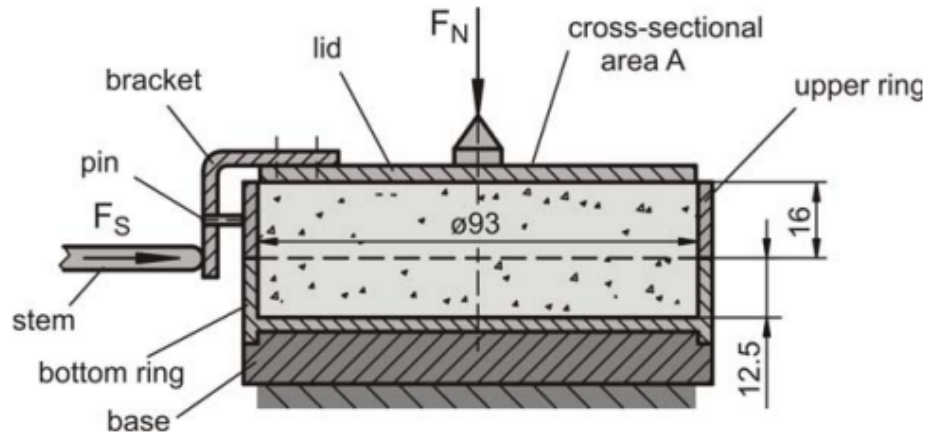
Figure 2.14: Shear Cell of the Jenike shear tester

The operation is detailed below; powder material is filled into a container that consists of a bottom ring, an upper ring and a mould. The upper ring is off-set against the bottom ring, Load is applied onto the lid to give a uniform force, F_N distribution across the powder surface. The mould is then removed and any additional powder material is scraped off. The powder material is now under the pre-consolidation condition with a certain pre-consolidation stress σ_1.

A bracket (Figure 2.14) is secured to the edge of the upper ring and is connected to a motor which provides an incremental force, F_S, to the upper ring. At a point when the upper ring shears against the bottom ring and slips, it is also the moment incipient failure occurs and the stress recorded at this point is the unconfined failure stress σ_c.

The Jenike shear test needs to be conducted several times with different pre-consolidation stresses to create a Flow Function, the Flow Function determines the flowability of the powder material.

However, the disadvantages of the Jenike shear tester are:

- time-consuming

- its requirement of high operational skill of the operator

- the maximum off-set distance is very limited

- the apparatus set-up requires the test to be repeated to generate the Flow Function, and the bulk density is not guaranteed to be repeatable as the nature of powder packing varies.

Walker improved the Jenike shear cell design to the ring shear cell [23]. The ring shear cell provides unlimited distance that the lid can travel, which is otherwise restricted in the Jenike shear cell.

The Walker shear tester was the srunner of several more widely used annular shear cells, including that of Schwedes and Schulze [21; 24; 25; 26] shown in Figure 2.15 below:
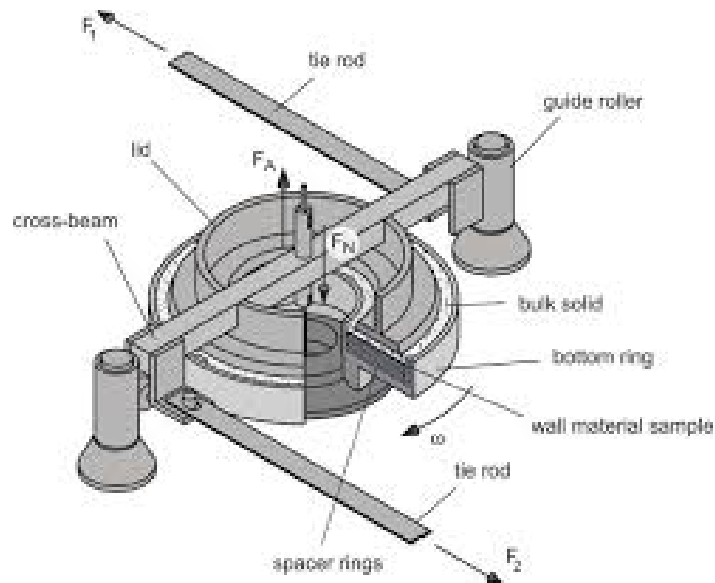
Figure 2.15: Ring shear tester of Schwedes and Schulze

Chapter 3

LITERATURE REVIEW ON NUMERICAL MODELS

Numerical simulations in powder mechanics can be categorised in three main areas: Discrete Approach, Continuum Approach and Hybrid Approach (Figure 3.1). Each categories has its own sub categories. This chapter will reviewed and detail the numerical models which are involved in powder mechanics on their strengths and shortfalls, in order to conclude the most suitable solution for this research project.
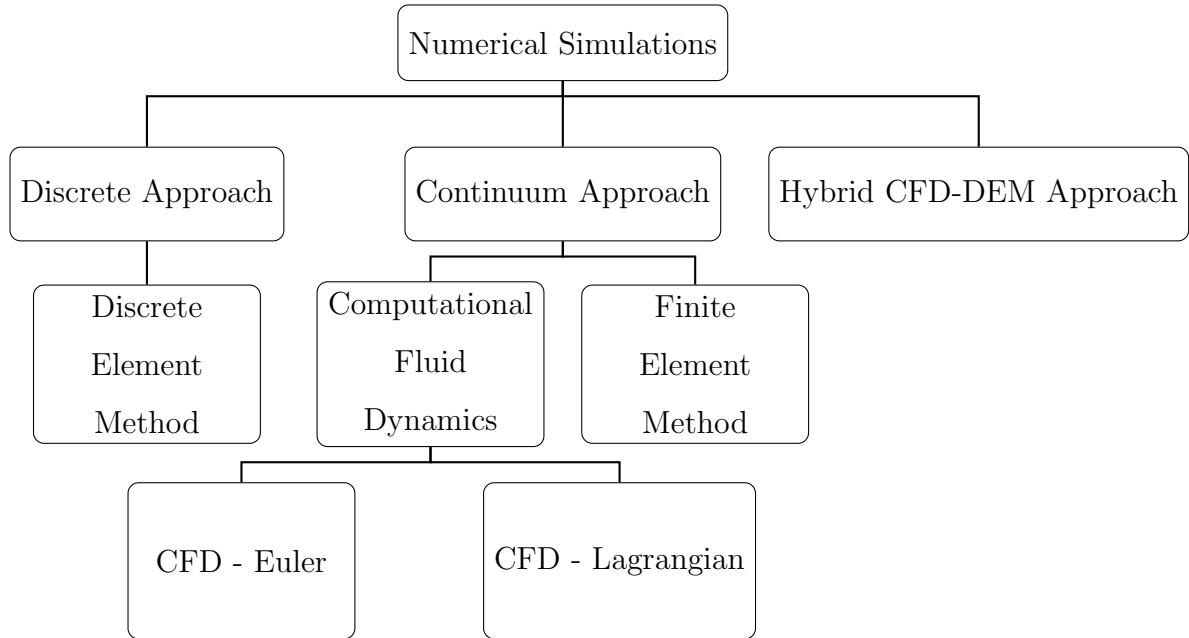
Figure 3.1: Numerical Simulation categories for powder mechanics.

3.1 Discrete Approach

This approach treats each particle individually and numerically simulates the motions and interactive force effects of each particle [27]. Due to the microscopic simulation and heavy usage of computational resources, Discrete Approach is only suitable for samples with a relatively small amount of particles to set bench mark for simulations for dynamic flow problem [28].

3.1.1 Discrete Element Method (DEM)

The Discrete Element Method(DEM) was first developed in late 1970's [29], it was for the purpose of simulating soil movement and geotechnical problems [30]. Powder Mechanics and Soil Mechanics share a large amount of similarities, therefore DEM has also been widely used in Powder Mechanics [31]. Due to modelling limitations,

most DEM powder simulations only consider monodisperse particles, ie all particles have a uniform size and shape. However, the assumption of monodisperse particles is seemingly unrealisetic , starting from last decade Kong, Lannutti et. al [32] have included multi-size particles in their simulations.

DEM simulates all forces acting on each individual particle, these include both normal and tangential forces. DEM numerically solves the equations of motion, Equation 3.1 is the integrated equation for all the interacting soft particles in a system of when they come into contact with each other.

$$m_i \frac{d^2}{dt^2} r_i = \sum_j \vec{f_i} + m_{ig} \tag{3.1}$$

where m_i is mass of particle i, r is the particle position, $\vec{f_i}$ is sum of all contact forces acting on the particle, and g is gravity.

Total force $\vec{f_i}$ on particle i from Equation 3.1:

$$\vec{f_i} = \vec{f^{ni}} + \vec{f^{ti}} \tag{3.2}$$

where $\vec{f^n}$ and $\vec{f^t}$ are normal and tangential contact force component, n and t are normal and tangential unit vector respectively.

3.1.1.1 Contact Force Model

The contact force models utilises the contact mechanics to define the deformation of solids that touch each other at one or more points, which is known as overlap, δ, shown in Figure 3.2. The contact force models are the most basic and widely employed model in DEM for granular simulations, the particles are assumed to be soft particles when they come into contact of each other [33; 34; 35; 36]. It has been used in both research and industry to simulate powder behaviours.
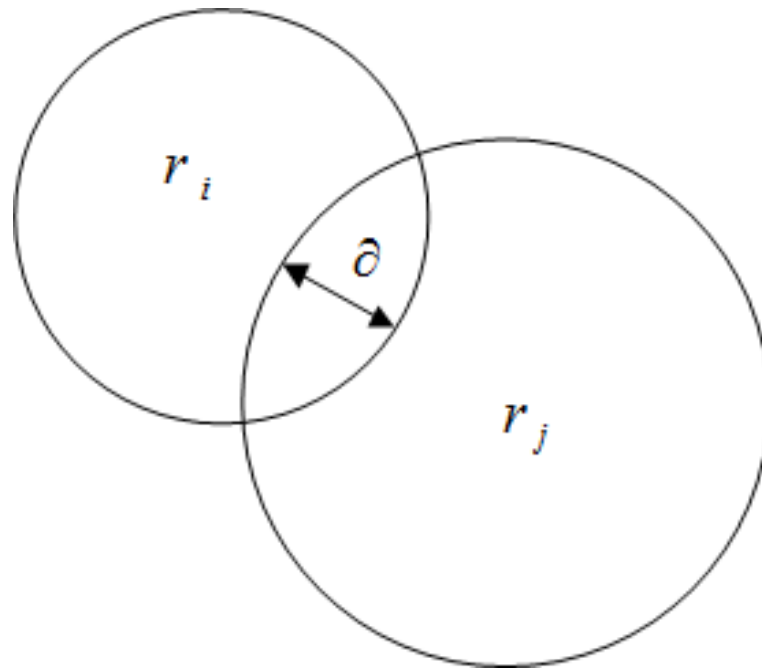
Figure 3.2: Overlap δ between two particles in contact

Linear Contact Model

The Linear Contact model employs Hook's law to represent the force-displacement relationship over the normal displacement, known as overlap δ, when two soft particles come into contact with each other as shown in Figure 3.2. In this model model two particles would have a displacement due to contact and the interaction is assumed to be linear elastic [37; 37; 38].

$$\vec{f^n} = k_n \delta_n \tag{3.3}$$

Hertz Model

The Hertz Model use the Hertzian theory in contact mechanics calculate the contact $\vec{f^n}$. Hertzian theory in contact mechanics promoted that the contact forces are usually

a nonlinear function of the deformation, due to complexity of forces and momentum exchanged during contact between solids. The normal contact force component $\vec{f^n}$ in Equation 3.2 then becomes:

$$\vec{f^n} = k_n \delta_n^{3/2} \tag{3.4}$$

Summary on Contact Force Models

Linear Contact Force models compute the equations of motions, different models represent different equations for stiffness coefficient k_n.

3.1.1.2 Tangential contact force

The tangential contact force term, $\vec{f^t}$, in Equation 3.2 is not as straight forward as the normal contact force term, $\vec{f^n}$. The tangential term takes consideration of the movement types of the particles: whether the particle is sliding or rolling [39]. There is a different model for each movement type.

Sliding

Sliding between contact particles will occur if the tangential force [40], in any direction, between them satisfies the Coulomb friction condition, which is:

$$|\vec{f^t}| > \mu |\vec{f^n}| \tag{3.5}$$

where μ is the friction coefficient.

The tangential contact force component $\vec{f^t}$ in Equation 3.2 then becomes:

$$\vec{f^t} = k_t \delta_t + \gamma_t v_t \tag{3.6}$$

where $k_t \delta_t$ is the spring conservative force term and $\gamma_t v_t$ is the dashpot dissipative damping force term of spring-dashpot system in this Linear Contact Force model. k is the spring stiffness of particle, γ_t is the viscous damping coefficient, and v_t is the relative velocity in tangential direction of the point of contact.

Rolling

There are two main factors that affect rolling mechanics, the contact force at the point of contact and the shape of particles [41; 42; 43], due to the depth of details, author will only review on models considering equal-sized particles.

The governing equation of motion for rolling of particle i is:

$$I_i \frac{d\omega_i}{dt} = \sum_j \vec{T_i} \tag{3.7}$$

where I_i is the moment, ω is the angular velocity due to rolling, T_i is the torque of particle i and t is the time increment. Torque $\vec{T_i}$ is given as:

$$\begin{aligned} \vec{T_i} &= R_i \vec{f^t} \\ &= -\mu R_i |\vec{f^n}| \end{aligned} \tag{3.8}$$

where R_i is the vector of rotational relative radius from the mass centre of the particle to the contact point, given as $R_i = a_i a_j / (a_i + a_j)$.

3.1.1.3   Collision models

The previous sections explained the more "static" models available in DEM, which are employed in simulations of dense flow of frictional granular materials [44]. In this section, Collision models are more "dynamic" models, they are employed in simulations for dilute flow of granular materials, due to their ability to capture action and reaction forces on each particle upon collision [45].

The collision model uses the Event-driven algorithm, which adapts variable time step interval in the simulation, the variable time step interval is determined by the occurring events (collisions) in the simulation. Whereas the time step interval is constant in classical DEM.

The event-driven method in DEM only started in 2007 by Theuerkauf [46] and its implementation can be found in most recent research since 2012 [47; 48; 49; 50; 51].

The nature of the collision models focuses on the motions during collision, which occurs frequently in fluidisation of powder flow [52; 53; 54]. However, this research is only interested in dense powder material.

3.1.2   Conclusion on DEM

DEM is the most popular approach in granular simulation nowadays, due to its ability to capture the microscopic behaviour and effect of granular material interaction with each other. The contact model simulates each particle interaction with particles in contact with it at every time step. This task alone may consume a large fraction of calculation time. This ability makes DEM cost a high computational resource. Some simulation scientists have applied the DEM approach to an industrial scale problem [55] with up to 1 million particles with particle size down to 30 mm. This maximum number of particles is not high enough and the particle particle size is not small enough for fine powder, as fine powder particle sizes range between 0 to 50 μm. A typical

hopper installed in a given production plant would contain tonnes of fine powder, that would be over trillions of particles. DEM falls short in terms of its ability to simulate small size particles in an enormously large quantity, but DEM can produce realistic simulations where there is sufficient computing resource available.

DEM originates from the soft particle molecular dynamics method, it also assumes that the granular particles are soft particles and the displacements are due to current forces exerted on the particles. However, as mentioned in the Introduction, cohesive material has the ability to contain its strength while the force is removed. That means the cohesive material is stress-history dependent. After reviewing the DEM approach in detail, the author's opinion was that DEM is not suitable approach in this research study.

3.2   Continuum Approach

Due to the high computational time that the discrete approach costs, the author has moved to viewing the continuum approach on powder simulation in detail to determine whether that is more suitable for this research project.

The continuum approach treats the powder as a continuum under the principle of continuum mechanics.

3.2.1   Computational Fluid Dynamics (CFD)

Computational Fluid Dynamics (CFD) models have been well studied and well established based on concrete underlying physics. The major capability of CFD is to solve the governing equations of the fluid; NavierStokes equations or Euler equations most of the time [56; 57; 58]. CFD started to gain its popularity in powder industry since the 1970's, starting to numerically simulate fluidised beds of powder [59; 60; 61],

as its application extended to multi-phase simulation: the simulation domain is consisted of not only fluid but also solid. There are two workframes: Euler-Euler and Euler-Lagrangian.

3.2.1.1 Euler - Euler

This workframe treats both gases and solid as a continuum. The powder (solid) is represented as a pseudo-fluid, hence it obeys the laws of conservation in fluid flow, in terms of mass, momentum and energy. Equation 3.9 is the Euler equations for mass conservation adopted with the volume fraction for both solid phase and gas phase.

$$
\begin{aligned}
\frac{\partial(V_g \rho_g)}{\partial t} + \nabla \bullet (\vec{f_g} \rho_g \vec{u_g}) = 0 \\
\frac{\partial(V_s \rho_s)}{\partial t} + \nabla \bullet (\vec{f_s} \rho_s \vec{u_s}) = 0
\end{aligned}
\tag{3.9}
$$

where subscript g and s indicates gas and solid respectively, V is the volume fraction, $\vec{f}$ is the phase fraction, ρ is the density and $\vec{u}$ is the velocity of different material accordingly.

The modified Navier-Stokes equations describes the motion of the domain for each phase is:

$$
\begin{aligned}
\frac{\partial}{\partial t}(\vec{f_g} \rho_g u_g) + \nabla \bullet (\vec{f_g} \rho_g \vec{u_g} \vec{u_g}) = \nabla \bullet \tau_g + \vec{f_g} \rho_g g - \nabla p - \beta(\vec{u_g} - \vec{u_s}) \\
\frac{\partial}{\partial t}(\vec{f_s} \rho_s u_s) + \nabla \bullet (\vec{f_s} \rho_s \vec{u_s} \vec{u_s}) = \nabla \bullet \tau_s + \vec{f_s} \rho_s g - \beta(\vec{u_s} - \vec{u_g})
\end{aligned}
\tag{3.10}
$$

where τ is the viscous stress tensor, g is the acceleration due to gravity, p is the thermodynamic pressure, which only exists in gas phase, and β is the interface momentum transfer coefficient.

On the microscopic scale, the vibration of any fluid molecules result in heat, a temperature is then introduced to the liquid. This concept was brought into bulk solid analysis by Savage in early 80's [22; 62] and had been widely used in bulk solid research [63; 64; 65; 66], especially in the field of powder fluidisation simulation where the applications are two-phase flow [67]. The collisions of particles cause velocity fluctuations, then a pseudo-temperature is introduced to the bulk solid due to the velocity fluctuations. The pseudo-temperature is called the granular temperature, is given as:

$$\theta = \frac{u'^2}{3} \tag{3.11}$$

where u' is the fluctuating velocity.

Hence the energy conservation equation is defined as:

3.2.1.2   Euler - Lagrangian

In the last decade, there has been a new technique emerging in granular simulations and it has been popular in powder dispersion [68; 69; 70] and in wall impingement [71] . In the CFD-Lagrangian workframe, granular material is no longer being treated as a pseudo-fluid, but a real particle as it is. The equations of motion are solved in the calculation of the solid phase, while gas remains as a fluid phase.

The Lagrangian workframe employs equation of motion to calculate acceleration for each particle, hence updates the particle velocity and feeds back to the fluid phase. Particle tracking is also embedded in this workframe to track the motion of each particle. Therefore this workframe is computationally expensive unless the number of particles is small.

3.2.1.3   Conclusion on CFD

CFD powder simulation allows the materials, air and powder to interact and exchange momentum and energy with each other. Hence the effect of fluid is a large contributor in powder simulation in comparison with DEM or FEM. In this study, air escapes through gaps between particles, and it does not interact or exchange information with the powder, air effect is minimal. Therefore CFD approach is not best suited for this project. The QPM project prior to this research came to difficulties in obtaining the effective viscosity of the powder (see Chapter 1.2). The focus of this research lays in the structure for the failure of the arch forming at the outlet. Section 2.4 explains that Mohr's circle analysis with stresses in different directions is crucial for prediction arching/failure condition. A model which can cope with deviatoric stresses is important. Most CFD models are only capable of providing hydrostatic pressure; it is not possible to analyse the failure with a stress that is not the same in all direction.

3.2.2   Finite Element Method (FEM)

The Finite Element Method is a continuum approach to granular numerical simulation, treating powder in bulk as a block of solid deformable continuum [72; 73].

3.2.2.1   Cam-Clay Model

In 1966, the Cam-Clay model was originally introduced by a Professor in Soil Mechanics from University of Cambridge, Schofield [74; 75]. It is a elastic-plastic numerical model that interprets a series of empirical data from axial testing and utilises the Critical State concept and Flow Rule of Theory of Plasticity [76] to predict the ideal behaviour of an isotropic-hardening soft clay. Hence the name Cam-Clay. The breakthrough of Cam-Clay model lies in its ability to allow the soft soil (usually wet clay)

to recover volume changes during axial testing by loading-unloading-reloading proce-
dure, this procedure can extract parameters of non-linear elasticity and of hardening
by plastic volumetric deformation of the soft soil. The soft soil is assumed to be a
ductile plastic continuum satisfying the associated flow rule.

Soil Mechanics and Powder Mechanics share a number of similarities, Cam-Clay model
is often employed in the simulations to predict dense powder behaviours.

Adapted Triaxial Powder Test for Cam-Clay

The schematic diagram in Figure 3.3 demonstrates the apparatus used in the triaxial
tester. The original triaxial test for soil submerges wet clay in water. In order to
accommodate dry powder testing, water is replaced with dry air. Therefore, this
adapted triaxial test submerges dry powder in dry air [77].

The test system is examined to be air-tight; there is no leakage anywhere throughout
the system. Powder is filled inside of the rubber sleeve, which is affixed to the pedestal.
There is a sintered metal plate inside of the rubber sleeve, between the pedestal and
the powder, to allow air to go through and to prevent powder from passing through the
porous medium. A plastic lid is mounted at the top end of the rubber sleeve. Powder
sample inside the rubber sleeve is air-tight and housed inside the glass chamber. Inlet
and outlet valves control the air pumping in and getting out off the glass chamber and
the fluid flow metre measures the air going into the chamber via the inlet.
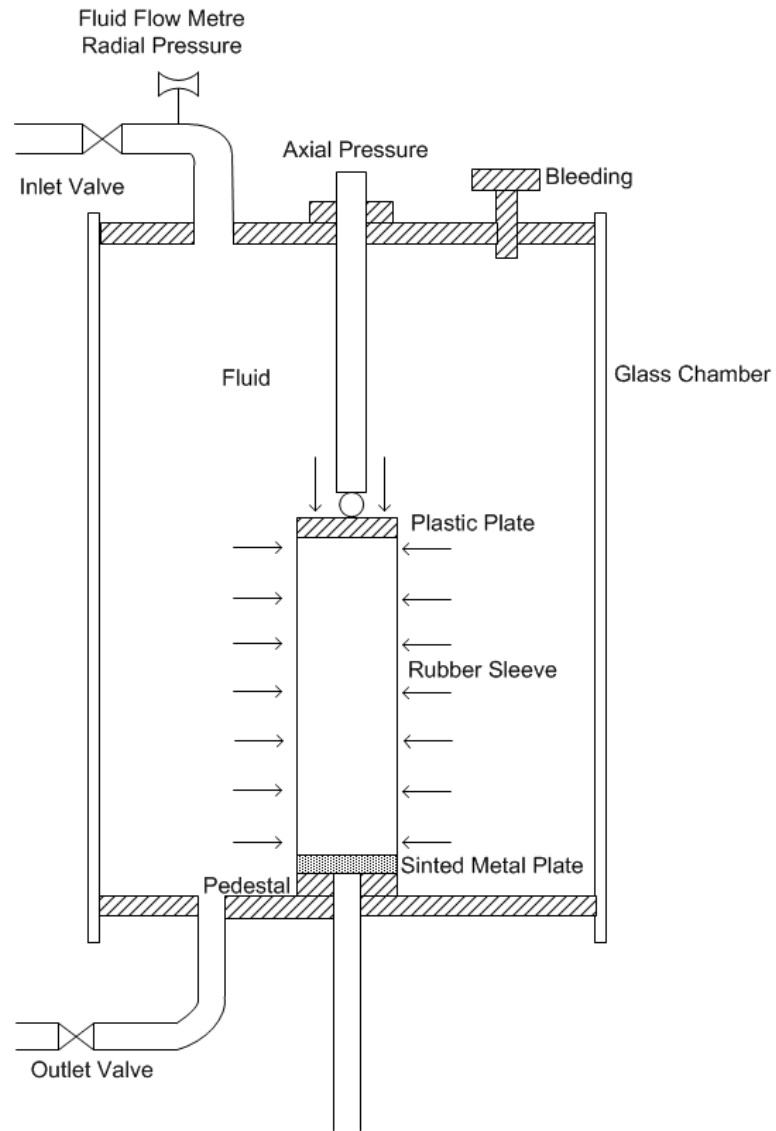
Figure 3.3: Triaxial test apparatus for Cam-Clay Model

Surrounding air in the glass chamber provides a radial air pressure of σ_r, and the axial shaft provides an axial pressure of σ_a onto the powder. The effective stress acts on powder is $\sigma' = (\sigma - u)$. The powder has its own pore air pressure u, which is negligible.

So the mean normal effective stress, p', and the traiaxial deviatoric stress, q, are:

$$p' = \frac{1}{3}(\sigma') = \frac{1}{3}(\sigma'_a + 2\sigma'_r)$$
$$q = \sigma'_a - \sigma'_r \tag{3.12}$$
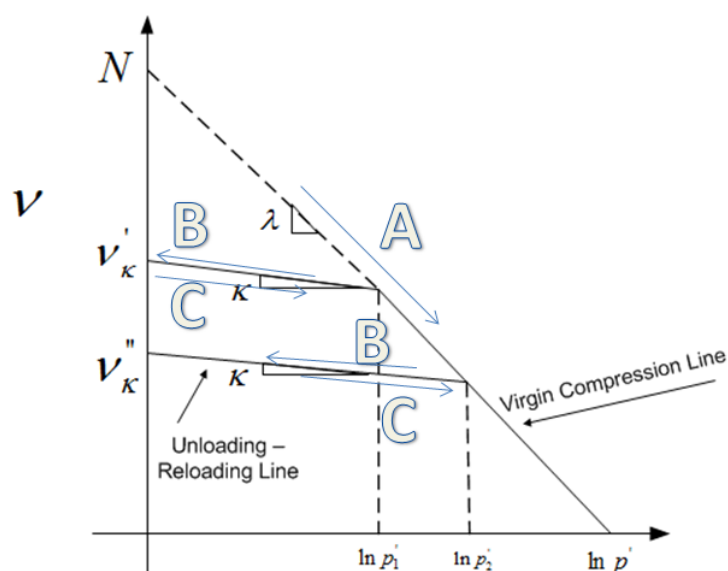
Figure 3.4: Correlation between specific volume and logarithmic
of normal effective stress

The advantage of Cam-Clay model lies in its establishment of a relationship between applied stress and relating strain, while taking account of the previous stresses acting on the material. Hence it was a break through on measuring material that is "stress history" dependent.

During compression, the powder specimen behaves as a ductile plastic continuum, its specific volume, v, is observed to decrease exponentially with increasing normal

effective stress, p', their correlation will be

$$v + \lambda \ln p' = v_\lambda \qquad (3.13)$$

Figure 3.4 Shows the relationship between the specific volume and logarithm of the normal effective stress. Material that is loosely pack is undergoing an increase of effective normal stress. The volume will reduce and follow the path on Line A with a slope of λ, until the effective normal stress reaches p'_1. Then the material is on relaxation; the applied stress is lifted and the material starts swelling. The material will follow a small elastic expansion. The specific volume of the material, v, follows the path on Line B with a slop of κ and increases slightly to v'_κ.

$$v + \kappa \ln p' = v_\kappa \qquad (3.14)$$

where v_λ and v_κ are the intercepts on the lines, v_κ differs from each unloading-reloading line and depends on the stress loading history.

After relaxation, the material is then under increasing compression again and the specific volume follows the path on Line C with a slope of κ until the effective normal stress reaches p'_1 again, then v will go back on Line A. Else if the effective normal stress does not research the p'_1, it will be in the region of between unloading and reloading, going back and forth on Line B and C. This is a very significant implementation of measuring material that is "stress history" dependent. This characteristic points out one of the crucial contributions of specific volume (or density) of the material in powder mechanics to predict its flow/no-flow condition, whereas the effect of density is minimal in conventional solid mechanics.

Critical State

Another crucial contribution of density in powder mechanics lies within the Critical State of the powder. Figure 3.5 details the shear failure for granular material and states that incipient flow only happens at shear failure when material is at its critical density.

Any granular material, under normal consolidation stress σ while shearing with a shearing stress τ for a horizontal displacement dx, would have a change in its thickness slightly, by a vertical displacement dy (Figure 3.5). dy/dx indicates the rate of dilation of the granular material. If it is continuously sheared, material strength reaches its maximum when dy/dx also reaches its maximum(Figure 3.6). Then slippage would occur and dy/dx becomes zero, this is said to be in Critical State condition [78].
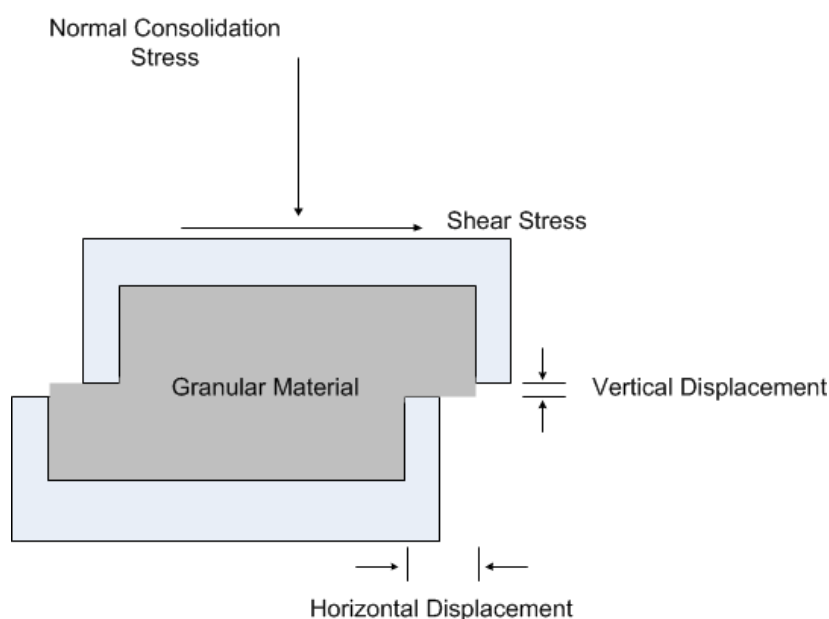
Figure 3.5: Direct shear box test

38
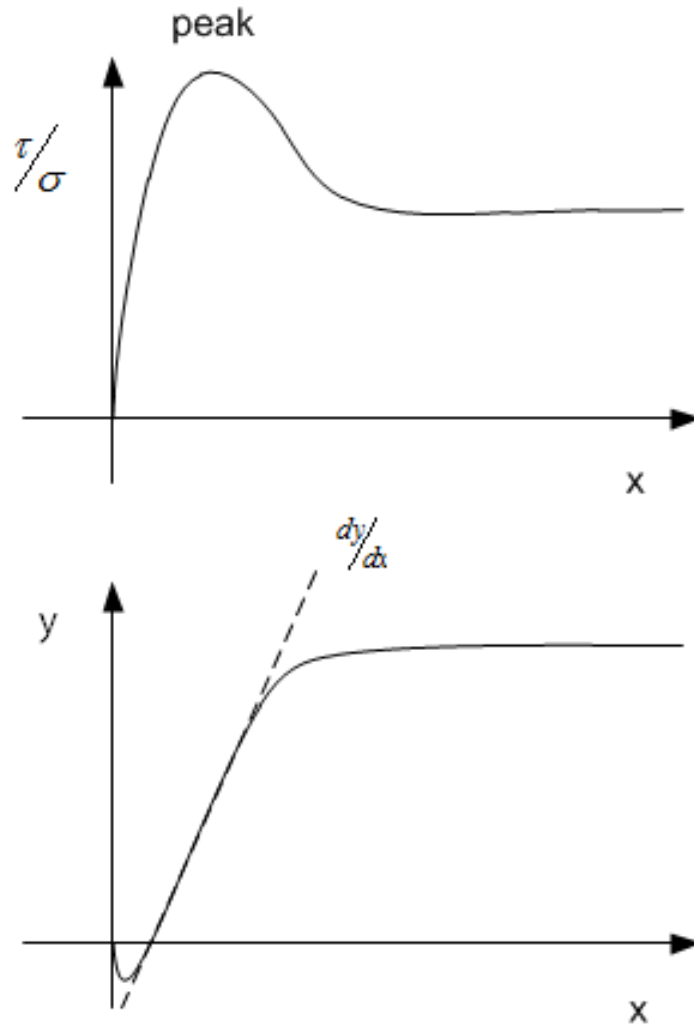
Figure 3.6: Strength and displacement during shear box test

In Critical State, granular material flows as a frictional fluid (similar to a Bingham fluid [1]), shear strain occurs without any further changes in effective mean stress p', deviatoric stress, q and specific volume v. This state can be represented by a Critical State Line in $p' - q$ plane (Figure 3.7) the Critical State Line is a straight line passing through the origin with the slope equal to M. The Critical State Line is also parallel

---

[1]The behaviour of switching from solid phase to fluid phase is very similar between the two, but there are still differences between the two, which will be discussed in later chapters

to the Virgin Compression Line in $v - \ln p'$, the parameter Γ is the specific volume at unit pressure in Critical State condition.
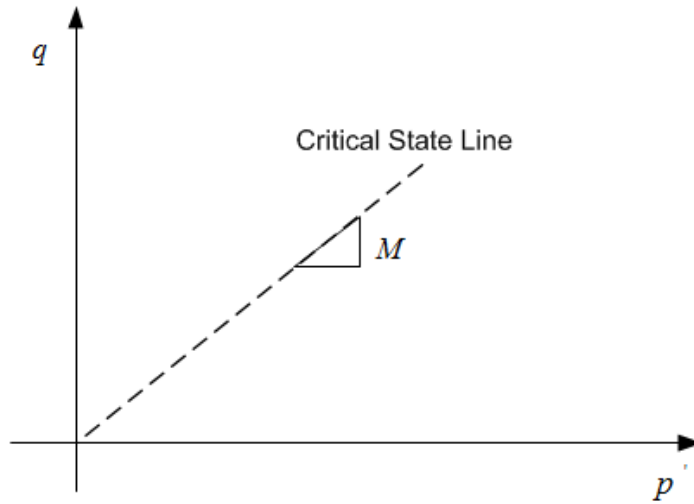
Figure 3.7: Critical state line in $q - p'$ plane
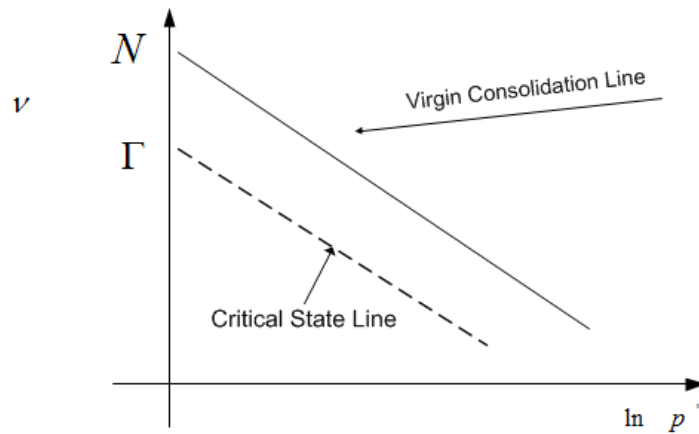
Figure 3.8: Critical state and virgin compression line in $v - \ln p'$ plane

Relation between Γ and N for Cam-Clay model is:

$$\Gamma = N - (\lambda - \kappa) \tag{3.15}$$

Hardening and Associated Flow Rule

Hardening of material in Cam-Clay is done by plastic deformation. Flow rules are used in plastic theory in solid mechanics to determine the plastic strain in any material which under goes plastic deformation. The name "associated" is given to its compatibilities with any certain yield criteria [79]. The original Cam-clay model has a yield function in the shape of a tear drop while the modified Cam-Clay model, by Roscoe and Burland [80], has a yield function of an ellipse as shown in Figure 3.9. In the Cam-Clay model, due to the usage of a critical state concept, the stress terms of yield function represent not the total stresses, but the mean effective stresses in $p' - q$ plane.
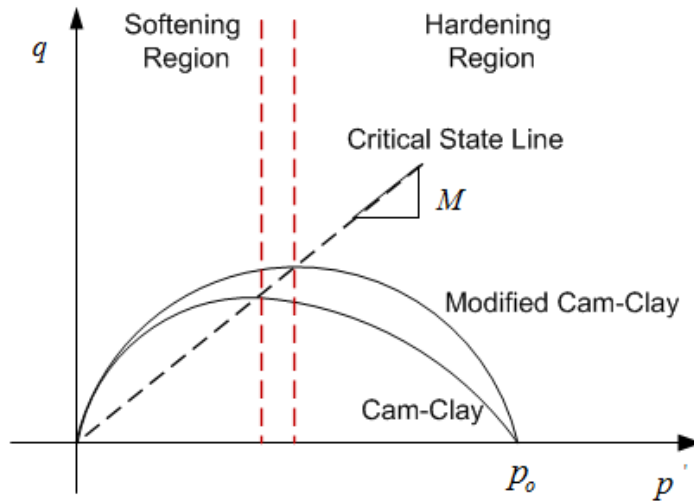
Figure 3.9: Yield surfaces for original Cam-Clay and modified Cam-Clay model

Yield function for Cam-Clay model:

$$q + Mp' \ln(\frac{p'}{p'_o}) = 0 \tag{3.16}$$

Yield function for Modified Cam-Clay model:

$$\frac{q^2}{p'^2} + M^2(1 - \frac{p'_o}{p'}) = 0 \tag{3.17}$$

where p'_o is the pre-consolidation stress and it controls the size of the yield surface.

Material hardening occurs in the region to the right of the intersect point of the Critical State Line and the yield surface, Figure 3.9 shows that material is in compression. The region to the left of the intersect point in the same figure represents material softening, which is associated with material dilatancy. The material is in tension in this region.

Conclusion on Cam-Clay Model

The cohesion of the powder is not a parameter in the Cam-clay model. Nevertheless cohesion is an essential parameter in the powder material property, therefore research has established a relationship between the elastic modulus and cohesion during the powder hardening stage [81; 82].

The Cam-Clay model is computationally inexpensive in comparison with DEM, its allowance for material to behave differently in either compression or tension makes it favourable among other numerical models for granular simulation. However the Cam-Clay model does lack some suitable prospects for the case study in this research, which is to predict the arching condition of cohesive powder in a hopper: a) Cam-Clay model only simulates compaction of powder, it lacks of the ability to examine the catastrophic failure of powder in the hopper, b) Cam-Clay model deals with isotropic compaction and treats the material as an isotropic material, which is not the case in cohesive powder.

If any researchers attempt to use the Cam-Clay model for failure/arching prediction in hoppers while taking consideration of cohesion. The author would suggest the research to focus on incorporating the cohesion in the yield surface and/or develop a yield surface that represents the failure of the powder.

3.2.3 Rheology Method

Powder behaviour classifies itself between being a fluid and being a solid, depending on its state [50], ranging from free-flow to non-flow situation. This transition zone is usually known as a state of "flowing solid" or "pseudo fluid". The term rheology is given to this area of study [83]. The rheology method in powder handling has been studied by researchers in the past two decades [84; 85]. If the powder, which is subjected to a constant stress, resists further deformation after an initial deformation, the powder is considered a solid. If the powder, which is subjected to a constant stress, continues to deform, the powder is considered a fluid. The rheology method allows the researchers to study both solid and fluid characteristics of the powder. Figure 3.10 shows that the classification of continuum materials.

Continuum Mechanics			
Fluid Meahnics		Solid Mechanics	
Newtonian Fluid	Non-Newtonian Fluid	Plasticity	Elasticity
	Rheology		

Figure 3.10: Classification of continuum materials

Viscoplasticity is a wide topic in rheology, its capability lies in providing both hydrostatic pressure and deviatoric stresses and its ability to considering both material properties plasticity(a solid's characteristics) and viscosity (a fluid's characteristics).

Viscoplastic models consist of two main elements; a Hookean spring element and a rate-dependent dash-pot element.

Bingham [86; 87] introduced a model in which under a certain yield stress [1] the solid

---

[1]Yield stress in this content is different from yield stress in normal standard solid mechanics, which is the stress threshold to determine the solid would behave either plasticity or elasticity.

material would start to flow. This phenomenon resembles the powder behaviour: a block of dense powder behaves as a solid until the exerted stress researches the critical point (yield stress).
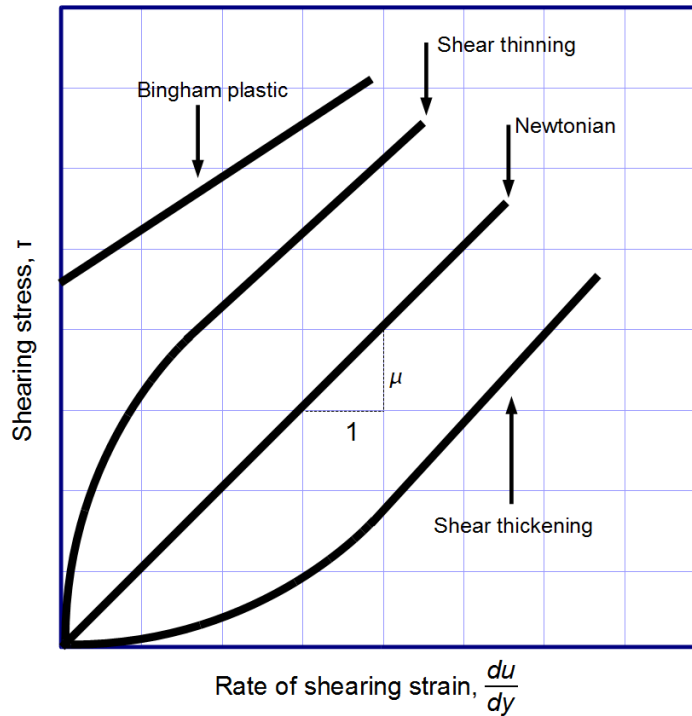
Figure 3.11: Viscosity regimes chart.

Figure 3.11 shows different material viscosity behaviours and Equation 3.18 shows that how a Bingham material switch from solid phase to fluid phase.

$$\frac{\delta u}{\delta y} = \begin{cases} 0 & , \tau < \tau_0 \qquad \text{solid phase} \\ \frac{\tau - \tau_0}{\mu_\infty} & , \tau \geq \tau_0 \qquad \text{fluid phase} \end{cases} \tag{3.18}$$

The ability of the model switching between two phases in the Bingham model resemble the behaviour of powder which also switches between two phases dependiing on the stress conditions.

3.3   Hybrid CFD-DEM Approach

The approaches mentioned previously in Section 3.1.1 and Section 3.2.1 have only one
solver. Some might have different elements interoperated into the solver to accommodate the situation. Figure 3.12 shows both CFD solver with incorporated DEM
element, which indicate DEM contributes sources to one or more than one CFD variable and vice versa for DEM solver with incorporated CFD.
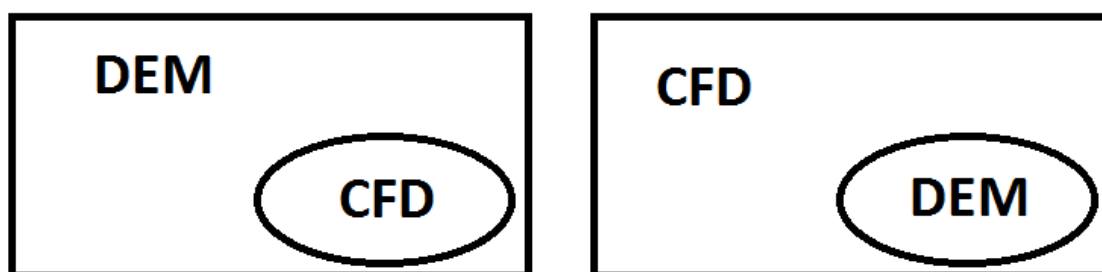
Figure 3.12: Solvers with incorporated element

Hybrid CFD-DEM Approach is a very sophisticated approach in Powder Mechanics
[88; 89; 90]. In Euler-Lagragian(Section 3.2.1.2), interaction between fluid and solid
phase is mentioned, but it is only the coupling between gas and particle. The interactions between particle and particle is absent. While the Hybrid CFD-DEM Approach
infuses the features from CFD and DEM. It couples gas-particle and particle-particle
interaction.

This approach focuses on running two solvers at the same time: the motion of discrete
particles is obtained by the DEM which solve the equations of Newton's law of motion
to each particle, while the flow of continuum fluid is calculated with local averaged
Navier-Stockes equations in CFD. The information is fed and exchanged between the
solid phase and the fluid phase, this interaion is described by using Newton's third
law. However this workframe is comparatively new in academic, and is still under
development [**?**].

Therefore there are two solvers running parallel to each other and exchanges information at the same time, demonstrated in Figure **??**. The function requires extremely complex coupling ability from the codes and also extremely high performance capability to conduct the calculation. Therefore this approach is the most computationally expensive of all.
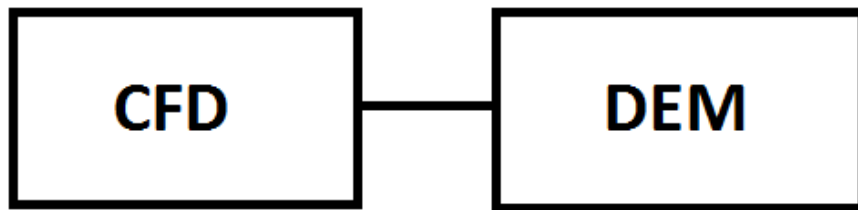
3.4 Chapter Summary

After reviewing the existing available models for powder behaviour simulations, the author decided to conduct a preliminary study to examine the closest models for powder behaviour for the problem of predicting arching.

Discreet Element Method(DEM) simulates the forces and dynamic motion for every single particle. Due to its extremely high computational requirements, it is only suitable for coarse granular materials or small benchmark samples of fine powders.

The existing models feature the flow end of granular materials and fine powders. However, this project is interested in the catastrophic failure of incipient flow in the hopper. The author felt there are none existing models that are perfectly suitable for this project as a whole, but only suitable for different individual aspects of the project, and moved to conduct preliminary simulations to extract the essence of each relevant aspect from different models, then establish a new constitutive model to predict arching conditions in a hopper.

Chapter 4

PRELIMINARY STUDY

The author's approach here was to start off by evaluating the available simulation tools. It was the best way to identify what worked, what did not work for the complex situation, and where the main difficulties were. This preliminary work was essential to establish the final simulation model approach.

4.1   Simulation of Powder behaviours by using viscoplastic fluid model

The rational starting point to simulate flow appeared to be using CFD. However to use CFD requires a constitutive law for the fluid, usually based on Navier-Stokes equation with the Newton's viscosity law (see Equation 4.1).

$$\frac{\partial}{\partial t}(\rho \overrightarrow{u}) + \bigtriangledown \bullet (\rho \overrightarrow{u} \otimes \overrightarrow{u}) + pI) = \bigtriangledown \bullet \boldsymbol{\tau} + \rho \boldsymbol{g} \qquad (4.1)$$

As yet the role of stress history would be ignored whilst trying to make a start on the

modelling knowing that this would have to be accountable for later.

Therefore the zone in the middle of the first arch in a discretised hopper was simulated (demonstrated in Figure 2.3) to determine if this model would be a suitable method for further development.

It was known that powders do not obey Newton's viscosity law, so it was necessary to seek a law that would be suitable to real powder behaviour. The powder behaves like a solid when it is filled and static in the hopper, but it behaves like a pseudo-fluid when it starts to flow. This phenomenon fits the definition of a viscoplastic material described in Section 3.2.3.

Bingham model features a material that behaves like a pseudo-fluid once the stress acting on the material exceeds the yield stress; the material would flow with a shear rate proportional to the amount by which the acting shear stress exceeds the yield stress.

The material in the zone is supported by its own weight and subjected to normal face acting on both side.

Figure 4.1: Simulation of arched element

Figure 4.1 is the simulation of an arched element circled in Figure 2.3 using Bingham model with one end fixed and external pressure acting on the end.

Boundary Conditions:

- fixed coordinates at $x = 0$

- applied pressure $36 \times 10 Pa$

Bingham Material Properties:

Yield stress	Shear rate	Viscosity
$1400 Pa$	$2000 Pa$	$1000 Pa$

Conclusion on Bingham model

Viscoplastic models are the well-known models in CFD that provide deviatoric stresses in additional to hydrostatic pressure. Powder materials do express different stress in different directions. Therefore Bingham model was chosen to be the first attempt, even though it has a few shortfalls when dealing with the prediction of arching behaviour in hopper.

However, standard CFD had no capability to deal with change in properties due to stress history, which was known to be important from the Cam-Clay model (Section 3.2.2.1). Bingham model assumes the material is incompressible, which is not the case for powder compaction. Cohesive powder increases its bulk density and decrease its volume under compaction, while the bulk density increases, the strength of the powder also increase.

In addition, in reality each layer of arch supports its own weight, stresses acting on the arch with the open outlet is less than the stresses when the outlet is close. According to the Bingham model the simulated element would always be in the solid phase; unless the assumption is made that the material sitting on top of the arch rests its weight onto the arch. This is a behaviour of flow condition, which is against conditions of this research project. This research project aims on predicting arching or flow condition with stress analysis.

Lastly, the viscosity in CFD, which is an important parameter in CFD simulation, does not fully represent the characteristics of the powder. Because during shear, the powder would break apart and become discontinuous instead of remaining continuous like a normal fluid. In normal CFD, the discontinuity in fluid is treated with extrapolation. However when the powder break apart, the failure is a catastrophic event, extrapolation over the discontinuous zone would not be a suitable approximation to the powder.

Discontinuity at arch failure is actually a quasi-static problem; it is like a bridge failure. The author hence moved to examine the use of Finite Element Method for arching

problem.

4.2 Simulation of an arched outlet and element removal by Using FE

Simulation of the arch was attempted using a continuum mechanics approach i.e. Finite Element (FE). The powder incipient flow at the outlet is a catastrophic failure event. Failure mechanics is well established in conventional solid mechanics [91; 92]. However, when the powder starts "flow" out of the hopper, the material which is "gone" would no longer have any effect on the stress-strain analysis of the rest of the powder. This is the reason why the author decided to model the failure event by changing powder elements to void elements. Below details how the study was conducted:

Arch geometry

Thickness	Hopper half angle	Mesh size
$100mm$	$45°$	$10 \times 26mm$

Most hopper and silo manufacturers design the geometry without the consideration of the powder behaviours and draw up the designs with CAD, hopper half angles across the industry are commonly found to be $30°$, $45°$ and $60°$. The half angle chosen to be $45°$ for this study, as it is one of the most common and problematic shapes across the industry.

Material properties

Bulk Density	Poisson Ratio	Young's Modulus
$720kg/m^3$	0.3	$220 \times 10^3 Pa$

Boundary conditions

- All degrees of freedom are restricted on the elements next to wall, that means the material is non-sliding along the wall. Because the preliminary study is only examining the removal of elements under the assumption that arching is already occurring. So the simulation will have a non-slip boundary condition at wall.

- The only forces existing are the gravitational force and force between powder and wall.

The same simulation with the unchanged material properties and boundary conditions were conducted on both ANSYS and PHYSICA. The reason for the comparison is to ensure the basic Solid Mechanics module in PHYSICA is bug-free, so further software development can be conducted in addition to the original source codes. The reason for choosing PHYSICA over ANSYS is that PHYSICA has a much easier access to its source codes and therefore more flexible to cope with user changes. Even though PHYSICA does not have a user friendly interface, it is necessary for software developers to develop the source codes, in order to make accommodating changes to the complex calculation system.
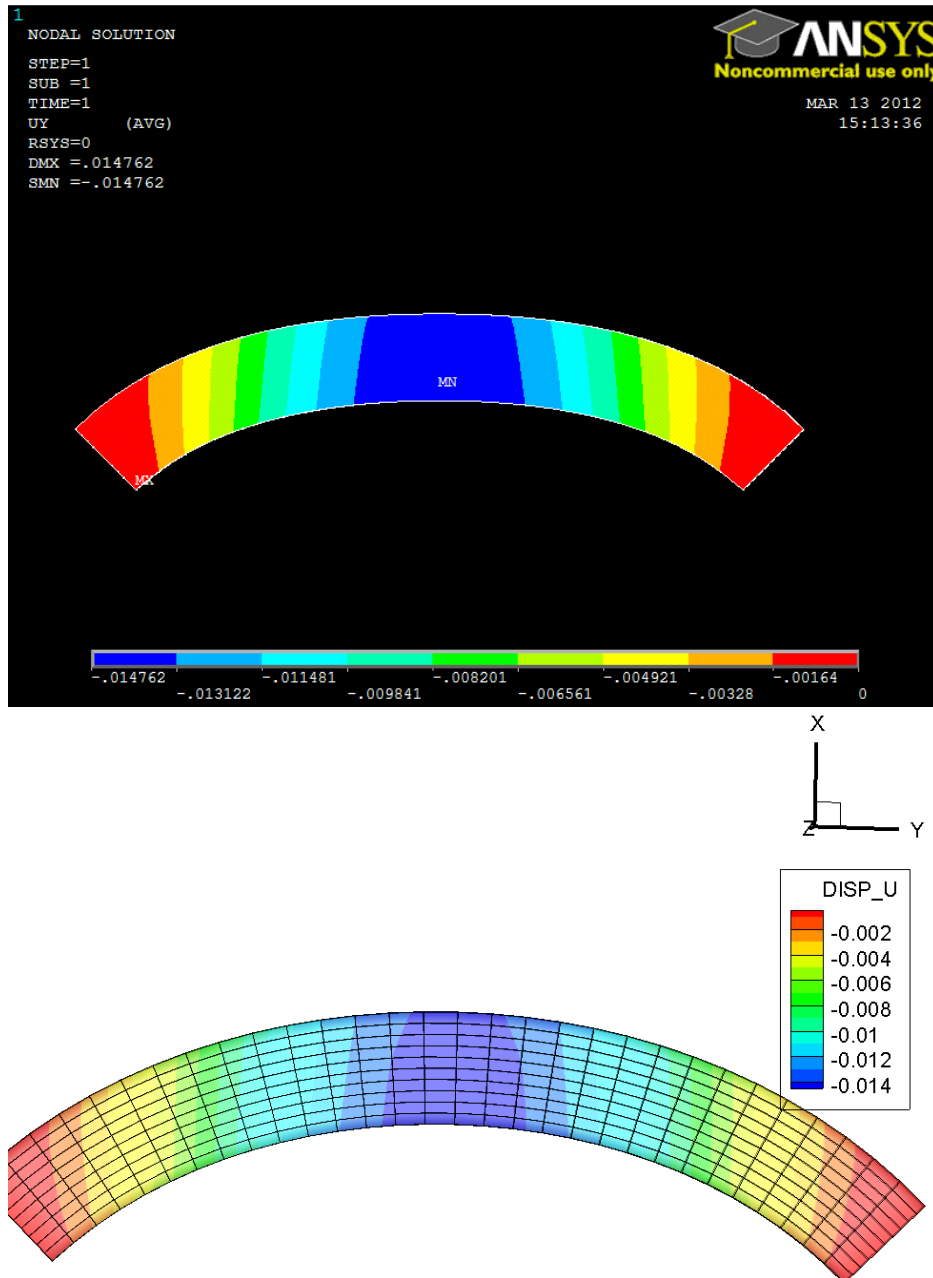
Figure 4.2: Comparisons between Ansys and PHYSICA on horizontal displacements.
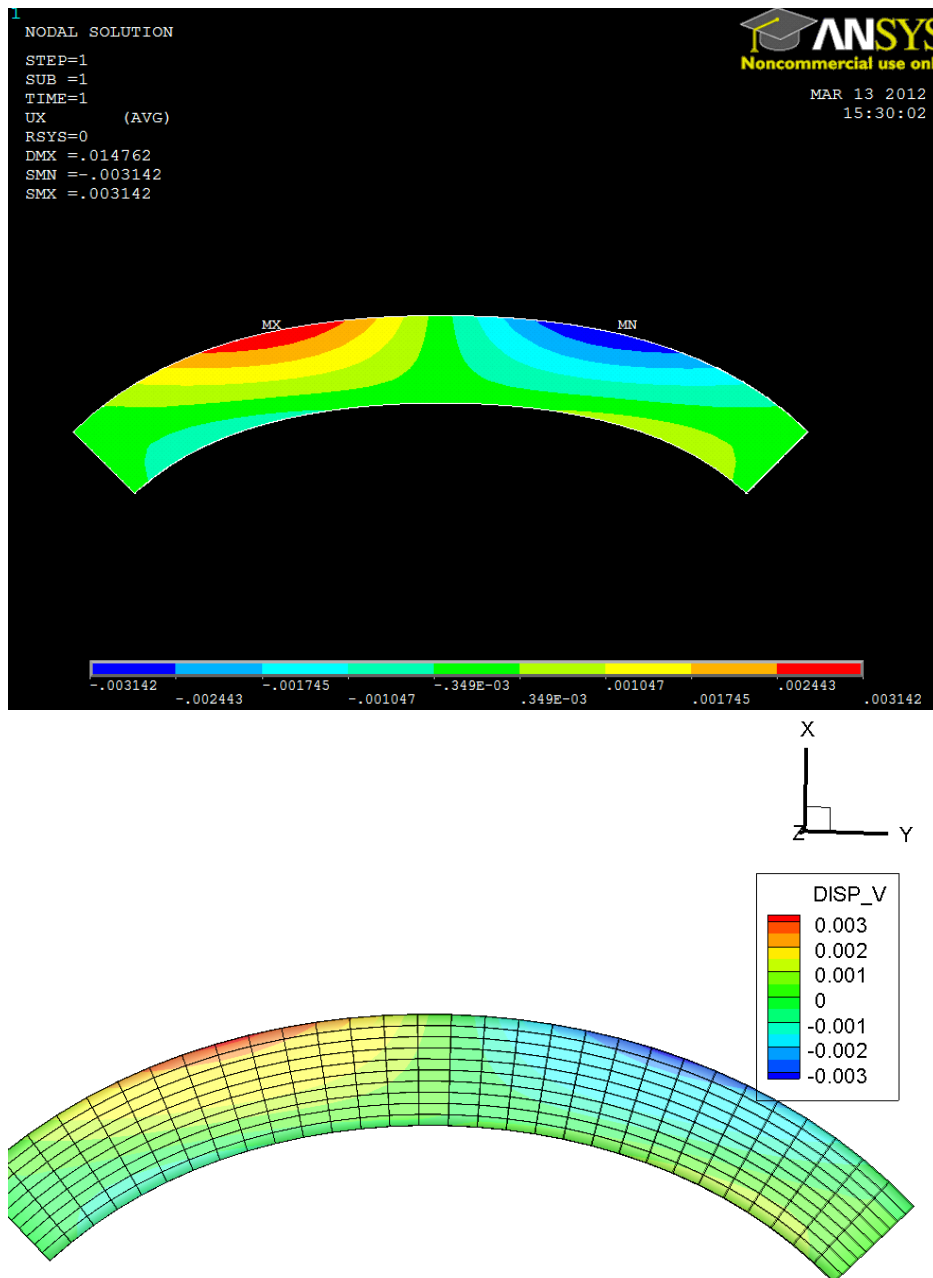
Figure 4.3: Comparisons between Ansys and PHYSICA on vertical displacements.

Both results on ANSYS and PHYSICA in Figure **??** show the same contour and value on displacements; range from $-0.0031m$ to $0.0031m$ for horizontal displacement,U, and range from $-0.0015m$ to $-0.0015m$ for vertical displacement,V.

To compare the stresses, the author has chosen the stress along the centreline of the arch (Figure 4.4), as it is where the largest movement in vertical displacements take place. The largest displacement is associated with largest stresses, for any discrepancy between Ansys and PHYSICA, the centreline will be the most obvious location to examine, as shown in Figure 4.4 maximum displacement is along the centreline.
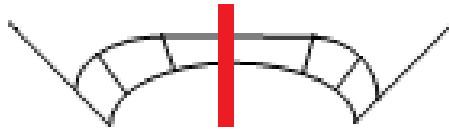
Figure 4.4: Schematic diagram for centreline of the arch, where the two results are compared.
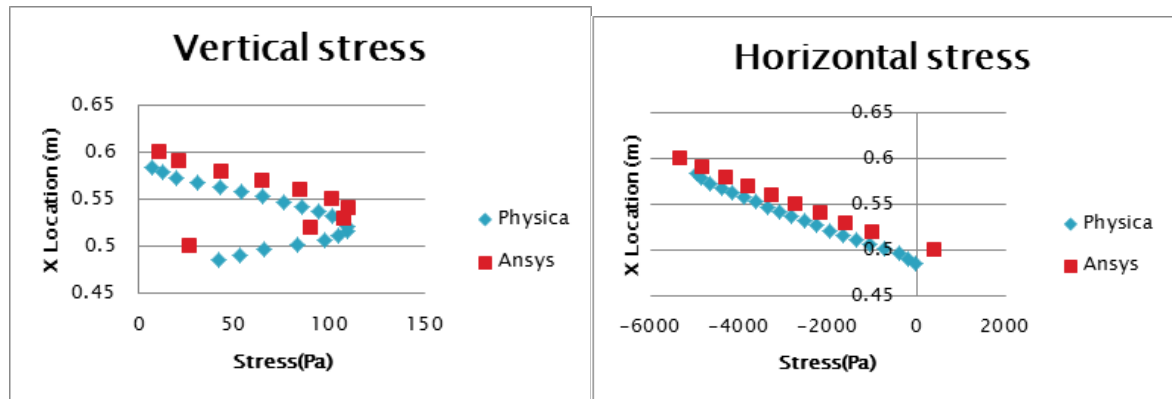
Figure 4.5: Comparisons between Ansys and PHYSICA on
vertical and horizontal stresses along the centreline

Figures 4.5 above show consistency in both vertical and horizontal stresses between ANSYS and PHYSICA results, even though there is a small shift in the results, this is due to the fact that the stress values in ANSYS are given at the nodes of each element

whereas in PHYSICA are given at the centre of each element. These comparisons show that the solid mechanics module in PHYSICA is suitable for further code development.

Elements are then removed to simulate the situation where bits of material from the arch start to fall. In the arch simulation there are two circumstances where the elements need to be removed. One is where elements experience tensile stress, the other, where the stresses of the element satisfy Mohr's Circle failure criteria.

PHYSICA gives stress results in global coordinates, which are in either global horizontal or vertical direction. In order to study the element stresses, local stresses need to be transformed from the global stresses to align with the orientation of each element. The stress transformation can be conducted as follows (see Figure 4.6):
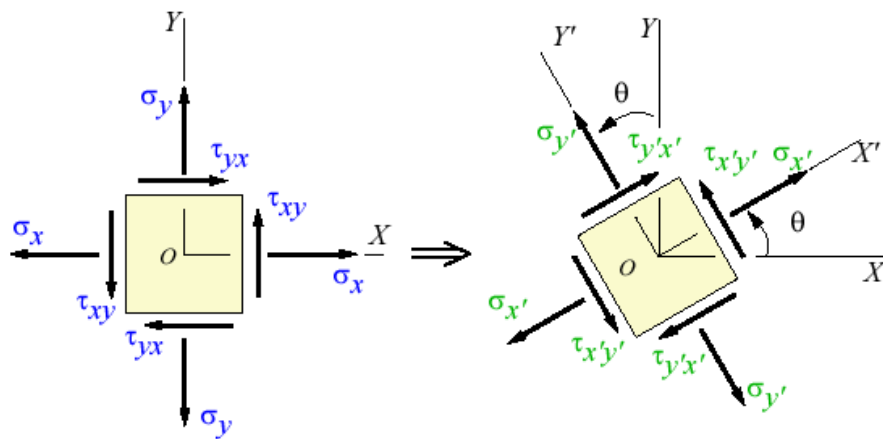
Stresses at given coordinate system   Stresses transformed to another coordinate

Figure 4.6: Stress transform and different co-ordinate system

Dieter (Ref [93]) has used ′ to denote the transformation coordinate, for simplification and coherence for later paragraphs, author will use notation as in the following

equations.

$$\sigma_{lh} = \frac{\sigma_h + \sigma_v}{2} + \frac{\sigma_h - \sigma_v}{2}\cos(2\vartheta) + \sigma_s\sin(2\vartheta)$$

$$\sigma_{lv} = \frac{\sigma_h + \sigma_v}{2} - \frac{\sigma_h - \sigma_v}{2}\cos(2\vartheta) - \sigma_s\sin(2\vartheta) \qquad (4.2)$$

$$\sigma_{ls} = \frac{\sigma_v + \sigma_h}{2}\sin(2\vartheta) + \sigma_s\cos(2\vartheta)$$

σ_{lh}, σ_{lv} and σ_{ls} are elemental local horizontal, vertical and shear stress respectively. σ_h, σ_v and σ_s are global horizontal, vertical and shear stress respectively and ϑ is the angle between local element orientation and the global x-y axes (shown as in Figure 4.7).
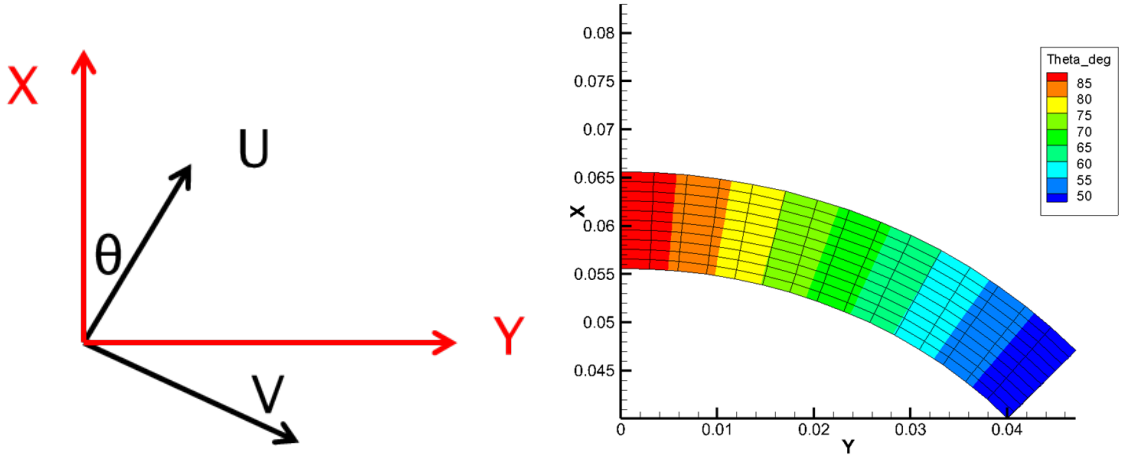
Figure 4.7: θ of an arbitrary element (left) and θ values across the arch

The local horizontal stress is shown in Figure 4.8 on the left and it is shown in a manner that positive and negative stresses are emphasised. In order to emphasise the switch between the compression elements and the tensile elements, the conture is scaled between $-1Pa$ to $1Pa$; the blue elements are all in tension and the red elements are in compression. The elements in tension are due to be removed. After the removal

of the elements in tension, the rest of the arch remains in compression. The figure on the right demonstrates the stress after removal of the elements in tension. The local horizontal stress on the rest of elements does not change before or after the removal. This shows that the rest of the arch is in compression and the compressive force makes elements interlock with its adjacent elements, therefore the arch can support its own weight.
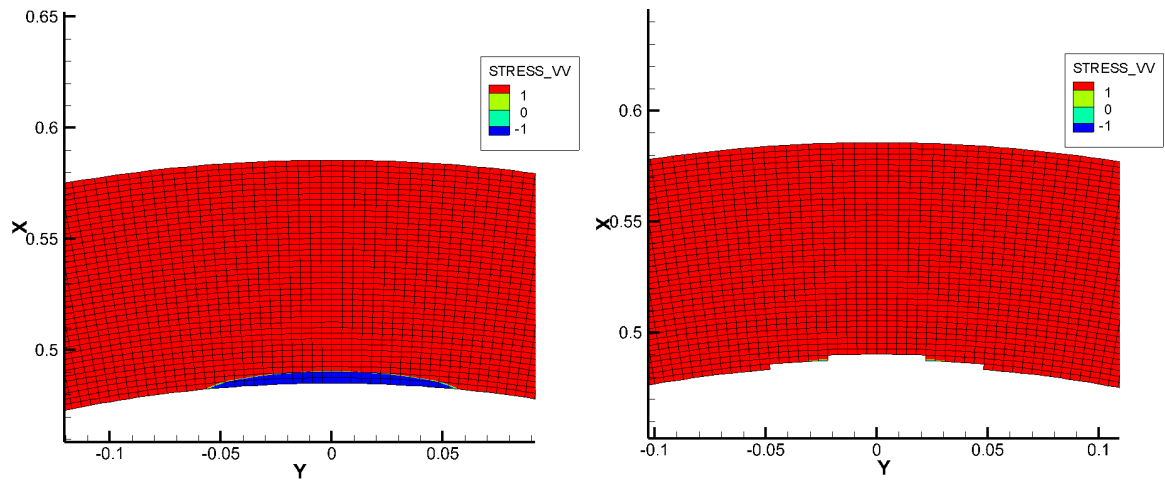
Figure 4.8: Local horizontal stress before (left) and after (right) removal of elements

As it has been mentioned in previous chapter, the other criterion for removing the element is to satisfy the failure criterion in Mohr's Circle analysis.

Mohrs circle analysis is the most fundamental principle in powder mechanics, Janikes introduction of Mohrs circle analysis paved the stress analysis in powder mechanics. Mohrs circle is a graphical expression of the state of stress at a point. The difference between the traditional Mohr's circle and the Mohr's circle for powder mechanics is that the traditional Mohr's circle by is derived for specimen in tensile stress (see Figure 4.9) and the powder mechanics are mostly in compression stress.
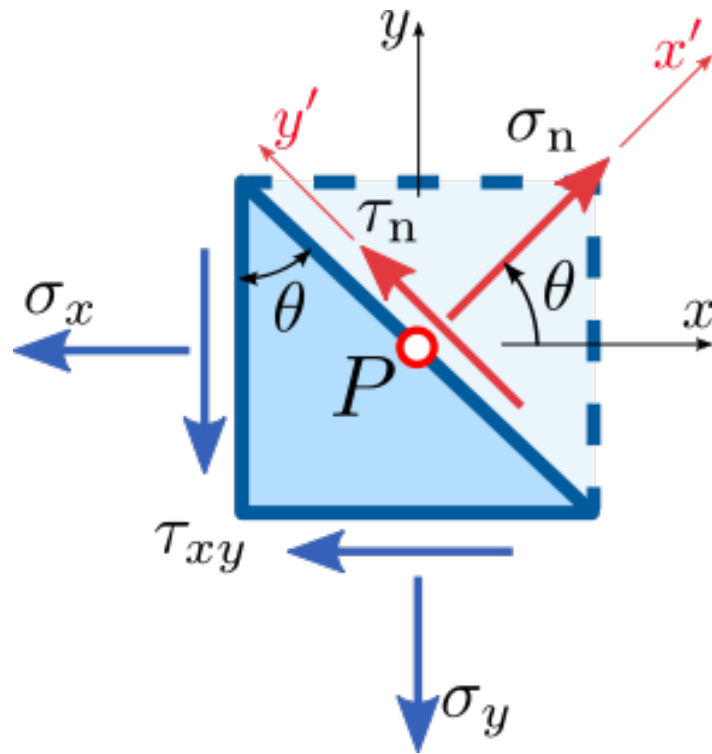
Figure 4.9: Stress components at a plane passing through a point in a continuum under plane stress conditions
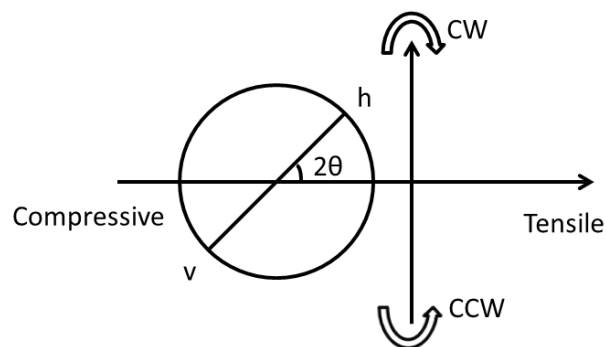
Figure 4.10: Sign convention of Mohr's Circle

Traditional Mohrs circle in Figure 4.10 has tensile stress as positive stress and compressive stress as negative stress. σ_1 and σ_2 are the major and minor principal stresses where shear stress is absent. The figure also shows the element needs to rotate 2θ clockwise (CW) to reach its principal stress state.

However, the sign convention is different in powder mechanics - compression is positive and tension is negative. The representation of the stress state for the same element will be as in Figure 4.11:
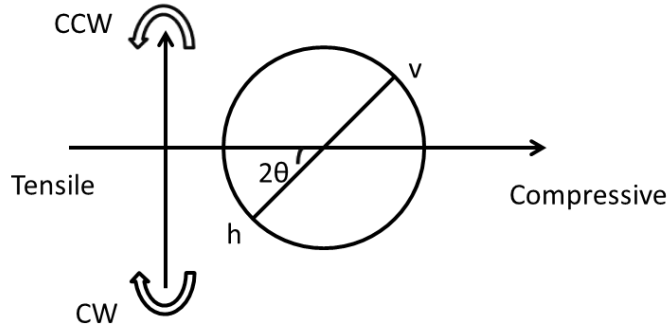
Figure 4.11: Sign convention of Mohr's Circle in Powder Mechanics

Values of mean stress σ_m, both principal stresses σ_1, σ_2 and maximum shear stress σ_{maxls} can be calculated as follows:

$$\sigma_m = \frac{1}{2}(\sigma_{lh} + \sigma_{lv})$$
$$\sigma_{maxls} = \sqrt{\frac{1}{2}[\sigma_{lv} - \sigma_{lh}]^2 + \sigma_{ls}^2} \qquad (4.3)$$
$$\sigma_1 = \sigma_m + \sigma_{ls}$$
$$\sigma_2 = \sigma_m - \sigma_{ls}$$

After studying the elements in the centre, another location with high tendency to shear has also been studied, where shear stress is at its maximum. The contour in Figure 4.12 shows that maximum shear stress occurs at the corner of the arch on each side,

the element at the corner of the arch on the right has been specifically studied using Mohrs Circle analysis. therefore the first principal, second principal and shear stress need to be calculated for each element.

For an arch to be formed in the hopper near the outlet, the arch is self-supported and it is believed to be rigid and static resting across the hopper outlet. Hence there would be a no-slip condition at the corner.
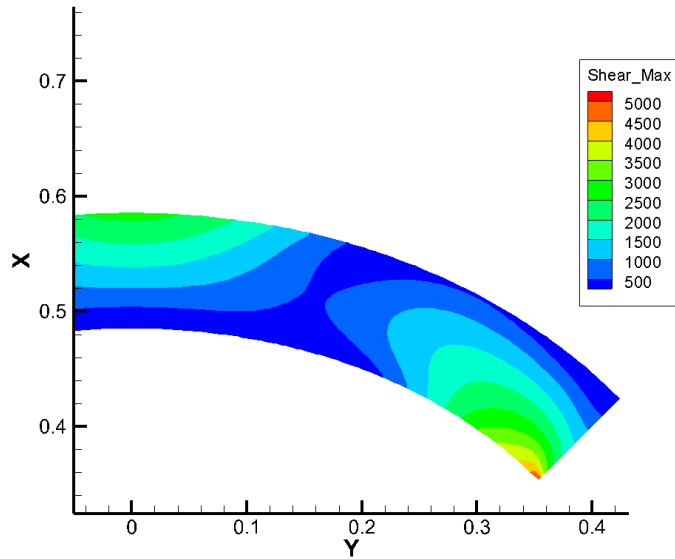
Figure 4.12: Contour of maximum shear stress in each element calculated from Equation 4.3

Stress data extracted from that point are tabulated as follows:

Local Vertical Stress	Local Horizontal Stress	Local Shear Stress
$11.6 \times 10^3 Pa$	$1.7 \times 10^3 Pa$	$14.5 \times 10^3 Pa$
Local Mean Stress	Local Max Shear Stress	
$6.0 \times 10^3 Pa$	$47.8 \times 10^3 Pa$	
Local Major Principal Stress	Local Minor Principal Stress	
$10.8 \times 10^3 Pa$	$1.2 \times 10^3 Pa$	

An empirical experiment has been conducted in accordance to the simulation. The cohesion and the internal friction angle are functions of pre-consolidation stress. The pre-consolidation stress is assumed to be the major principal stress, therefore the cohesion and the internal friction angle can be found accordingly for each element. The corresponding Yield Locus is then obtained as a failure criterion to examine whether or not the element will fail. Hence the author used the stresses to analyse the condition with the Mohr's circle analysis.
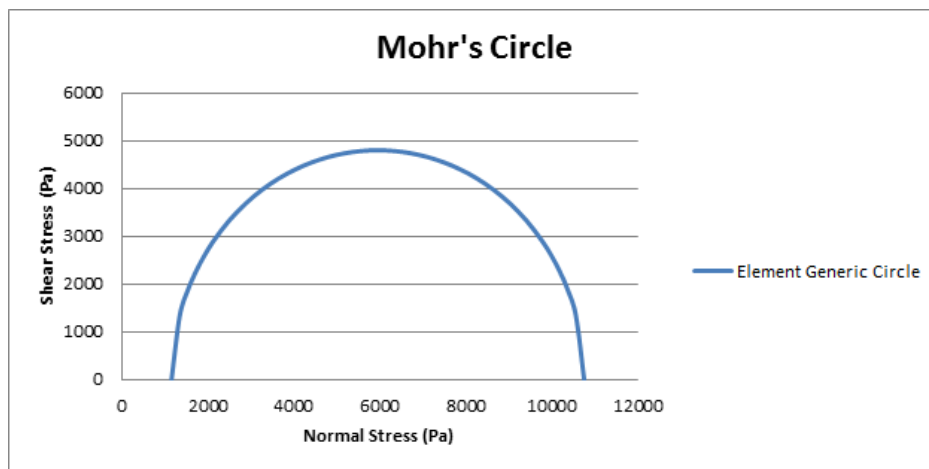
Figure 4.13: Generic Mohr's Circle using given stress data, maximum and minimum principal stresses
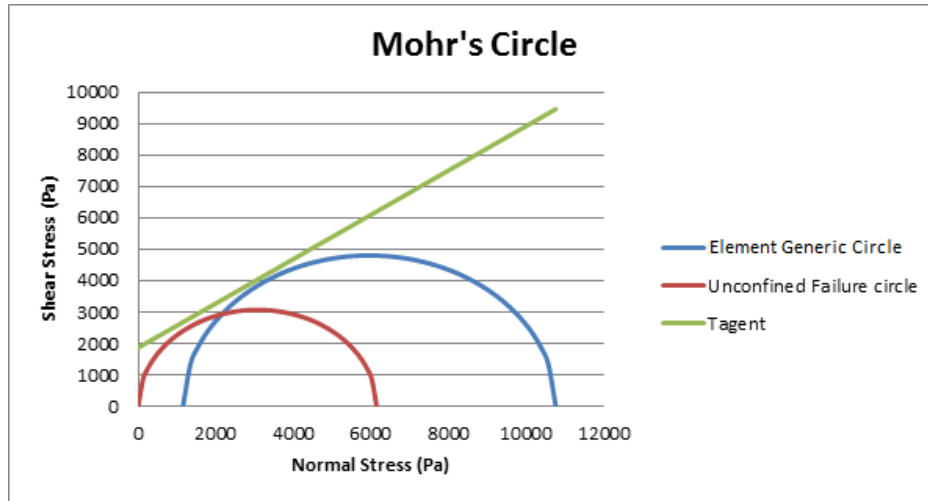
Figure 4.14: Genetic Mohr's Circle and its predicted Yield Locus

For any powder specimen, failure occurs when the element generic Mohr's circle touches the Yield Locus. However, at this point of the research, the author came to the realisation that a history of stress needs to be created in order to carry out the Mohr's circle analysis with a failure criterion. The preliminary simulation leads to further research after realising the problems and the the adoption of PHYSICA, whose ability allow users and developers to create code to accommodate complex calculation, these two aspects are explored on later chapters.

The author also carried out simulations on different outlet spans and different hopper angle to support the preliminary simulation:

Radius of curvature(mm)	Silo outlet span (mm)	Cell size (mm)	No. of cell	Max vertical disp. (mm)	Stresses at corner			Sigma C (Pa)
					Stress VV (Pa)	Stress UU (Pa)	Stress UV (Pa)	
600	848	2.5x5.2	7200	20	12700.45	2069.594	1667.642	7249.414
500	707	2.5x4.4	7200	14	11593.4	1950.493	1620.921	6617.515
400	565	2.5x3.5	7200	8.5	10100.59	1781.116	1528.805	5765.415

Figure 4.15: Different outlet span for preliminary stimulation
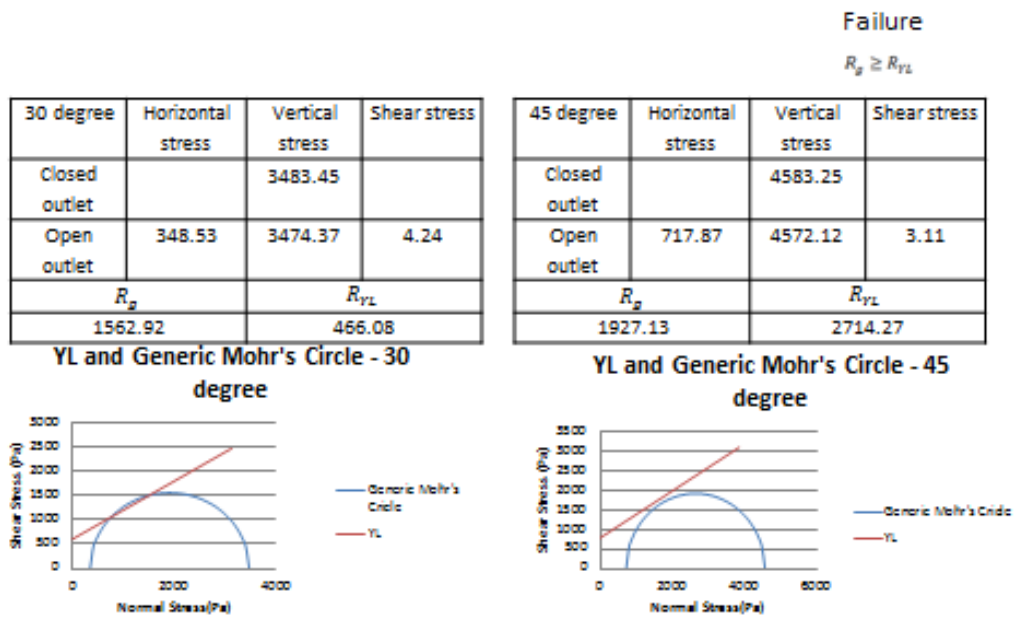
Figure 4.16: Different hopper angle for preliminary stimulation

The findings of conducting two analysis with different hopper geometry; hopper half angle of 30° and 45°. The results shows that the Generic Mohr's circle from the 30° case touches the Yield Locus therefore it would fail. The Generic Mohr's circle from the 45° does not satisfy the failure criterion, the material therefore remains arched.

This is the true to most real situations across the industry. The steeper the hopper (smaller hopper half angle), the more free-flowing the material will be.

Chapter 5

THEORY

This chapter outlines the hypothesis of this research project and modelling and the theories behind the hypothesis.

5.1   Model Theory

Through Literature Review and the Preliminary Study, we know that there is no current existing continuum numerical model that is good for predicting cohesive arching in a hopper. The author decided to extract the relevant essential aspects from the well-established models to assemble and develop a model that represents the underlying physics in cohesive arching condition in a hopper.

The author identified FEM as a feasible approach in Preliminary Study Chapter 4, and this decision has been upheld after reviewing the relevant literature. The full modelling approach is set out in Figure 5.1. Subsequent sections will describe the model in greater detail in terms of empirical property determination, numerical simulation, and

the links between the two. The author conducted the confided compression test for powder characteristics which are used in the compaction aspect of modelling and the Brookfield PowderFlow test for the powder characteristics which are used used in the failure of the arch.
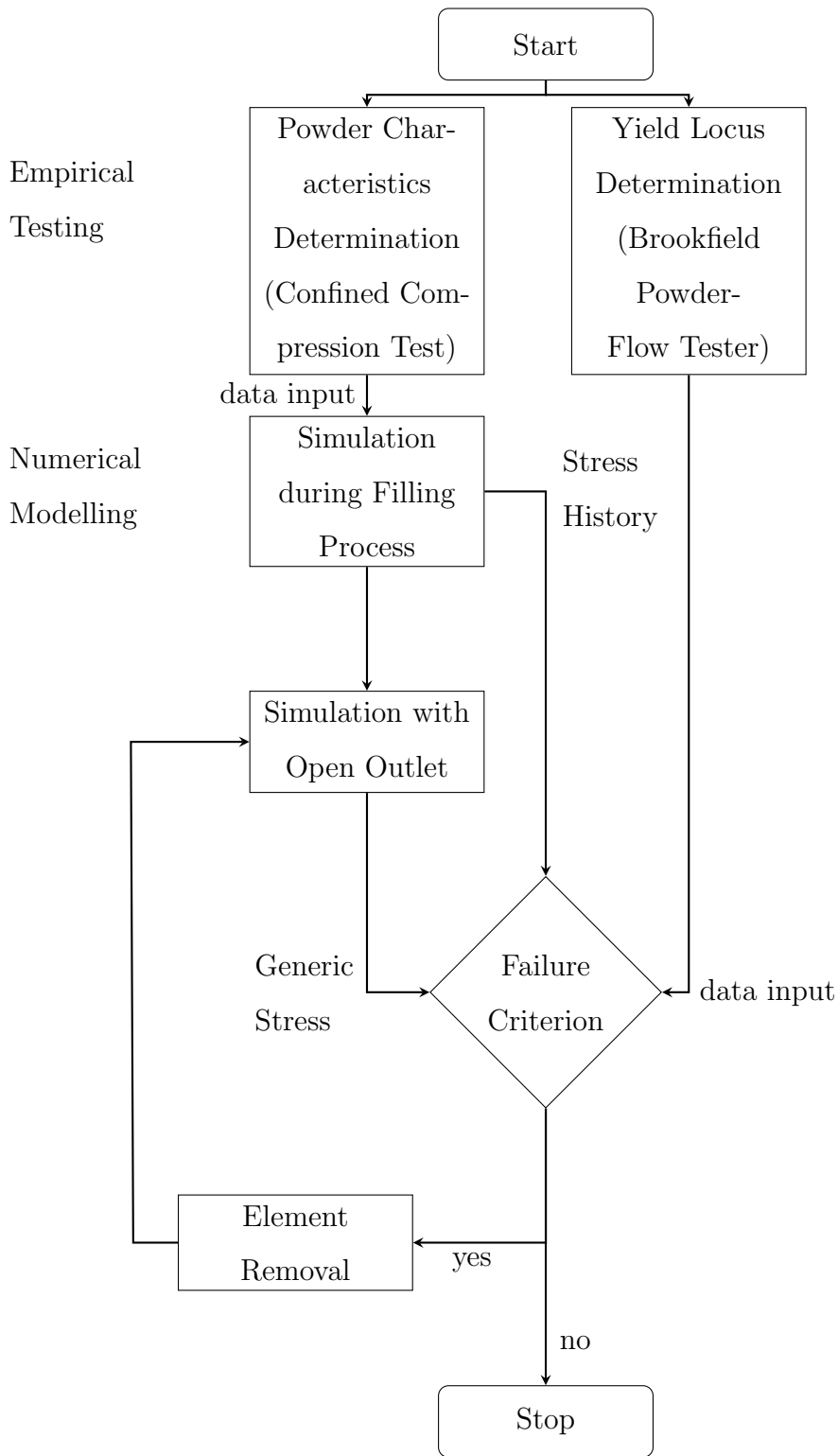
Figure 5.1: Modelling Flowchart

5.2 Powder Compressibility and Young's Modulus

In order for the simulation to function properly, it needs a new relationship for Young's modulus which relates the strain to applied stress according to powder behaviour. Whereas, for a solid, this relationship is well established, for powder it is much more complex. The complete arise in the under-defined powder concepts in FEA.

During filling, the powder is under compaction, ie. its volume is reducing. The Cam-Clay model (Section 3.2.2.1) shows how powder behaves under both increase and decrease of stress.

The use of the plasticity law in Cam-Clay for flow is not employed in author's model, because the Cam-Clay model was introduced having in mind that the material will flow as an extremely ductile solid or frictional fluid after the critical state is reached. However, for the cohesive powder arching condition, once the shear failure happens, it will be a catastrophic failure event, similar to fracture events but not the same. So the deformation mechanism from plasticity law is of no use in this model.

The author knows that during compaction the powder is behaving plastically in reality. But for computational convenience, the author introduced the effective "Young's Modulus" to trick the software package, with a high yield stress[1]. Because the yield stress in the simulation is ensured to be high enough for the calculations to be conducted within the elastic region of the material.

The relationship between applied stress and related strain are given in Chapter 3.2.2.1, where a powder starts at a low density (eg. filled into a hopper under low stress) and stress is applied, the volume reduces along the steep part of the curve. The slope is a function of density, but can be modelled as an equivalent Young's modulus,"E", where can be produced from this curve, as a function of stress, to use in the simulation for filling. According to the Cam-Clay model, if at any point the stress is reduced an

---

[1]The yield stress here is the yield stress in which if exceeded, material deforms plastically

elastic expression will occur at a different slope, for which a different stress-strain relationship (effective "E") can be determined, again dependent on stress because the line is a curve if plotted on linear axes.

To implement the effective "E" in the simulation, it requires a different function for "E", one for plastic volume reduction for filling stage when the powder is in compaction and one for the elastic behaviour during opening when the powder is in relaxation. Both relationship of "E" are liked by density and with respect to stress σ.

As mentioned in previous Section 3.2.2.1 about Cam-Clay, there are two coefficients λ and κ for the virgin compression situation and unloading-reloading compression situation. For the numerical model to be able to implement two different compression situations, two functions are needed for effective "E".

5.3   Finite Element Method for "Elastic" Material

The typical stress and strain analysis on a given element is illustrated in Figure 5.2 with stresses in each direction [94]:
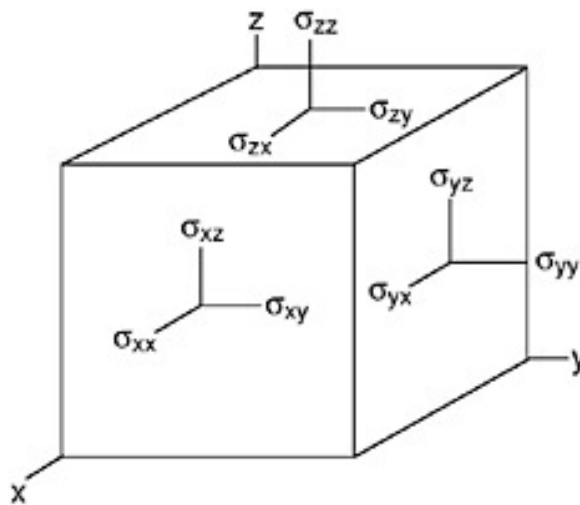
Figure 5.2: Stress components on an infinitesimal element.

The equilibrium equations for three-dimensional elastic stress are:

$$\frac{\partial \sigma_{xx}}{\partial x} + \frac{\partial \sigma_{xy}}{\partial y} + \frac{\partial \sigma_{xz}}{\partial z} F_x = 0$$

$$\frac{\partial \sigma_{xy}}{\partial x} + \frac{\partial \sigma_{yy}}{\partial y} + \frac{\partial \sigma_{yz}}{\partial z} F_y = 0 \qquad (5.1)$$

$$\frac{\partial \sigma_{zx}}{\partial x} + \frac{\partial \sigma_{zy}}{\partial y} + \frac{\partial \sigma_{zz}}{\partial z} F_z = 0$$

where σ_{xx}, σ_{yy} and σ_{zz} are normal stresses, σ_{xy}, σ_{xz} and σ_{yz} are shear stresses, F_x, F_y and F_z are body forceses.

The equilibrium equations are integrated:

$$\iiint (\frac{\partial \sigma_{xx}}{\partial x} + \frac{\partial \sigma_{xy}}{\partial y} + \frac{\partial \sigma_{xz}}{\partial z}) \quad dxdydz = \iiint -F_x \quad dxdydz$$

$$\iiint (\frac{\partial \sigma_{xy}}{\partial x} + \frac{\partial \sigma_{yy}}{\partial y} + \frac{\partial \sigma_{yz}}{\partial z}) \quad dxdydz = \iiint -F_y \quad dxdydz \qquad (5.2)$$

$$\iiint (\frac{\partial \sigma_{zy}}{\partial x} + \frac{\partial \sigma_{zy}}{\partial y} + \frac{\partial \sigma_{zz}}{\partial z}) \quad dxdydz = \iiint -F_z \quad dxdydz$$

The system of Partial Deferential Equations are coded to be solved in PHYSICA, which is a numerical solver developed in the Department of Mathematical Sciences at University of Greenwich. In this study the above equations are simplified into two-dimensions to simulate a cross-section of a wedge hopper.

$$\iint (\frac{\partial \sigma_{xx}}{\partial x} + \frac{\partial \sigma_{xy}}{\partial y}) \quad dxdy = \iint -F_x \quad dxdy$$

$$\iint (\frac{\partial \sigma_{xy}}{\partial x} + \frac{\partial \sigma_{yy}}{\partial y}) \quad dxdy = \iint -F_y \quad dxdy \qquad (5.3)$$

Approximation made in this case is the thickness of the hopper in z-axis direction is extremely small compared to its other directions. A two-dimensional plane stress

condition is defined to be a state of stress in which normal stress σ_{zz}, shear stress σ_{xz} and σ_{yz} directly perpendicular to the $x-y$ plane are zero.

$$\sigma_{zz} = \sigma_{xz} = \sigma_{yz} = 0 \tag{5.4}$$

Using Green's Theorem, which gives the relationship between a line integral around a line and a double integral over an area, Equation 5.3 becomes:

$$
\begin{aligned}
\oint (\sigma_{xx} dy - \sigma_{xy} dx) &= \iint -F_x \quad dxdy \\
\oint (\sigma_{xy} dy - \sigma_{yy} dx) &= \iint -F_y \quad dxdy
\end{aligned}
\tag{5.5}
$$

Using the plane stress condition, the Hook's Law strain-stress compliance matrix for an orthotropic material is [95; 96; 97]

$$
\begin{bmatrix} \varepsilon_{xx} \\ \varepsilon_{yy} \\ \gamma_{xy} \end{bmatrix}
=
\begin{bmatrix}
\frac{1}{E_x} & -\frac{v_{yx}}{E_y} & 0 \\
-\frac{v_{xy}}{E_x} & \frac{1}{E_y} & 0 \\
0 & 0 & \frac{1}{2G_{xy}}
\end{bmatrix}
\begin{bmatrix} \sigma_{xx} \\ \sigma_{yy} \\ \sigma_{xy} \end{bmatrix}
\tag{5.6}
$$

$$
\begin{aligned}
\varepsilon_{xx} &= \frac{\partial u}{\partial x} \\
\varepsilon_{yy} &= \frac{\partial v}{\partial y} \\
\gamma_{xy} = \varepsilon_{xy} + \varepsilon_{yx} &= \frac{\partial u}{\partial y} + \frac{\partial v}{\partial x}
\end{aligned}
\tag{5.7}
$$

where ε_{xx}, ε_{yy} and ε_{xy} are strain in x direction, strain in y direction and shear strain, E_x and E_y are Young's Moduli in x and y direction, v_{xy} and v_{yx} are Poisson's ratio and G_{xy} is shear modulus. Equation 5.7 is the two-dimensional compatibility equations for strain. In orthotropic materials, there is no interaction between the normal stresses σ_{xx}, σ_{yy} and the shear strain σ_{xy}. The factor $1/2$ multiplying the shear modulus in the

compliance matrix results from the difference between shear strain and engineering shear strain, γ_{xy}, which is a total measure of shear strain in the x-y plane. In contrast, the shear strain ε_{xy} or ε_{yx} is the average of the shear strain on the x face along the y direction, and on the y face along the x direction [98; 99; 100].

The correlation between Shear Modulus, Young's Modulus and Poisson Ratio for orthotropic material[101] is:

$$2G_{xy} = \frac{E_x E_y}{E_x + E_y + 2E_x v_{xy}} \tag{5.8a}$$

$$\frac{v_{xy}}{E_x} = \frac{v_{yx}}{E_y} \tag{5.8b}$$

The Hook's law stiffness matrix for orthotropic materials, the inverse of the compliance matrix, is given as follows:

$$
\begin{bmatrix} \sigma_{xx} \\ \sigma_{yy} \\ \sigma_{xy} \end{bmatrix} =
\begin{bmatrix}
\frac{E_x}{1-v_{xy}v_{yx}} & \frac{v_{xy}E_y}{1-v_{xy}v_{yx}} & 0 \\
\frac{v_{xy}E_y}{1-v_{xy}v_{yx}} & \frac{E_x}{1-v_{xy}v_{yx}} & 0 \\
0 & 0 & 2G_{xy}
\end{bmatrix}
\begin{bmatrix} \varepsilon_{xx} \\ \varepsilon_{yy} \\ \gamma_{xy} \end{bmatrix} \tag{5.9}
$$

where

$$2G_{xy} = \frac{E_x E_y}{E_x + E_y + 2E_y v_{xy}}$$

5.4   Confined Compression Test

The confined uniaxial compression test is conducted to obtain Young's Moduli E_x and E_y required in simulation. This method is introduced by the author for this research.

The confined compression test procedure is very similar to the Unconfined Uniaxial Compression Test.

Powder is filled into a cylindrical confinement and the redundant powder at top is scraped off to give an even surface. The cylinder is then securely positioned under the Texture Analyser (Figure 5.3) which applies and measures the load onto the lid to compress the powder.

Figure 5.3: Confined Uniaxial Compression test.

The Texture Analyser applies a load at a speed of $0.5mm/s$ onto the lid with diameter of $50mm$ until the load researches $10kg$ to compress the powder in the cylinder wit length of $104mm$.

At each specific time, i, the Texture Analyser records the load exerted, F_i, and the displacement, u_i, from original position of the lid in the direction of load exerted.

Therefore stress, strain and density at each specific time are:

$$\rho_i = \frac{m}{A(L - u_{i-1})}$$
$$\sigma_{xx,i} = \frac{F_i}{A}$$
$$\varepsilon_{xx,i} = \frac{u_i - L}{L}$$

(5.10)

where A is the area of where load is exerted, L is the original height of the powder and m is the mass of the powder.

Density , ρ, is plotted against compression stress , σ_{xx}, to obtain a correlation between them, density is represented in a function of compression stress.

$$\rho = F(\sigma_{xx})$$

(5.11)

From compliance matrix Equation 5.6, we know:

$$\varepsilon_{xx} = \frac{1}{E_x}\sigma_{xx} - \frac{v_{yx}}{E_y}\sigma_{yy}$$

(5.12)

$$\varepsilon_{yy} = -\frac{v_{xy}}{E_x}\sigma_{xx} + \frac{1}{E_y}\sigma_{yy}$$

(5.13)

In the simultaneous equations, there are 3 known variables, ε_{xx}, σ_{xx} and ε_{yy}, which are 0 and also five unknown variables, E_x, E_y, v_{yx}, v_{xy}, and σ_{yy}. There are more unknown variables than equations.

Researches [102; 103] have methods to determine the Poisson's ratio and the results

show the Poisson's ratio has a typical value of 0.3 for powder:

$$
\begin{aligned}
\upsilon_{xy} &= -\frac{\varepsilon_{yy}}{\varepsilon_{xx}} \\
\upsilon_{yx} &= -\frac{\varepsilon_{xx}}{\varepsilon_{yy}}
\end{aligned}
\tag{5.14}
$$

K ratio of powder is defined as a ratio between transverse stress, σ_{yy}, and axial stress, σ_{xx}. The value of K can be measured and varies widely. The assumption of using K to linked the two stresses is that the calculation needs to update the value of K every iteration.

$$
\sigma_{yy} = K\sigma_{xx}
\tag{5.15}
$$

Now there are only two unknown variables, E_x and E_y, remain in Equation 5.12 and 5.13.

Therefore, the Young's moduli, E_y and E_y, have a strong coupling with stress σ_{xx} and σ_{yy}. This strong coupling might disrupt the irritative procedure. Therefore the Young's moduli will be represent with density ρ using correlation in Equation 5.11 in this research model.

5.5   Yield Locus and Failure Criterion

In previous Chapter 2.3, the author stated that the stress history is the only considered impact on cohesion. The underlying physics and the measurement will be detailed in this section. Hence how cohesion is associated with the flowability of any given powder.

The mathematical equations for Failure Criterion is introduced by the author and it's derived from stress analysis of Mohr's Circle. Possible incipient flow begins at the

opening of outlet in the hopper. The material at that particular moment has internal shear strength stored within the material, the shear strength is generated from stress history. In order to have occurrence of failure, the generic (current) external stress Mohr's circle needs to either touch the Yield Locus at the its tangent point or research the Yield Locus and follow the Yield Locus. This section is dedicated to the custom equations derived from the Mohr's circle by the the author for the element failure criterion.
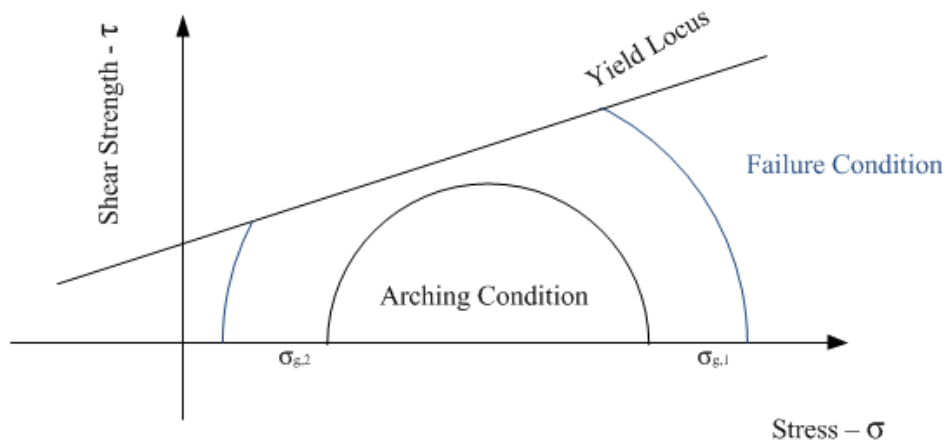
Figure 5.4: Mohr's Circle consisting of generic stresses at the opening of outlet, each half circle represents 1) the arching condition and 2) the failure condition of the powder.

Figure 5.5 shows an arbitrary stress condition, which is used to derive a mathematical expression required for the computer to differentiate between these two stress conditions. The parameters; Cohesion(c) and the gradient(m) of Yield Locus, $\tau = m\sigma + c$, are obtained from the Brookfield PowderFlow Tester detailed in Chapter. 6.1.1.

Figure 5.5: Mohr's Circle consisted of arbitrary generic stresses at the opening of outlet and a Yield Locus generated with stress history.

The Arbitrary Line is perpendicular to the Yield Locus, because initial failure happens when the Mohr's circle touches the Yield Locus. In failure condition, the Yield Locus is tangent to the Mohr's circle, R_F is the shortest distance between mean stress, $\sigma_{g,m}$, and the Point (τ, σ). R_g is the longest distance within the generic Mohr's circle. For failure to occur:

$$R_g = R_F \tag{5.16}$$

Stress $\sigma_{g,h}$ and $\sigma_{g,v}$ are the generic horizontal and vertical stresses, the local mean stress, $\sigma_{g,m}$ is:

$$\sigma_{g,m} = \frac{\sigma_{g,v} + \sigma_{g,h}}{2} \tag{5.17}$$

$$R_g = \sqrt{(\frac{\sigma_{g,v} - \sigma_{g,h}}{2})^2 + (\sigma_{g,s})^2} \tag{5.18}$$

78

Yield Locus and the Arbitrary Line are perpendicular to each other:

$$\tau = m\sigma + c \qquad \text{Yield Locus(Stress History)} \qquad (5.19)$$

$$\tau = n\sigma + k \qquad \text{Arbitrary Line (Generic Stress)} \qquad (5.20)$$

$$m \cdot n = -1$$

$$n = -\frac{1}{m} \qquad\qquad\qquad\qquad\qquad\qquad\qquad\qquad (5.21)$$

where m and n are gradient to each line separately, c is cohesion and k is an arbitrary constant.
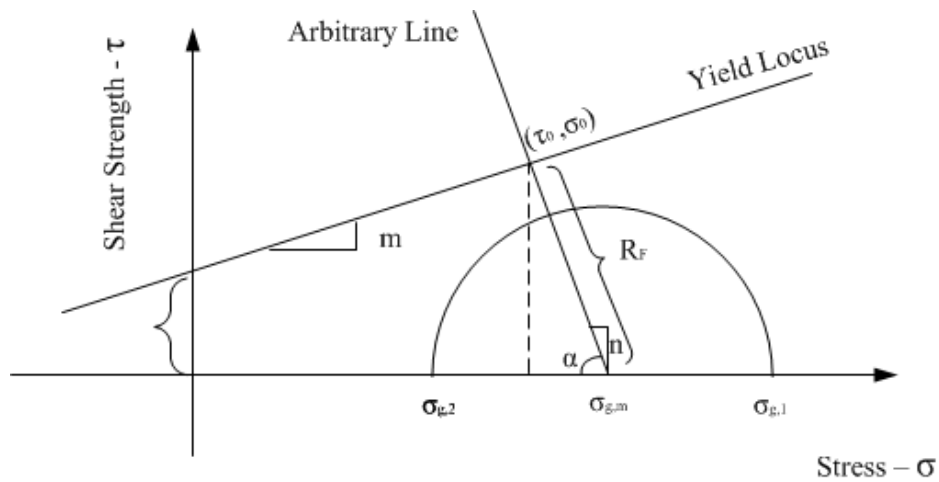
Figure 5.6: Mohr's Circle and Yield Locus intercept.

Arbitrary Line also crosses the Yield Locus at $(\sigma_{g,m}, 0)$ and (τ_0, σ_0) in Figure 5.6, Equation 5.20 becomes:

$$k = -n \cdot \sigma_{g,m}$$

$$= -(-\frac{1}{m}) \cdot \sigma_{g,m}$$

$$= \frac{\sigma_{g,m}}{m} \tag{5.22}$$

Both lines cross at (τ_0, σ_0),

$$
\begin{cases}
\tau_0 = m\sigma_0 + c \\
\tau_0 = (-\frac{1}{m})\sigma_0 + \frac{1}{m}\sigma_{g,m}
\end{cases}
$$

Obtaining coordinates for τ_0 and σ_0 by solving the simultaneous equations above:

$$\sigma_0 = \frac{\sigma_{g,m} - mc}{m^2 + 1} \tag{5.23}$$

$$\tau_0 = m\frac{\sigma_{g,m} - mc}{m^2 + 1} + c \tag{5.24}$$

$$\tag{5.25}$$

R_F is the distance between centre point of the Mohr's circle $(\sigma_{g,m}, 0)$ and Point (σ_0, τ_0).

$$R_F = \sqrt{(\frac{\sigma_{g,m} - mc}{m^2 + 1} - \sigma_{g,m})^2 + (m\frac{\sigma_{g,m} - mc}{m^2 + 1} + c)^2} \tag{5.26}$$

Now R_g, Equation 5.18, and R_F 5.26 can be compared to exam whether the powder would fail under the current generic stress condition. So the failure criterion will be:

$$F = R_g - R_F \tag{5.27}$$

The powder material will fail if F reaches zero.

5.6 Chapter Summary

The introduced model aims to predict incipient arching or flow conditions in a hopper using stress history. This model is developed with the understanding of the overlapped areas in the powder mechanics and numerical simulation which these two principles does not share prior to this research.

The advantage of combining the aspects of empirical testing and numerical modelling is to have a better representation of powder behaviours. The model does not only consider the effect of generic stress but also the stress history. The author would use Confined Compression Test to determine powder characteristics for the effect of generic stress on the shear strength of the powder and Brookfield Powderflow Tester for the effect of stress history on failure condition of the powder.

In order to capture the stress history development, the model starts when the filling starts in a closed hopper. When the filling is complete, the outlet will be open to simulate generic stress. The model will then trigger the failure criteria for the powder to determine whether the element of the powder will fail or remain intact. The failed elements will be removed and the removal will be fed back to the stress calculation with an open outlet, in order to simulate the failure of each cell again until there is no failure occurs.

The model addresses the effect of stress history on cohesive powder in arching/failure condition in numerical calculation.

Chapter 6

IMPLEMENTATION

Every successful simulation model consists of three different procedures of implementation: a) Initial Particle Property Determination, b) Numerical Simulation with specific parameters and boundary conditions, and c) Validation against experimental data. This chapter describes the first two in detail.

6.1 Empirical Testing for Initial Particle Property Determination

As for any another simulation, input parameters need to be determined beforehand. The model proposed in this Thesis utilises the stress-density-strength relationship to approximate a powder phenomenon, which is that the material is not only affected by its current stress state, but also affected by its historical stress state.

6.1.1 Brookfield Powder Flow Tester

With reference to Figure 6.1the Brookfield Powder Flow Tester which a more advanced tester than the other analytical tester described in Chapter 2.4.2, the Yield Locus obtained will be used in predicting failure for each element. The results from the Brookfield will be used in the Yield Locus Determination section in the modelling Flowchart (see Figure 5.1).

In Chapter 2.4.2, the author briefly introduced shear failure and powder's critical state, Brookfield Powder Flow tester utilises these characteristics to measure flowability of powder material.

The Brookfield Powder Flow tester was developed in the Wolfson Centre at University of Greenwich. It measures the characteristic properties of any fine powders, which include the Flow Function, the effective angle of internal friction, the cohesion and the gradient of Yield Loci of any given powder with respect to consolidation stress σ_1. The results from the tests focused on obtaining the gradient of loci m and the cohesion from the test to put into Equation 5.26. Because they are the two contributors from the stress history to the failure criteria.

Figure 6.1: Brookfield Powder Flow tester

Figure 6.2: Cross-section of part of the powder in the Bookfield Powder Flow tester during operation

The mesh at the bottom of the trough, shown in Figure 6.1 and 6.2, prevents slippage between the powder and the bottom surface. A trough filling tool is designed to attain a uniform surface of the powder. Powder is filled in the trough, the trough is affixed onto the base mechanism. The base mechanism can rotate with a constant velocity and measures the torque required to turn it. The internal friction lid is mounted onto the axial shaft which is connected to the loading mechanism.

The powder needs to be consolidated until reaching the steady-state or "critical state" condition, at which it has researched a constant volume under shear. Then it is sheared to failure under either the same critical stress or a lower one. In the following paragraph, the subscript $_{ss}$ is given to parameters at steady-state condition, and $_{sf}$ is given to parameters where the powder is sheared to failure.

The powder is consolidated with a normal stress, σ_1, exerted on the lid. The trough

starts to rotate with a constant velocity and this rotation generates a horizontal shear stress, τ_{ss}. Shear stress increases with time until it remains constant even though the powder continues shearing. At this point the strength and the density of powder do not increase any further. Therefore powder is now shearing under a constant normal stress, σ_1 and a constant shear stress, τ_{ss}, with a constant density, ρ_{ss}, at a constant velocity, this condition of shearing is known as steady-state flow and the powder is defined as critically consolidated.

Steady-state flow is followed by a pause of rotation and reversal to relax τ then the trough restarts to rotate again to shear the powder to failure. The normal stress resumed during shear-to-failure, σ_{sf}. The powder will start to rearrange and dilate: ρ_{sf}, will be less than ρ_{ss}. As the trough rotates at a constant velocity, the shear stress increases until the incipient flow occurs, at which point the failure of the sheared powder is achieved. The shear stress at this point is recorded as τ_{sf}.
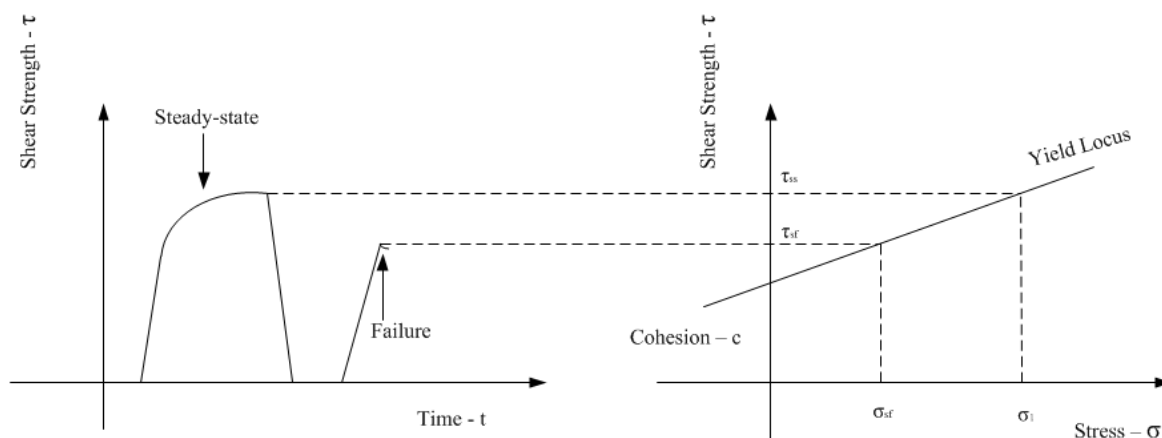
Figure 6.3: Plot of shear stress with respective of time (left) and of normal stress (right)

Each shear stress for a simple value, τ_{sf} has its corresponding normal stress value, σ_{sf}, these are used to obtain the Yield Locus, $\tau = m\sigma + c$.

The whole procedure is repeated using several different values of σ_1, to obtain a family of yield loci for different powder stress history.

6.1.2 Uniaxial Compression Test

With reference to the modelling flow chart Figure 5.1, the Uniaxial Compression test has been employed to obtain the parameters to determine the powder strength with respect to stress. Figure 6.4 shows the apparatuses for the uniaxial compression test The cylindrical column wall is greased with a plastic sheet and the friction between the wall and the powder is minimised because the plastic sheet slides along the wall with the powder during compression. The powder fills in the cylindrical column and the top is scraped off to give an even surface, the specimen is then placed under the Texture Analyser, which applies and measures the load onto the lid during compaction of the powder.

Figure 6.4: Texture Analyser

The author intended to deduce an institutive relationship between the material properties and the stress exerted on it. There are two relationships deduced from the test results, one between stress and density, the other one between density and tangent modulus.

The tangent modulus here is the slope of a stress-strain curve at any stress point. For simplicity of a complicated numerical model, the tangent modulus is imposed as an elastic modulus in the simulation, even though tangent modulus is the slope of the curve beyond the yield stress point and elastic modulus is the slope before the yield stress point. The numerical purpose and reasoning are detailed in Chapter 5.2

The Texture analyser recorded the position (x_i) and the applied load (m_i) of the piston at each specific time. The height (L_0) and the diameter (D) of the cylinder are given, the weight (M) of powder specimen is measured prior to the test. The following parameters can be calculated from the data obtained.

Height of cylinder	L_0
Diameter of cylinder	D
Weight of powder specimen	M
Cross-section area of cylinder	A
Distance of piston between current and original position	u_i
Displacement between each given time	$\delta L_i = u_i - u_{i-1}$
Load applied by Texture analyser at given time	m_i
Force exerted on specimen at given time	$F_i = (m_i + \frac{1}{2}M)g$
Height of specimen at given time	$L_i = L_0 - u_i$
Strain of specimen at given time	$\epsilon_i = \frac{\delta L_i}{L_i}$
Density of material at given time	$\rho_i = \frac{M}{A \cdot L_i}$
Stress at given time	$\sigma_i = \frac{F_i}{A}$
Specific volume at given time	$\upsilon_i = \frac{1}{\rho_i}$
Tangent modulus at given time	$E_i = \frac{\sigma_i}{\epsilon_i}$

Data of density ρ_i and stress σ_i at any specific time can be plotted on the same graph

and output as an empirical correlation between the data.

6.2   Numerical Implementation for Empirical Relationships

Numerical simulation mimics a situation where fine powder, flour in this case study, was filled in a wedge hopper with a closed outlet, then released from the hopper by opening the outlet. The simulation predicts whether or not the powder arches at the outlet when it is opened. The highlighted codes will be detailed in the following sections, for full coding, please see Appendix A.

The following sections detail all the numerical models attempted. All hoppers in the simulation are with a hopper half angle of 45° due to the limitation of PHYSICA in boundary condition.

6.2.1   Code development in PHYSICA

PHYSICA is a numerical solver package to calculate a system of mathematical equations for engineering problems, developed at the University of Greenwich. It is a powerful solver which allows users have access to the source codes, its accessibility is much welcomed in research because it provides tailoring for each different complex scenario.

PHYSICA does not have a Graphical User Interface (GUI), therefore the geometry file and the "Inform" test input file contain the information and command inputs for the

Figure 6.5: PHYSICA Processing Flowchart

executable. The executable, physica3g.exe, is developed in Fortran. It reads in the geometry and the Inform files to numerically calculate the system and to generate data files. Data files generated are in binary form, then they are fed to a post-processor TecPlot to produce visual results. This is a typical user procedure for PHYSICA, as shown in Figure 6.5

The executable, physica3g.exe, contains a casecode.f in addition to its source codes. Advanced users of PHYSICA use casecode.f to add extra subroutines, linked with the standard source codes of physica3g.exe. However, adding extra subroutines in casecode.f is not enough for this study, it needs even more development in the source codes as well. The source codes are written in Fortran, structured with many different modules by utilising structure-oriented programming. The development for this study focuses on casecode.f and the structure module, which is the module for Solid Mechanics. There are three main areas developed to accommodate this special scenario: changing material properties during filling of the hopper, introducing wall friction during the filling of the hopper and removing failed elements at the opening of the hopper.

The overall simulation process consists of two stages: 1) the filling stage which includes changing material properties and introducing wall friction. 2) the opening stage which includes the opening outlet and the removal of failure elements.

6.2.1.1 Changing Material Properties during Filling

With reference to the modelling flowchart (Figure 5.1), material changes contribute in the section of Simulation during Filling Process. The filling of material is coded as these elements of each layer that switch from having the material properties of air to powder; the switch progresses uniformly upward as time steps advance. This is triggered by the command `USER_ROUTINE` in Inform file with subroutines named "layered" for density and "powderE" for Young's modulus, the modulus used is plastic modules (practically) from the Cam-Clay model dependent of stress. However, they

are identified (numerically) under elastic material properties section in casecode.f (see a copy of the complete code in Appendix A.1), the reasoning can be found in a previous Chapter 5.3. The command `USER_ROUTINE` in the Inform file allows physica3g.exe to bypass the built-in codes in corresponding sections which are set up for standard Solid Mechanics calculations.

New variables, which are needed to predict arching failure, are also introduced into the module under material property.

In the Inform file under `MATERIAL_PROPERTY_MODULE`, both the density and the Young's Modulus are set to bypass the original source codes with subroutine "layered" and "powderE" separately with initial values.

In the casecode.f, the author coded if PHYSICA reads "layered" under the original subroutine `case_mat_prop` (casecode for material properties) then PHYSICA would perform the following:

1. Read in arrays and their locations from source codes

2. Introduce the angle of friction m

3. Allocate memory space for new variables, nx for number of layers in x-direction, $iStr$ for stresses, $iCohe$ for the cohesion, $Einit$ for the initial Young's modulus, $iTheta$ for the angle between principle stress and generic stress, $iTantheta$ for the tangent of $iTheta$. $iRyl$, iRg and $iFail$ are variables introduced for element failure criterion.

4. Stress tensors are stored in array, $[\sigma_{1xx}, \sigma_{1yy}, \sigma_{1xy}, \sigma_{2xx}, \sigma_{2yy}, \sigma_{2xy} \dots]$ The code creates individual stress arrays corresponding to each direction. Array Str_{xx}, Str_{yy} and Str_{xy} in respective of normal stress in x-direction, normal stress in y-direction and shear stress on xy-plane.

5. Data initialisation at the start of the simulation

6. If the layer position is equal to 1 at the first time step. then the density is equal to 1.2 which is the density of air.

7. If the layer position is equal to the time step number then the density would change to be equal to "dens".

in the casecode.f, the author coded if PHYSICA reads "powderE" under the original subroutine `case_mat_prop` (casecode for material properties) then PHYSICA would perform the following:

1. if the position of the layer is larger then the current time step number, then the Young's modulus will be the one of air, which is calculated with $C_{solid} = \sqrt{\frac{E}{\rho}}$ [104]

2. else if the position of the layer is less and equal to the current time step number, then the Young's modulus will be under compaction, performed as $E = f(\rho)$ to account for the "hardening" of the powder with increasing compaction, as per the Cam-Clay model.

The author also coded the Failure Criterion at the filling stage to prepare for the opening stage.

1. Calculating the cohesion c, R_{yl} and R_g

2. Establish failure criterion which represents Equation 5.26
$R_F = \sqrt{(\frac{\sigma_{g,m}-mc}{m^2+1} - \sigma_{g,m})^2 + (m\frac{\sigma_{g,m}-mc}{m^2+1} + c)^2}$

3. Determine if the failure criterion is satisfied for each element. The variable Failure will have positive value when criterion is satisfied.

4. The cohesion is the identifier for stress history in the opening stage, so it is calculated and stored here in order to be called for future calculation.

6.2.1.2 Wall Friction

There was no built-in wall friction model in PHYISCA, the "wall friction forces" had to be "borrow" the wall the subroutine `pressure_load`, so that the author could control the effective angle of wall friction in the Inform file.

$$\tan \varphi_w = \nu_w \tag{6.1}$$

where φ_w is the effective angle of wall friction, For example, for φ_w of 10°. ν_w is 0.176

The friction coefficient is control in the Inform file under Boundary Condition as.

BOUNDARY_CONDITIONS

F_PATCH   4   PRESSURE   VALUE   0.176

The value in the Inform file is read in to the subroutine `get_pressure_load` as `value`

```
call get_pressure_load ( Ia, Ra, ipat, ipres, value )
```

However, the subroutine `pressure_load` is over a face are and the structure calculation is conducted at points. A new subroutine `tangnor` is introduced to a) storing displacement tangential component to accommodate the transfer from face calculation to point calculation, and b) storing normal force to calculate the frictional tangential force.

$$F = \nu_w N \tag{6.2}$$

where F is the frictional force and and ν is the coefficient of friction, N is the normal force.

```
fricmax = Max( -sn6, 0. ) * value
```

Then the frictional force is transferred to stress and applied as an opposite frictional pressure to its displacement.

6.2.1.3 Storing Stress History

After closely reviewing the Cam-Clay model, the author appreciated its ability to store and recover the the characteristics of powder specifically the varying modulus with the stress history. However the model was developed using isotropic compaction, which is not the case for powder.

The Cam-Clay model is the only model across the field of powder mechanics which has the accountability for stress history. The author decided to extract the concept of restoring stress history from the Cam-Clay model to be part of the implementation of the model in this research project.

The order of calculation in Structure Module PHYSICA is listed below:

1. Input geometry, boundary conditions and material properties

2. Calculate the stiffness matrix and elasticity matrix

3. Calculate the displacement

4. Obtain strain

5. Obtain stress

Due to the nature of PHYSICA, the simulation has had to be paused to make changes in the Inform file and the casecode.f to storage the stress history from the filling state to be used in the opening stage. This is done under `DATABASE_MODULE`, this module in PHYSICA allows users to restart a previous simulation under either the same or changed source code.

```
DATABASE_MODULE
    INPUT_DATABASE    hopperStr
#                     name = filename without extension of
    PRINT_READ_VARIABLES   ON

    OUTPUT_DATABASE    hopper_open
#                     nam1 − change database filename to prevent
    overwriting
END
```

The old stresses and variables are stored and compared with the new stresses and variables in the post-structure section.

6.2.1.4   Initial Flow at Opening outlet

During the filling stage the powder is simulated under a complex code to establish the failure for each element. At the opening stage, the restriction at the bottom is removed to represent the opening of the valve.

Geometry file in PHYSICA is represented in a numerical way. Each point in the geometry file is represented by corresponding location co-ordinates and corresponding patch numbers. The patch numbers are the boundary condition identifiers used in the Inform file to command PHYSICA what to do when the identifiers are read.

Example of how points are created in the geometry file:

```
0.00000E+00   0.00000E+00   0.00000E+00   1   3   5
6.00000E−03   0.00000E+00   0.00000E+00   0   3   5
1.20000E−02   0.00000E+00   0.00000E+00   0   3   5
        .
        .
        .
        .
        .
```

The author then has employed and tailored an external application with Fortran to make changes on the patch file, in order to identify number "1" is used to represent all the points at the outlet in every direction.

```
C       Make changes to the .geo data in memory:


        do  i = 1, np

          if  ( ixp(i) .EQ. 1 )  then
            iyp(i) = 1
          endif

        enddo
```

The geometry file becomes:

```
0.00000E+00   0.00000E+00   0.00000E+00   1   1   5
6.00000E−03   0.00000E+00   0.00000E+00   0   3   5
1.20000E−02   0.00000E+00   0.00000E+00   0   3   5
        .
        .
        .
        .
        .


   BOUNDARY_CONDITIONS

!   P_PATCH   1   DISPLACEMENT   VALUE   0.0
    P_PATCH   3   DISPLACEMENT   VALUE   0.0
        .
        .
        .
        .
        .
```

The simulation is then resumed with a changed Inform file, a changed casecode.f.

6.2.1.5 Failure Criteria

This is conducted in the `case_output_results` in the new casecode.f. So the stress history and the current stress can be employed in the Failure Criteria.

The most crucial component to represent the stress history in the Equation 5.26 is the cohesion. In the new casecode.f, instead of calculating it with the generic stress, it is called from the previous database after the paused-restart procedure.

```
call save_restart_variable ( 'Cohe',  ierr ,  failed )
```

So the $R_y l$, R_g and R_F are then re-calculated, the Failure Criterion is overwritten and properly compares the stress history with the generic stress. So the author can examine the failed elements to be removed in the next step.

6.2.1.6 Removal of Elements

After the initial opening of the outlet, each element has a Failure value. If the failure value is larger or equal to zero, the element is considered to meet the failure criterion. The code then needs to change to remove the failed element by changing the material properties to air.

1. examine each element with failure criterion

2. for satisfied element, change the material properties to air

3. for unsatisfied element, the material properties stay the same.

6.2.2 Results monitoring

During the simulation, the author made certain results are converged properly by monitoring each time step. Therefore the Post-process files (Tecplot files) will have more accurate results in terms of computational iterations.

Figure 6.6: Screen-shot of simulation monitoring

The residual error is set to be less than 10^{-7} to ensure convergence.

6.3 Chapter Summary

This chapter outlines the developed numerical model that is implemented in the study for simulation of cohesive powder in a hopper, along with the conducted experiments to obtain the parameters required for the numerical model.

The model combines the experimental aspects for powder characterisation and the numerical modelling aspects to deliver a model, which accounts for the impact of stress history in the powder for failure criteria.

The advantage of this model lies in its ability to precisely predict the failure condition

by using the Jenike's failure criteria. The traditional Jenike's model has been limited to only three hopper geometries: cynical hopper; square hopper with a circular outlet and wedge hopper with a rectangular outlet.

The study cases with the developed model, which is detailed in the next chapter, benchmark against the traditional hopper geometries to ensure the practical functionality of the model and prepare it for further development in the future.

Chapter 7

RESULTS AND DISCUSSION

The results are presented here for a series of case studies, which are able to reflect the practical application of the model to industrial processes.

Prior to the numerical simulation, empirical experiments have been conducted to obtain input parameters.

7.1 Empirical Results for Powder Property Determination

As mentioned in previous chapter, the author detailed the reasoning to employ the Texture Powder Analyser to obtain the relationships among the stress, the density and the effective Young's modulus "E".

Time	Distance	Load		x-dir		strain_xx		sigma_xx		rho
(s)	u_n(mm)	(g)		(u_n)-(u_n-1)	L-(u_n-1)			F_n (NE-3)	(Pa)	(kg/m3)
0	0	0								
0.1	0.04	29		0.04	104	0.000385		284.49	144.9261	390.5423
0.2	0.09	28		0.05	103.96	0.000481		274.68	139.9287	390.6926
0.3	0.14	29		0.05	103.91	0.000481		284.49	144.9261	390.8806
0.4	0.19	30		0.05	103.86	0.000481		294.3	149.9236	391.0688
0.5	0.24	30		0.05	103.81	0.000482		294.3	149.9236	391.2571
0.6	0.29	31		0.05	103.76	0.000482		304.11	154.921	391.4457
0.7	0.34	34		0.05	103.71	0.000482		333.54	169.9134	391.6344
0.8	0.39	33		0.05	103.66	0.000482		323.73	164.9159	391.8233
0.9	0.44	35		0.05	103.61	0.000483		343.35	174.9109	392.0124
1	0.49	36		0.05	103.56	0.000483		353.16	179.9083	392.2017
1.1	0.54	37		0.05	103.51	0.000483		362.97	184.9058	392.3911
1.2	0.59	37		0.05	103.46	0.000483		362.97	184.9058	392.5807
1.3	0.64	39		0.05	103.41	0.000484		382.59	194.9007	392.7706
1.4	0.69	40		0.05	103.36	0.000484		392.4	199.8981	392.9606
1.5	0.74	41		0.05	103.31	0.000484		402.21	204.8956	393.1507
1.6	0.79	41		0.05	103.26	0.000484		402.21	204.8956	393.3411
1.7	0.84	40		0.05	103.21	0.000484		392.4	199.8981	393.5317
1.8	0.9	41		0.06	103.16	0.000582		402.21	204.8956	393.7224
1.9	0.94	42		0.04	103.1	0.000388		412.02	209.893	393.9515

Figure 7.1: Sample of raw data from Texture Powder Analyser
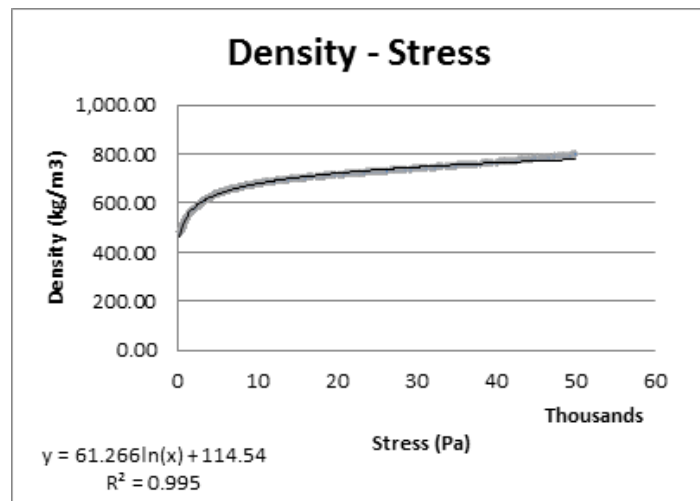
Figure 7.2: Constitutive relationship between the density and applied stress

The Constitutive relationship, shown in Figure 7.2 between the density and applied

stress, is

$$\rho_i = 61.266 \ln \sigma_i + 144.54 \tag{7.1}$$

Data of Tangent Modulus E_i is also plotted against density ρ_i is collected as in Figure 7.3
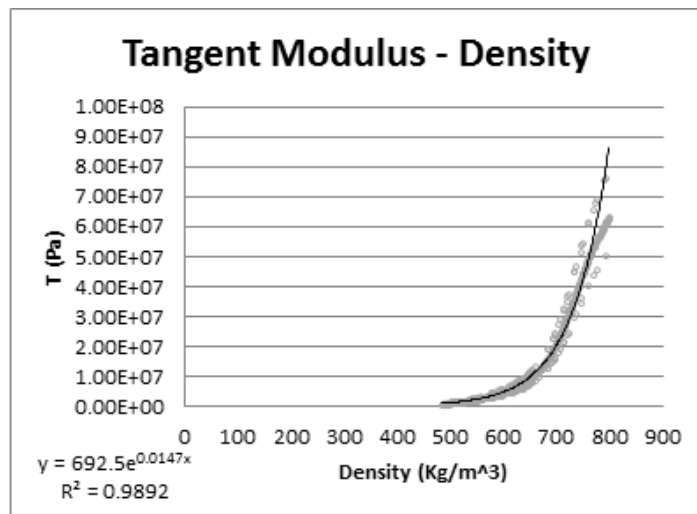
Figure 7.3: Constitutive relationship between the Tangent Modulus and density

$$E_i = 692.5 e^{0.0147 \rho_i} \tag{7.2}$$

These two correlations are employed in the numerical simulation of a wedge hopper.

7.2 Empirical Results for Yield Locus Determination

Also mentioned in previous chapter, the proposed empirical experiment for obtaining parameters of yield loci is by using the Brookfield Powder Flow Tester.

flour		Batch:		1	Sample:
Stress		Normal Stress	Shear Stress	Density	
Setpoint		sigma 1	sigma c		
(kPa)		(kPa)	(kPa)	(kg/m³)	
0.289000004		0.280000001	0.286000013	562.2000122	
0.096		0.125	0.212999999	561.4000244	
0.289000004		0.305999994	0.252000004	562.5999755	
0.193000003		0.211999997	0.257999986	563.2000122	
0.289000004		0.305999994	0.25	564.2000122	
0.14		0.158999994	0.224000006	563.0999755	
0.289000004		0.305999994	0.252999991	565.2000122	

Figure 7.4: Sample of raw data collection

Major Principal Consolidating Stress	Major Principal Consolidating Stress	Unconfined Failure Strength	Gradient	Angle	Cohesion	Density	Effective Angle of Internal Friction
(kPa)	(Pa)	(kPa)		(°)	(kPa)	(kg/m³)	(°)
0.061	61					518.6	%
0.525	525	0.483	0.48	25.5	0.152	564	69.7	8.754339
1.046	1046	0.735	0.59	30.4	0.21	615	55.3	18.58851
2.162	2162	1.344	0.58	30.3	0.385	653.9	51.1	26.08947
4.087	4087	2.33	0.6	31.1	0.658	703.3	49.4	35.61512
7.553	7553	4.249	0.49	26.1	1.324	736.2	45.2	41.95912

Figure 7.5: Clean data

The value for m with respective of σ_1 is:

Figure 7.6: The gradient of the loci with respective of σ_1 from the Brookfield Powder Flow Tester

The value of m in the Failure Equation 5.26 is evaluated to be 0.6 for the powder specimen.
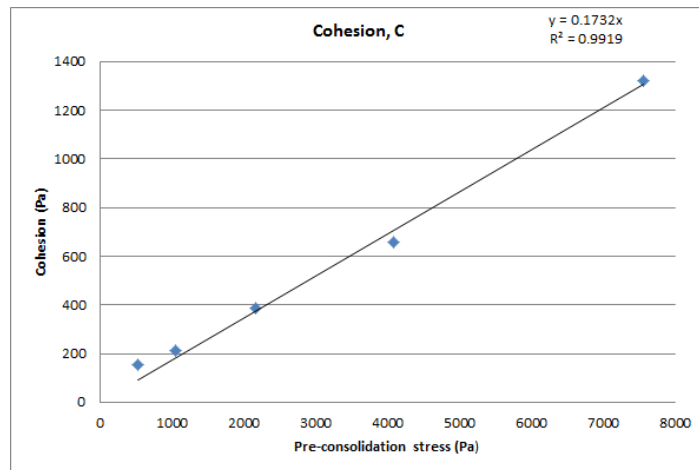
Figure 7.7: The cohesion with respective of σ_1 from the Brookfield Powder Flow Tester

$$c_i = 0.1732\sigma_{1,i} \tag{7.3}$$

105

7.3 Case Study 1

The first case study that powder is being poured into a hopper with the closed outlet, then the hopper outlet is opened to examine if there would be arching formed across the outlet. The simulation is a slice of a wedge hopper with dimension of 1650 mm in total height; 1410 mm in the straight section and 240 mm in converging section, 550 mm in width and outlet of 80 mm. The geometry is chosen according to the experiment conducted in the thesis of Dr Rob Berry [105]. The wall friction for this case is 10°.

The continuous change of properties, density and Young's Modulus, are formulated in case code. The properties are also switched from those of air to those of powder during the filling process. The switch is triggered by each time step in accordance with each element's location. All elements in the domain are initialised to have a density of $1.2kg/m^3$ and Young's Modulus of 1.40×10^5. The density of the powder is also changing when it is being compacted during the filling stage.

The author is aware that there is not a proper Young's Modulus for air, as air is a fluid. However, it is treated as if the air is a solid in the simulation. The Young's Modulus of air can be found from the speed of sound. According to Kinsler [104], speed of sound of any solid in one-dimension is:

$$C_{solid} = \sqrt{\frac{E}{\rho}} \tag{7.4}$$

Therefore the initial Young's modulus of air is estimated as 1.40×10^5 with the speed of $340m/s$ and density of $1.2kg/m^3$

Powder in bulk is compressible if subjected to external forces. The relationship for this case study is classified with Equation 7.1 and 7.2.

The continue change is detailed in Chapter 6.1.2. Figures **??** demonstrate property changes during filling stage of the hopper with time step increment of 1 second. The powder's strength increases when the density of the powder increases.

The chosen time step of 1 second is not relevant to the flow rate of the powder during filling. It is merely a counter to accommodate the subroutines to work properly with the layer as the hopper is filled. All results shown in the figures across this chapter are outputs of every 50 time steps.

Figure 7.8 shows the densities and Young's Moduli of powder during the filling stage. Only half of the hopper is simulated by symmetry to save computational resources. Figures on the left-hand side show the changes in density. Blue contour represents the density of air, the contour for powder changes in accordance with higher density as time steps advance. The density of air is 1.2 kg/m^3 and the initial density for powder is 483 kg/m^3 (which is obtained from experiment). The maximum density of powder reaches 650 kg/m^3 during compaction. Figures on the right-hand side show changes in Young's Moduli. The Young's Modulus of air is $1.40 \times 10^5 Pa$ and the initial value of powder is $8 \times 10^5 Pa$ (which is also obtained from experiment). The maximum Young's Modulus of powder reaches $1.5 \times 10^7 Pa$ during compaction.
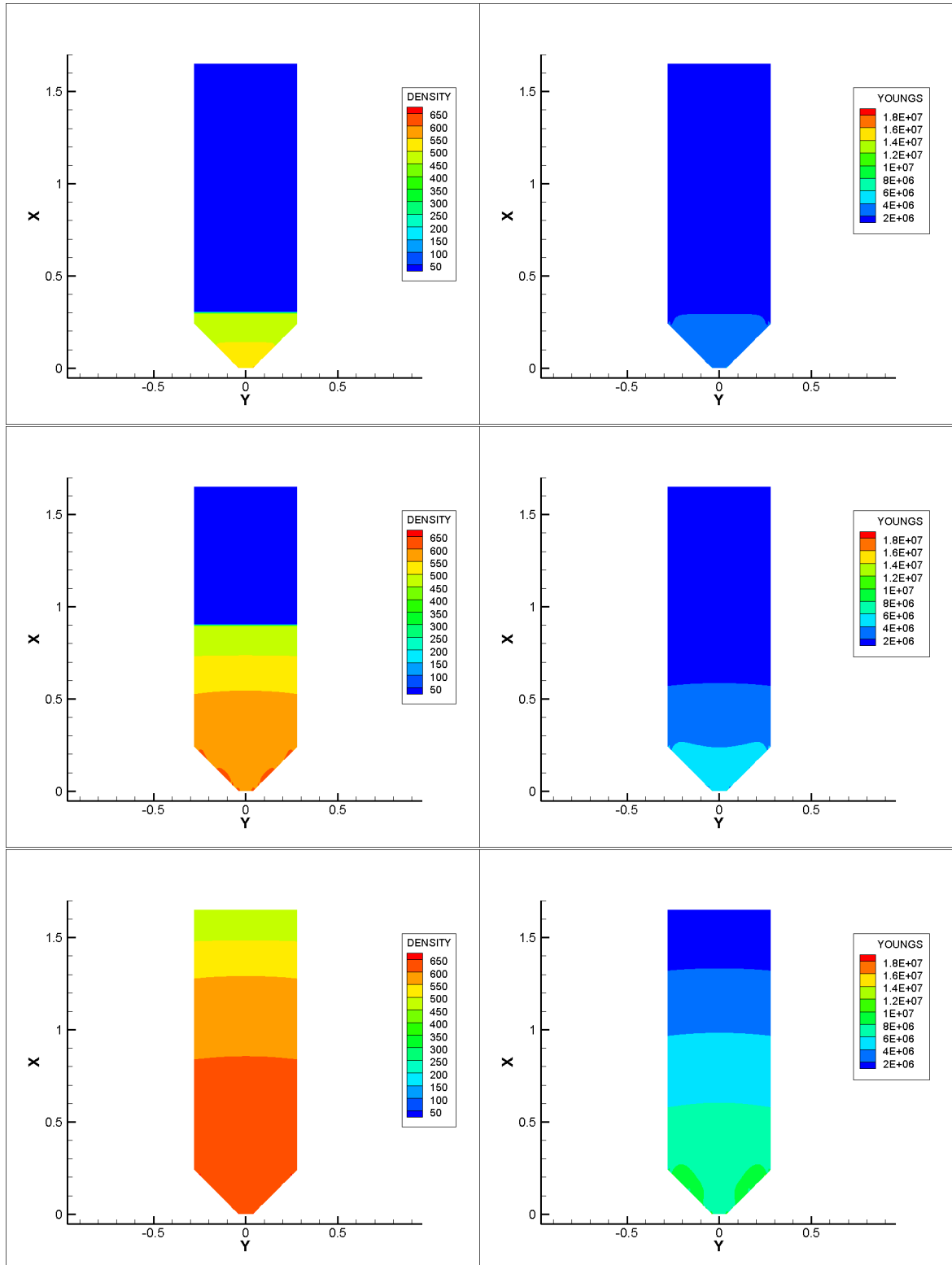
Figure 7.8: Density (left) and Young's Moduli (right) during filling stage with different time steps.

7.3.1 Stress Profile

The normal stress to the wall in a filled hopper is well documented in the literature [106; 107; 108].

Referring to the stress profile (Figure 2.6) in Chapter 2.3, the normal pressure to wall increases as the depth from the top of the hopper, z, increases. The theoretical method, Janssen's slice method provides a stress profile for a cohesionless granular material in a straight cylindrical vessel.
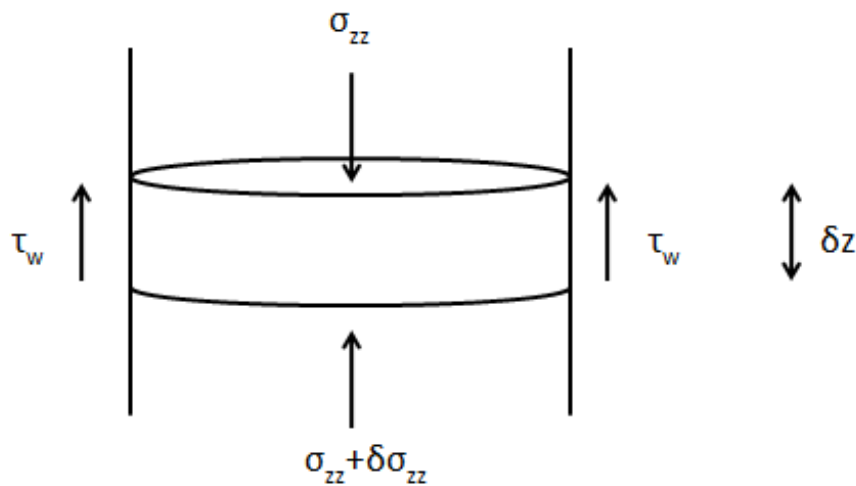
Figure 7.9: Stresses acting on a differential slice of cylindrical element.

Figure 7.9 illustrates a slice in a cylindrical column and all the stress acting on it. σ_{zz} is the vertical stress, τ_w is the wall frictional shear stress. For every increment in depth, there is a linear incremental increase in stress $\delta\sigma_{zz}$. This is a simply hydrostatic pressure. However, with the presence of wall friction, the profile becomes exponential as the wall stress also increases as the depth increases (see Appendix B.1 for Janssen's equations).

Even though the pressure profile provided by Jassen is for cohesionless materials in

a cylindrical section, it still serve the purpose to indicate a general pressure profile across any straight sections of any hopper. Therefore Figure 2.6 represents a general wall stress profile for any hopper.

Extracting raw data near the wall from the simulation by using post-processor TecPlot, the author can analyse the data. Figure 7.10 shows the extracted raw data.

	A	B	C	D	E	F	G	H	I	J	K	L	M	N	O	P	Q
1	X	Y	Z	gFpat	gVpat	DISP_U	DISP_V	DISP_W	STRESS_XX	Perp to Wall	STRESS_YY	Norm to Wall	STRESS_Z	STRESS_X	STRESS_Y	STRESS_X	STRAIN_X
2	1.649727	0.267219	0	6	2	-0.00088	-1.28E-06	3.09E-19	-15.22486371	15.22486371	79.04394103	-79.04394103	19.14572	1.864893	-1.08E-12	-7.63E-12	-5.22E-05
3	1.637214	0.267244	0	6	2	-0.00088	-9.87E-07	-1.85E-19	-63.86295371	63.86295371	43.66984334	-43.66984334	-6.05793	6.29949	-2.91E-12	1.37E-11	-8.78E-05
4	1.624702	0.267268	0	6	2	-0.00088	-8.44E-07	-1.14E-18	-130.0309297	130.0309297	3.57649722	-3.57649722	-37.9363	11.30884	-1.79E-12	-9.05E-12	-0.00014
5	1.61219	0.267293	0	6	2	-0.00088	-7.88E-07	-2.07E-18	-197.7492175	197.7492175	-32.25273138	32.25273138	-69.0006	16.71375	-8.06E-13	-3.12E-11	-0.0002
6	1.599677	0.267317	0	6	2	-0.00087	-7.62E-07	-2.96E-18	-264.347576	264.347576	-64.38262031	64.38262031	-98.6191	22.94408	-4.13E-14	-5.16E-12	-0.00025
7	1.587165	0.267341	0	6	2	-0.00087	-7.39E-07	-3.80E-18	-328.279756	328.279756	-93.79366716	93.79366716	-126.622	30.02449	1.31E-12	3.65E-13	-0.00031
8	1.574653	0.267366	0	6	2	-0.00087	-7.17E-07	-4.60E-18	-389.4834394	389.4834394	-121.5489051	121.5489051	-153.31	37.38471	7.26E-13	-1.27E-11	-0.00036
9	1.562141	0.26739	0	6	2	-0.00086	-6.94E-07	-5.36E-18	-448.2135261	448.2135261	-148.0840136	148.0840136	-178.889	44.69225	1.77E-12	-7.25E-12	-0.00041
10	1.549628	0.267414	0	6	2	-0.00086	-6.70E-07	-6.10E-18	-504.6277995	504.6277995	-173.5358369	173.5358369	-203.449	51.70365	1.01E-12	1.16E-11	-0.00046
11	1.537116	0.267439	0	6	2	-0.00085	-6.45E-07	-6.81E-18	-558.8229722	558.8229722	-197.7774558	197.7774558	-226.98	58.19923	2.69E-12	2.71E-12	-0.0005
12	1.524604	0.267463	0	6	2	-0.00084	-6.26E-07	-7.48E-18	-611.1230381	611.1230381	-220.2915239	220.2915239	-249.424	64.081	4.45E-13	2.31E-11	-0.00055
13	1.512092	0.267488	0	6	2	-0.00084	-6.31E-07	-8.11E-18	-662.3124871	662.3124871	-239.5682239	239.5682239	-270.564	70.38967	-8.06E-13	1.33E-11	-0.00057
14	1.499579	0.267512	0	6	2	-0.00083	-6.18E-07	-8.74E-18	-713.3066463	713.3066463	-258.114538	258.114538	-291.426	77.74385	-3.61E-13	7.91E-12	-0.00058
15	1.487067	0.267536	0	6	2	-0.00082	-5.95E-07	-9.38E-18	-764.6831963	764.6831963	-278.1585401	278.1585401	-312.853	85.42612	-1.09E-12	2.14E-11	-0.00058
16	1.474555	0.267561	0	6	2	-0.00082	-5.68E-07	-1.00E-17	-816.6016271	816.6016271	-299.182384	299.182384	-334.735	93.28221	-7.47E-13	1.73E-11	-0.00058
17	1.462043	0.267585	0	6	2	-0.00081	-5.40E-07	-1.07E-17	-869.051311	869.051311	-320.93032	320.93032	-356.994	101.2706	8.87E-13	1.15E-11	-0.00058
18	1.44953	0.26761	0	6	2	-0.0008	-5.12E-07	-1.14E-17	-921.9760031	921.9760031	-343.2355032	343.2355032	-379.563	109.3706	-3.07E-12	-4.95E-12	-0.00058
19	1.437018	0.267634	0	6	2	-0.00079	-4.84E-07	-1.21E-17	-975.3090891	975.3090891	-365.9834975	365.9834975	-402.388	117.5692	1.59E-12	2.61E-12	-0.00058
20	1.424506	0.267658	0	6	2	-0.00079	-4.58E-07	-1.28E-17	-1028.988748	1028.988748	-389.0878665	389.0878665	-425.423	125.8541	7.82E-13	-5.40E-12	-0.00058
21	1.411993	0.267683	0	6	2	-0.00078	-4.33E-07	-1.35E-17	-1082.963023	1082.963023	-412.4820737	412.4820737	-448.634	134.2128	5.12E-12	-2.27E-11	-0.00058
22	1.399481	0.267707	0	6	2	-0.00077	-4.09E-07	-1.42E-17	-1137.18176	1137.18176	-436.1135148	436.1135148	-471.989	142.6352	1.37E-12	-7.33E-12	-0.00058
23	1.386969	0.267732	0	6	2	-0.00076	-3.86E-07	-1.49E-17	-1191.601264	1191.601264	-459.9353846	459.9353846	-495.461	151.1113	6.16E-13	3.67E-12	-0.00058
24	1.374457	0.267756	0	6	2	-0.00076	-3.65E-07	-1.56E-17	-1246.18863	1246.18863	-483.9145112	483.9145112	-519.031	159.6311	6.62E-13	1.36E-11	-0.00059
25	1.361944	0.26778	0	6	2	-0.00075	-3.45E-07	-1.63E-17	-1300.906307	1300.906307	-508.0137091	508.0137091	-542.676	168.1863	9.78E-13	-1.91E-12	-0.00059

Figure 7.10: Sample of raw data from simulation.
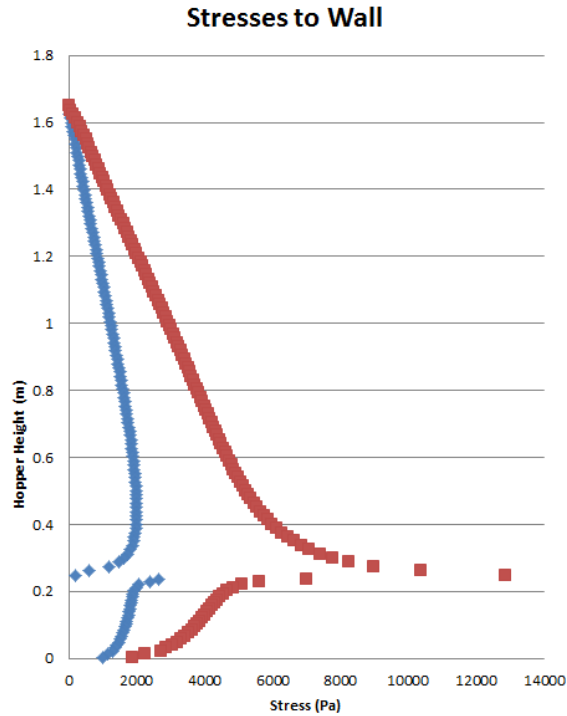
Figure 7.11: Stress profiles from simulation.

Figure 7.11 shows both parallel stress (red) and perpendicular stress profiles (blue) to wall. The perpendicular stress profile matches the general normal stress profile in the literature (Figure 2.6). Stress increases with depth, peaks at switch point (at 0.24m from the outlet) then comes back down to zero at the outlet. Jassen's theoretical method introduces a K ratio of the horizontal stress to the vertical stress in straight section:

$$K = \frac{\sigma_h}{\sigma_v} \qquad (7.5)$$

The value of K-ratio for powder is between zero to one, where zero is for flat solid plate particles and one is for liquids [109; 110; 111; 112]. Figure 7.12 shows the value of K-ratio at wall from the simulation. The majority of the data points fall in range between 0.3 and 0.5, which resembles the values for powder from the literature [112; 113]
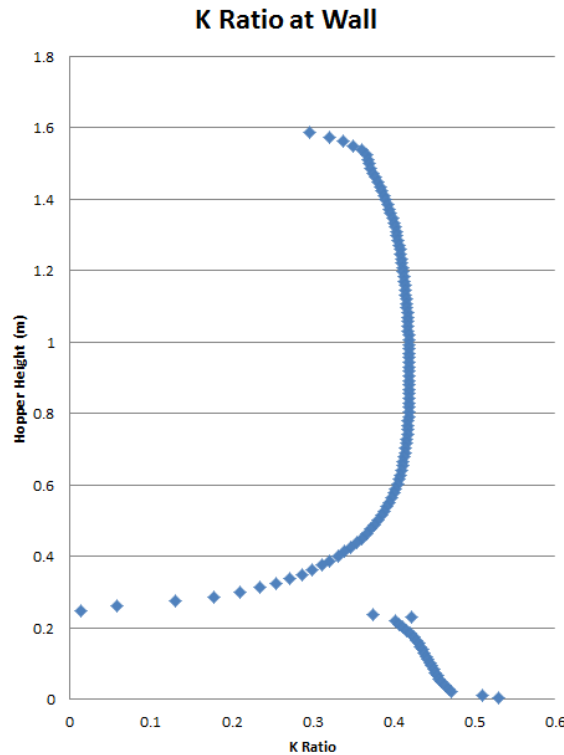
Figure 7.12: K-ratio at wall.

7.3.2   Arching Prediction

The author is aware that in real practice once the outlet is opened, the failed element should be under the "elastic" region [1] of the Cam-Clay model while the element is relaxed. However, the author was only to able to obtain the constitutive relationship during compaction, which is the virgin compaction curve in the Cam-Clay model. The author decided to also employ the virgin compaction curve in the outlet-opening stage, further suggestion on how to obtain the "elastic" region will be detailed in Chapter 8.2.1 Expansion Curve of E.

_____

[1]The "elastic" region here refer to the unloading-reloading zone in Cam-Clay model, no the elastic region in traditional Stricture Mechanics.

After the hopper outlet is opened, some powder falls off naturally. Every element is coded to be examined with the failure criterion which is derived by the author and detailed in Chapter 5.5. Equation 5.27 indicates that positive Failure value (coloured red in Figure 7.13) is associated with element failure. Every element, which satisfies the failure condition, will fall off. The associated elements will be removed for the next time step. The rest of the powder remains as a rigid solid, which is associated with a negative Failure value (coloured blue in Figure 7.13). The red contour in the corner of the switch point is falsely caused by the mathematical singularity at the sharp corner, therefore no elements from the this corner would be removed. The material properties of powder in that corner zone remain as those of powder.

After the initial opening of the hopper, elements of failed powder are removed from the simulation. This is archived via changing the material properties from those of powder to those of air to model the fallen-off powder, before continuing any further simulation. Figure 7.13 also shows that density of air ($1.2kg/m^3$ coloured green) at the outlet.
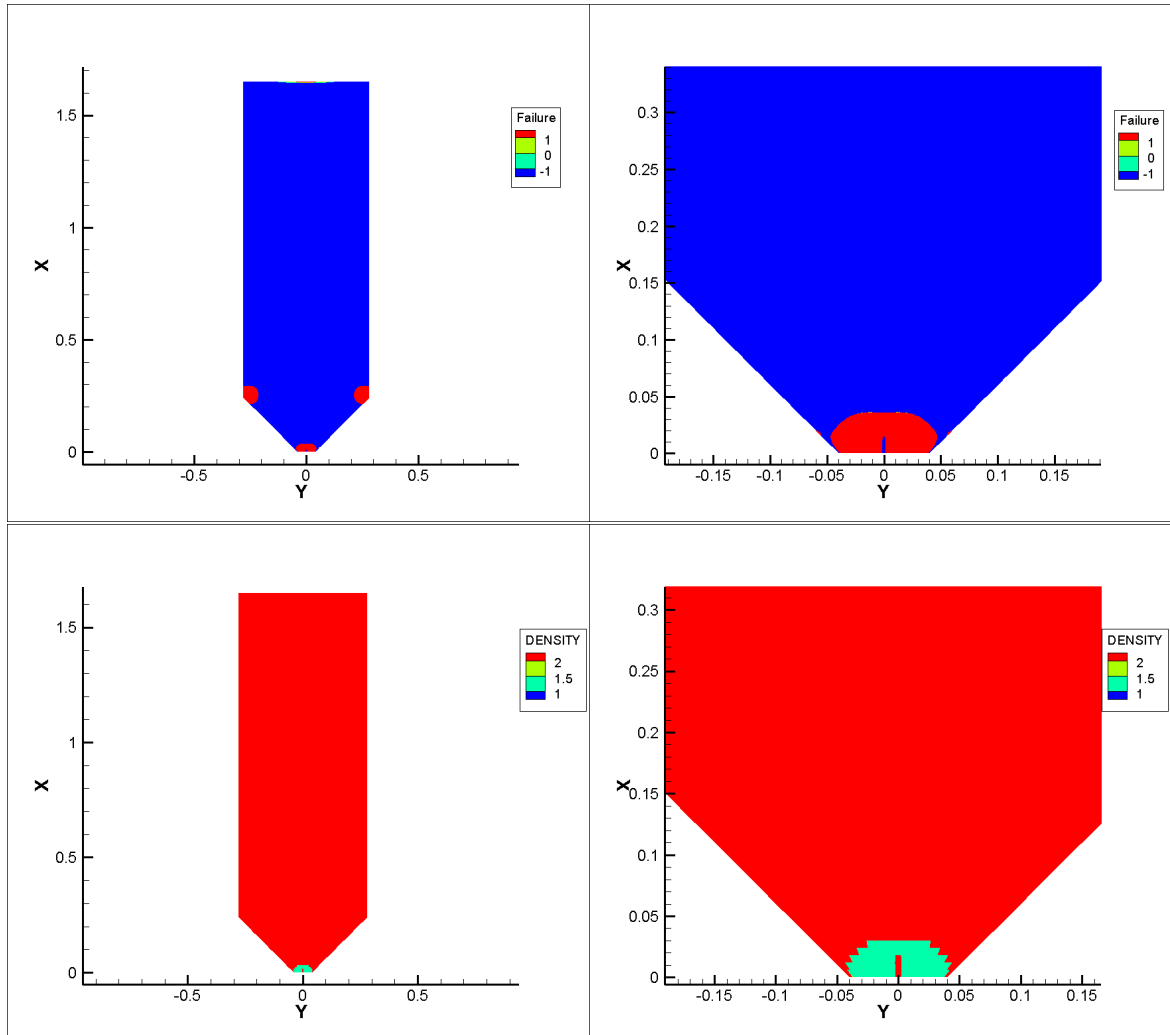
Figure 7.13: Arching condition at the outlet right after initial opening (top) and removal of the failed elements (bottom) (Time Step 1 at opening).
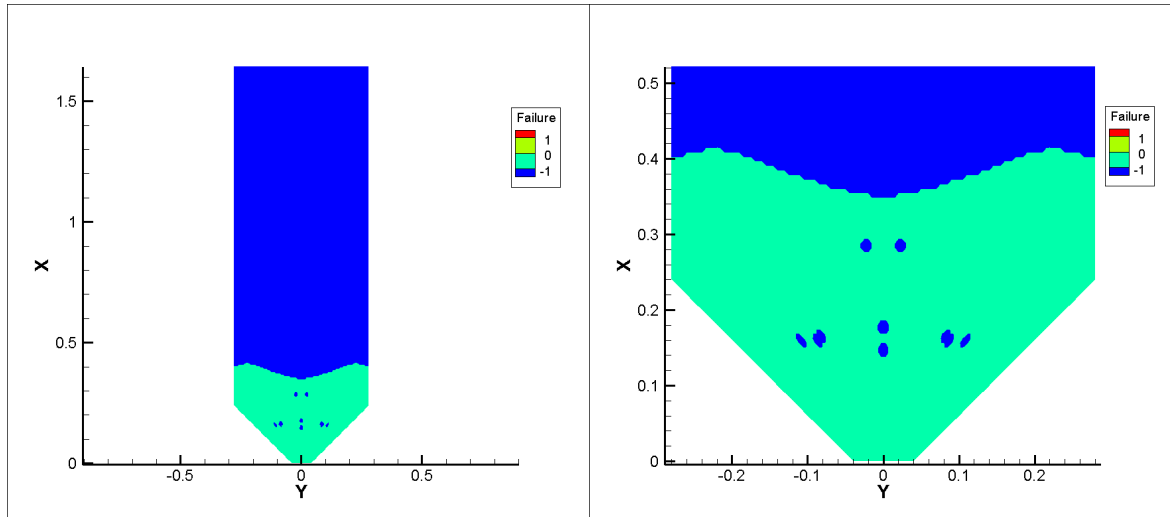
Figure 7.14: Arching condition at the outlet right after removing the falling
material (Time Step 8 at opening).

The random "dots" in Figure 7.14 are due to numerical errors. The failed areas are
removed as the failure criteria are satisfied. Even though the simulation shows no
further failure shown in red, the failure zone has reached beyond the switch point.
Hence it will continue to fail to the top, the simulation predicts a mass flow for this
geometry.

7.3.3 Hopper Outlet Design Calculation for Case 1

In 1961 [15], Jenike enlightened the field of bulk solid handling with his ground-
breaking solution method to hopper design, 50 years on the design method has retained
its reputation and widely employed across bulk solid handling industries. The author
used the same method to determine the minimum outlet size for a reliable flow of the

cohesive powder in this case study, for comparison against the simulation.

$$B_{min} = \frac{\sigma_{c,crit} H(\alpha)}{\rho_{b,crit} g} \tag{7.6}$$

where B_{min} is the minimum outlet size, $\sigma_{c,crit}$ and $\rho_{b,crit}$ are the unconfined yield strength and the bulk density of the powder at critical consolidation. $H(\alpha)$ is an empirical dimensionless factor which depends on the shape and the half angle of the hopper (see Figure 7.15). For a 45 degree wedge hopper, which has a rectangular outlet, the value of $H(\alpha)$ is 1.3.
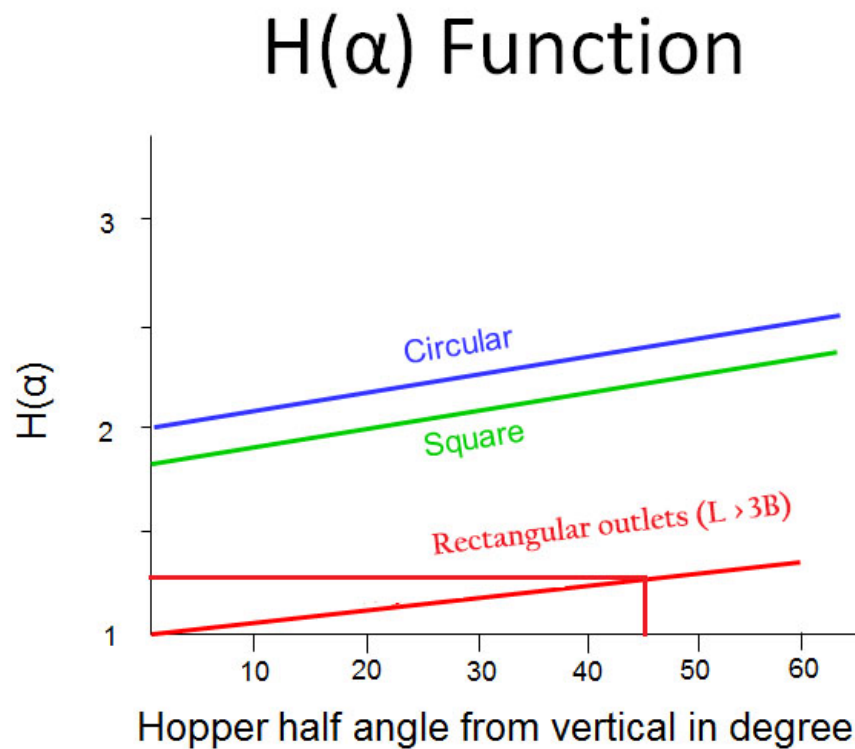
Figure 7.15: $H(\alpha)$ function.

With reference to Figure 7.16 In order to obtain $c,crit$ and $\rho_{b,crit}$, the critical point needs to be identified with Flow function (FF) and flow factor (ff). The intersection

of FF and ff is the critical point which determines the flow-or-no-flow condition, FF must lie under ff for a flow condition (as seen in Figure 7.16). Flow Function (FF) is explained in Figure 2.12 and flow factor (ff) is a constant ratio of effective wall stress (σ_a) to pre-consolidation stress (σ_1) for a given hopper.
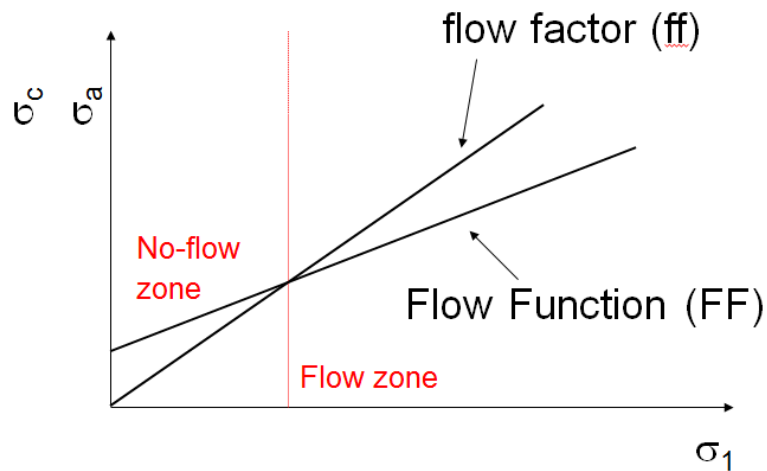
Figure 7.16: Flow and no-flow criterion for a hopper

For any given hopper, the hopper half angle α, the effective angle of internal friction δ and the effective angle of wall friction φ_w. Each line will has its own function and the intersect point is calculated with Equation 7.7.

The powder has been put under the Brookfield Powder Test to obtain the effective angle of internal friction δ along with other parameters.

7.3 Case Study 1
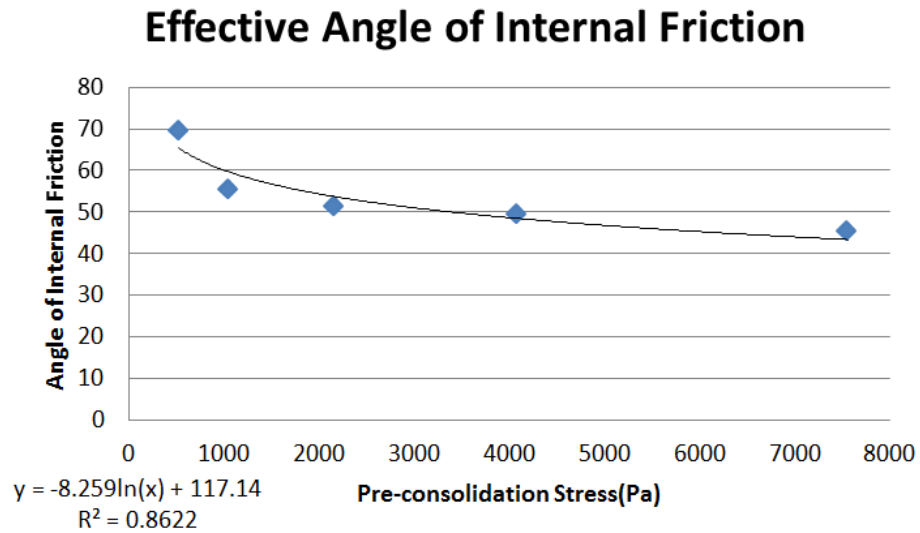
Figure 7.17: Effective angle of internal friction for flour

Figure 7.17 shows the effective angle of internal friction, δ, for flour from the Brookfield PowderFlow tester. However, the effective angle of friction is a function of temperature and moisture content, while the environmental factors remain unchanged, δ remains constant [16]. δ will be taken at an average of $50\,^{\circ}$ for this study.

118
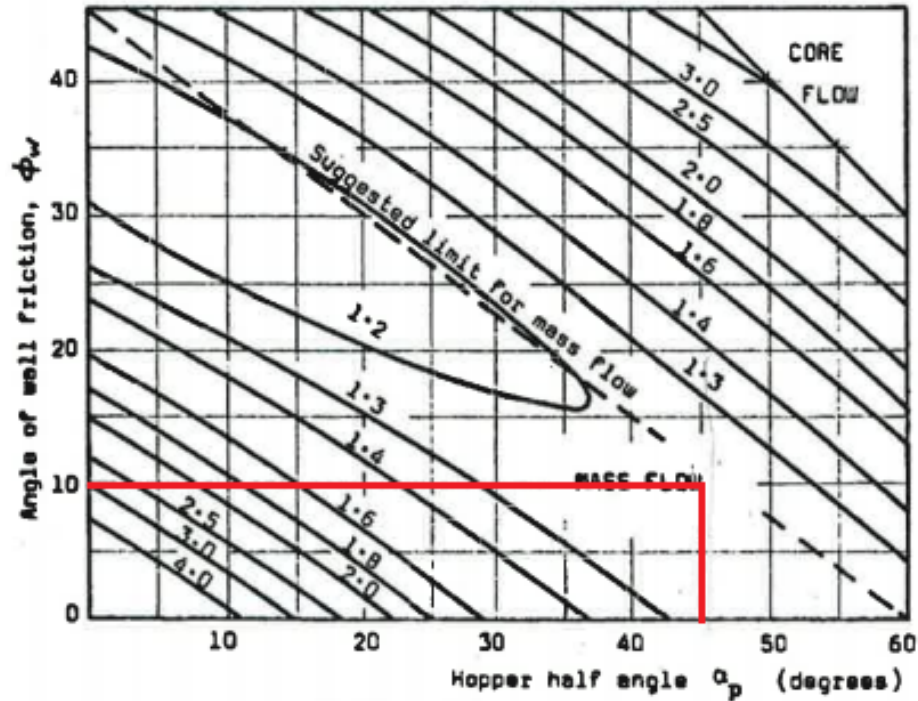
Figure 7.18: Flow factor (ff) contour for symmetrical wedge hopper for effective angle of friction of $50\,^\circ$

For every given hopper shape and effective angle of wall friction, flow factor (ff) can be read off the contour in Figure 7.18. For a $45\,^\circ$ wedge to have a flow pattern of mass flow, the flow factor is 1.3 and the effective angle of wall friction, φ_w, as previous mentioned, is $10\,^\circ$ for this study case.

$$\begin{cases} \sigma = 1.3\sigma_1 & \text{for ff} \\ \sigma = 0.5361\sigma_1 & \text{for FF} \end{cases} \qquad (7.7)$$

The critical pre-consolidation stress $\sigma_{1_{crit}}$ is calculated at $235.6 Pa$, and the σ_{crit} is $306.25 Pa$. The critical density at $\sigma_{1_{crit}}$ of $235.6 Pa$ is $550.0 kg/m^3$.

Calculation from Equation 7.6 obtains minimum outlet width B_{min}:

$$B_{min} = \frac{306.25 \times 1.3}{550.0 \times 9.81} = 0.07379m \tag{7.8}$$

The calculated minimum outlet for the given hopper in Case 1 is 0.07379m, which is less than in Case 1 (0.08m). Case 1 simulation is predicted to have a mass flow pattern, which is satisfied with the calculated value. Case 1 is with an outlet of 0.08, hopper half angle of 45 $^\circ$ and a wall friction angle of 10 $^\circ$.

The proposed method benchedmark against the Jenike hopper design. As previously mentioned in Chapter 2, the limitation of Jenike lies in the hopper geometry. As the design equation, Equation 7.6 and Figure 7.15 suggest. The Jenike's method is functional for only three hopper geometries. The proposed method would have the potential to provide flexibility on hopper geometry while predicting the arching/failure condition.

7.4 Case Study 2

With the second case study. All geometry aspects, material properties and boundary conditions will be the same expect. The angle of friction between the wall and powder, it changed from 10 $^\circ$ to 20 $^\circ$.

Case 1 shows that the model is capable of simulating mass flow in the hopper with the correct given conditions. Case 2 ensure that with changing angle of friction between the wall and the powder, the model would be also capable of simulating a different flow pattern. In order to verify the model is not limited to mass flow only.
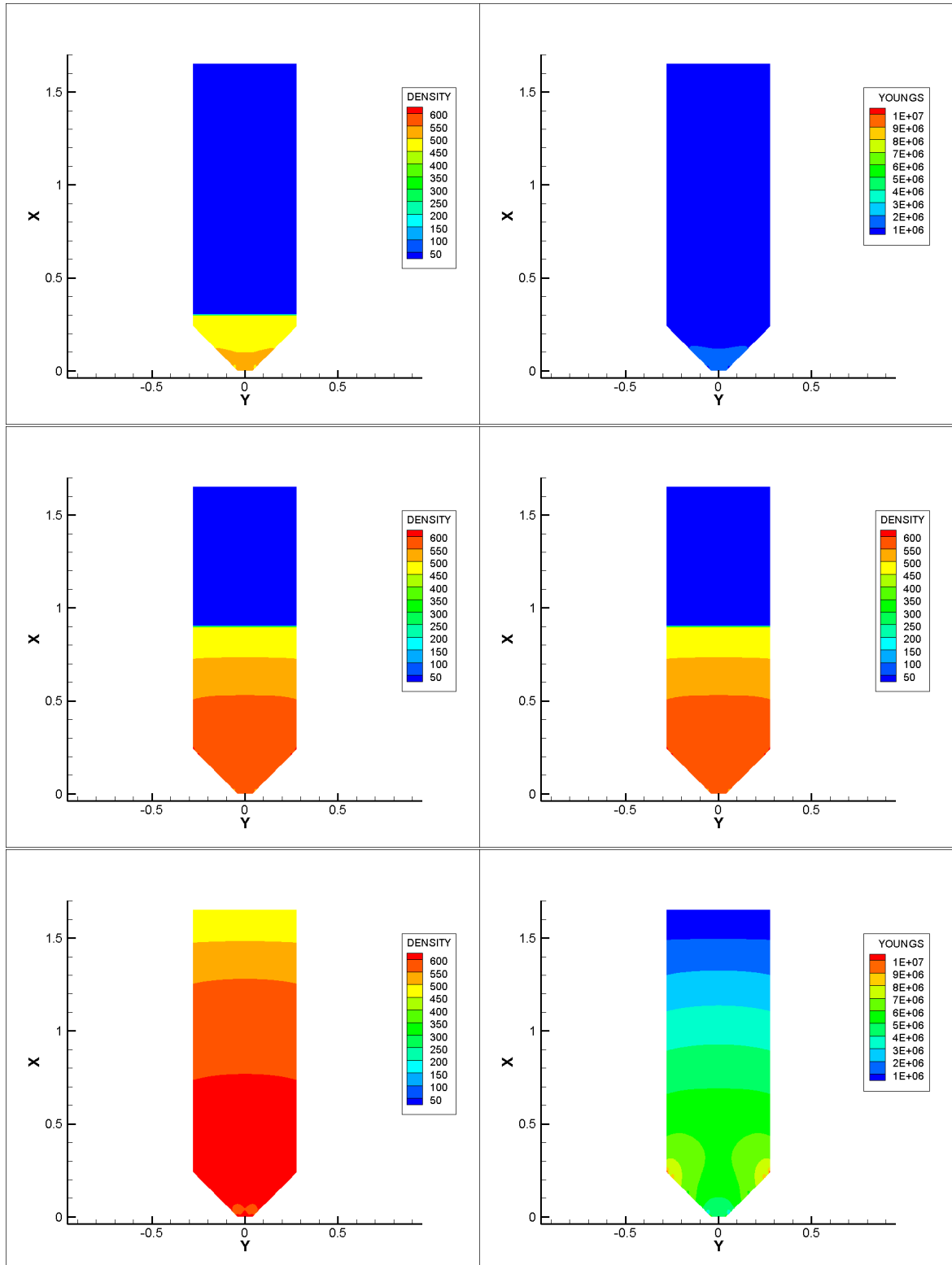
Figure 7.19: Density (left) and Young's Moduli (right) during filling stage with different time steps.

7.4.1 Stress Profile

Figure7.20 shows the shape of the stress profile is the same as Figure 7.11.
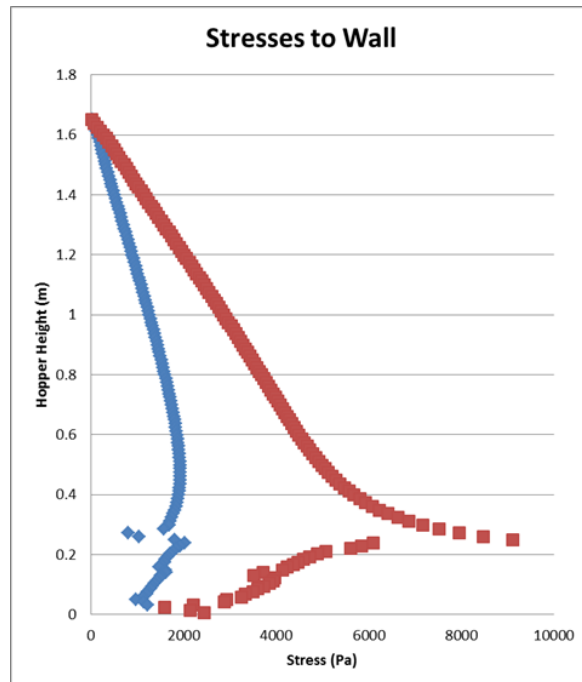
Figure 7.20: Stress profiles from simulation.

7.4.2   Arch Prediction
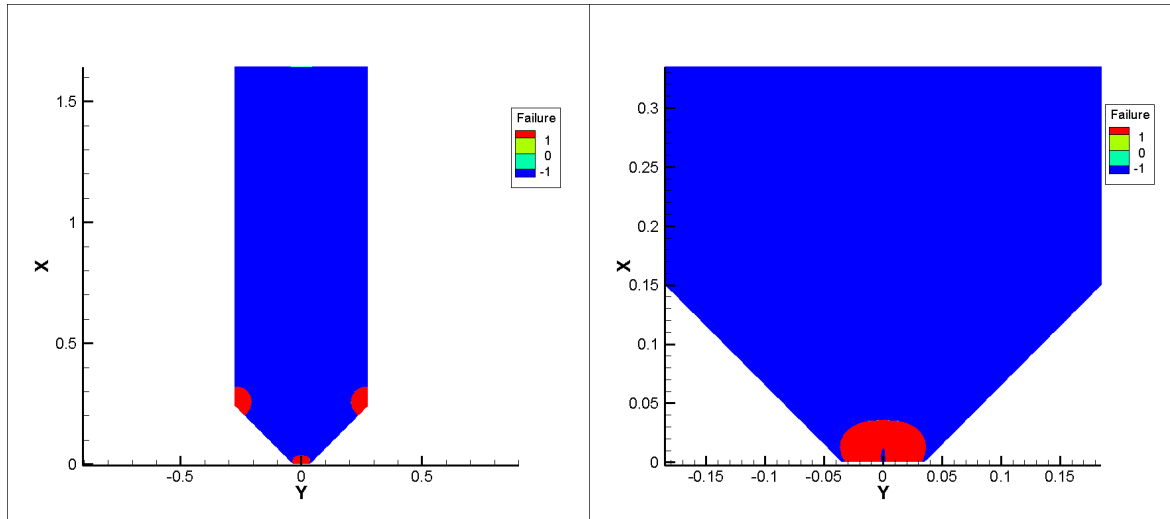
Figure 7.21: Arching condition at the outlet right after removing the falling
material (Time Step 1 at opening).

At initial opening of the outlet, the area (contoured in red)of elements at the outlet
satisfies the failure criterion, the elements are then "removed" by changing the material
from those of powder to those of air.
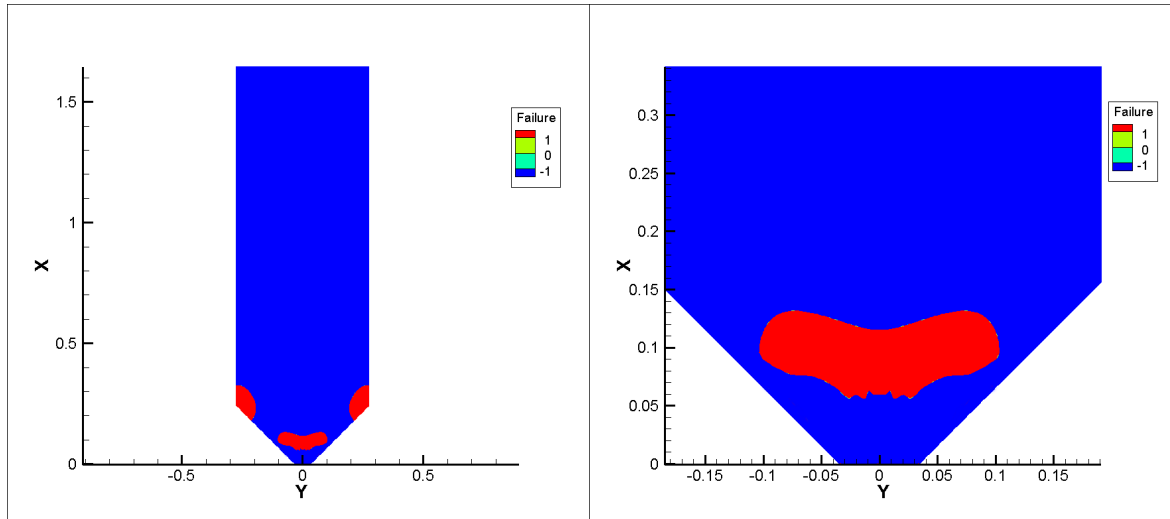
Figure 7.22: Arching condition at the outlet right after removing the falling material (Time Step 3 at opening).

At Time Step 3 after opening, the arching prediction was "floating" in the middle. Failure of the arch mainly happen from the edge of the wall. If there the elements at the wall do not satisfy the failure criterion, the author suggests that there is an arch formed or "rat-holing" is occurring. In Case 2, the hopper is expected to not have a mass flow pattern, due to the increase in angle of friction changed from $10\,^\circ$ to $20\,^\circ$.
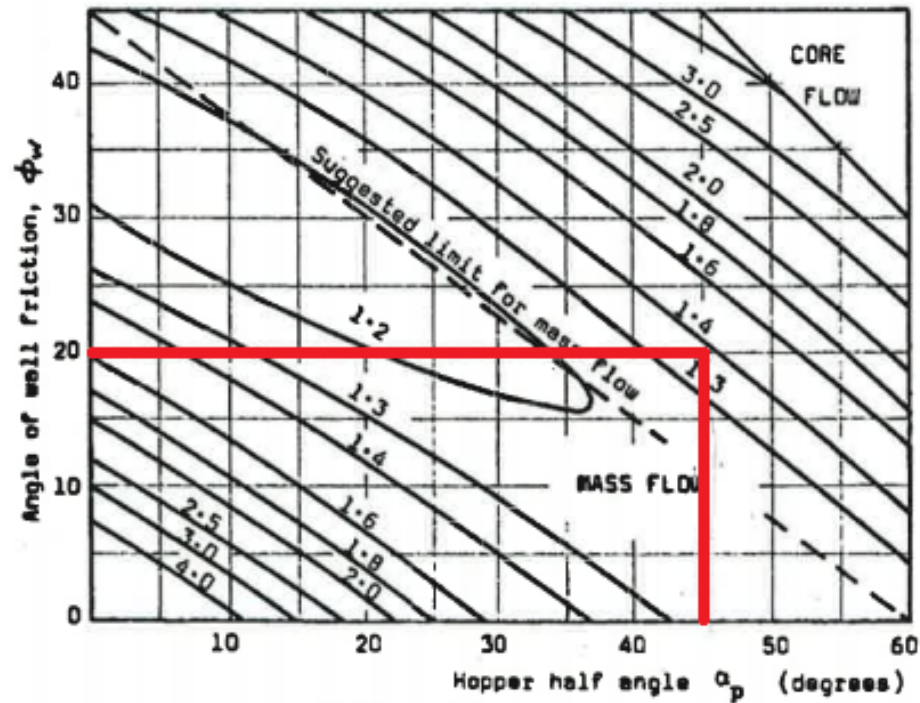
Figure 7.23: Flow factor (ff) contour for symmetrical wedge hopper for effective angle of friction of 50°

According to Jenike calculation in Figure 7.23 a 45° hopper with 20° angle of wall friction will most likely lack the ability to create any mass flow pattern, which is in-line which the results from the simulation that predicts the hopper will have a "rat-holing" condition (see Figure ??).

The results from Case 2 prove that the model is not restricted to only predict mass flow pattern.

7.5 Case Study 3 - Changes in Cohesion

The simulation is based on FE approach. As Chapter 2.3 explains in detail for Cohesion, Cohesion is one of the controlling factors in powder flowability. There have not been any attempts to correlate the cohesion and Young's modulus in powder mechanics before this research. Nevertheless, in the last decade, researchers in Soil Mechanics [81; 82; 114]

Brahma promoted:

$$E = 600c \tag{7.9}$$

where E is Young's Modulus and c is cohesion.

Schanz promoted the following in Hardening Soft Clay model:

$$E = E^{ref}\left(\frac{\sigma_3 + c\cot\phi_p}{\sigma^{ref} + c\cot\phi_p}\right)^m \tag{7.10}$$

where E^{ref} is a reference Young's modulus corresponding to the reference stress p^{ref}, which is the stress recorded in the tri-axial test in order to carry out the Cam-Clay model. σ_3 is the minor principal stress, m is the stress dependency index. For more details about the parameters in Cam-Clay model, please see Chapter 3.2.2.1.

In this Study Case, Equation 7.9 is employed for its simplicity. The cohesion of the powder increased two-times, so the Young's Modulus of the material also increase two-times.

Figure 7.24: Density (left) and Young's Moduli (right) during filling stage with different time steps.

The author observed a flow pattern of "rat-holing" after increasing the Young's modulus, E.
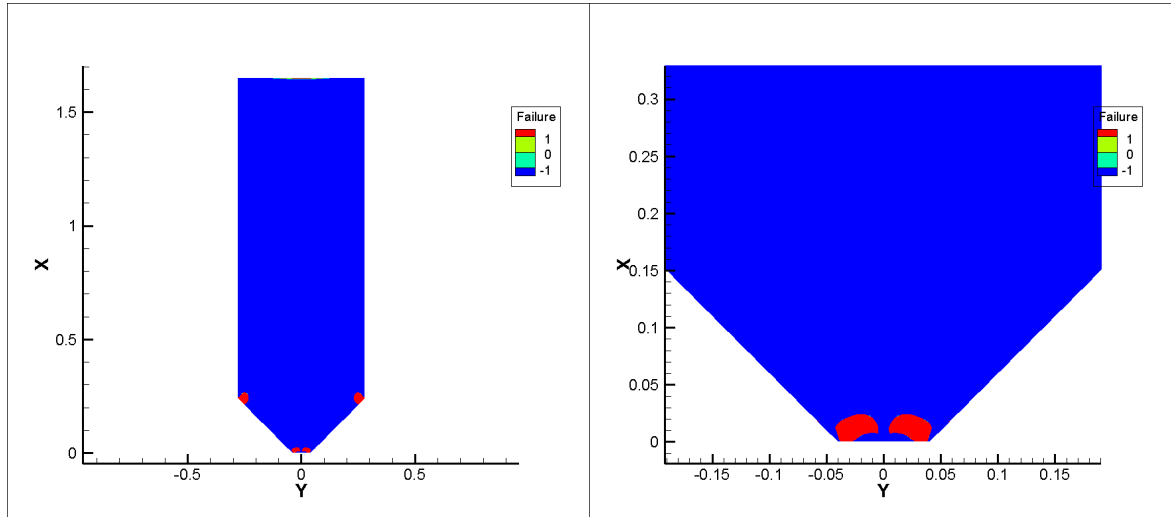
Figure 7.25: Arching condition at the outlet right after initial opening (Time Step 1 at opening).
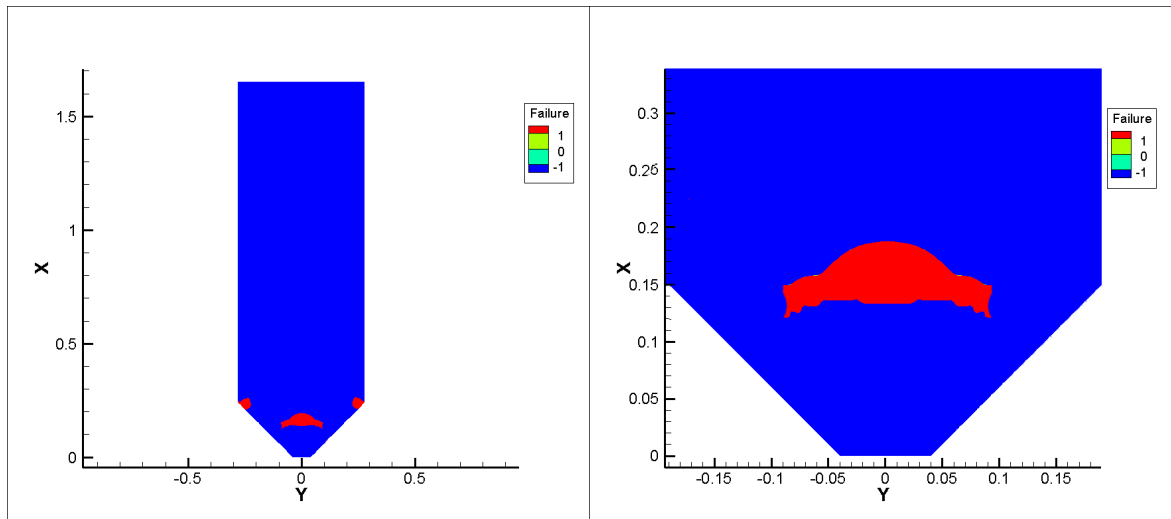
Figure 7.26: Arching condition at the outlet right after removing the falling material (Time Step 5 at opening).

In Case 3, the cohesion was doubled numerically to simulation the situation with a powder material whose strength is doubled. The simulation shows that the material is having a rat-hole condition in Case 3.

The new material in Case 3 is only implemented numerically, did not undergo any empirical experiments to obtain parameters such as the effective angle of internal friction. The analytical method, Equation 7.6, cannot be conducted to obtain the exact minimum outlet size for mass flow condition. However, the increase of material strength is known to be one of the contributors to flow obstruction. The rat-holing results from the simulation reflects the criterion.

Therefore the author concluded that Case Study 3 is also a valid results from the model.

7.6   Chapter Summary

The introduced numerical model successfully simulate the free-flowing in Case 1 validated against analytical model. The author tested the model with an increase of the wall friction in Case 2 and the cohesion in Case 3. The contributors to arching forming or flow obstruction are a) increase in wall friction and b) increase in material strength. The results from Case 2 verifies the former and the results from Case 3 verifies the latter.

In order for the model to function properly, users must conduct both empirical experiments and the numerical simulation together according to the model flowchart 5.1

The case studies shown that the capability of the model to predict arching/failure condition. The model may provide a potential foundation of numerical simulation which is tailored to powder mechanics.

Chapter 8

CONCLUSIONS AND FUTURE WORK

8.1   Conclusion

8.1.1   Summery of the Research

This PhD project suggests on a new constitutive numerical model that predicts arching at the outlet of a hopper of a hopper. This model also takes consideration of stress history which is "stored" in the powder under a FEA approach. This has never been achieved before.

To take account of the stress history, the simulation follows the filling an empty hopper with powder. As the hopper gets filled, the powder properties, Young's Modulus and Density change, according to the stress acting on it, due to self-weight of the powder. The constitutive relationship for charging material properties were obtained

by conducting the following experiments: Uniaxial Compression Test and Brookfield Powder Flow Tester. The tests were conducted in The Wolfson Centre at the University of Greenwich.

Complex coding was required to accommodate the complexity of the material. The Young's Modulus and Density of powder is changing as a function of stress, and the variable parameters are coded into the source codes in a software package Physica. Physica is a numerical solver package that solves a system of engineering equations, it was developed at the Department of Mathematical Sciences at University of Greenwich.

The importance of wall friction between powder and the wall lays in that it is one of the main factors for forming an arch at the outlet.

After coping with the complex non-linear constitutive material properties, study cases were conducted with the improved codes.

What the author has concluded from this research is that FEA is still a promising approach for large scale in industry applications to simulate powder behaviour in hoppers and silos. However, to this date, it has certain limitations to yet to be addressed.

From the viewpoint of PHYSICA, it is indeed an extremely nested software with a high number of modules and subroutines. However, the modules and subroutines are written in a very neat manner, and they provide a high degree of flexibility and the potential of improvement. If PHYSICA were to have a graphic user interface (GUI) and a database of material properties, the application has the prospect to be more affordable to use than the analytical model and be widely employed in the industry, especially for companies which do not have in-house laboratory facilities.

8.1.2   Contribution to Knowledge

8.1.2.1   Combining Two Fields

The main contribution of this project to the exiting knowledge is the function of the model which brings together established powder mechanics with numerical simulation to deliver a feasible measure to predict hopper arching in industry.

The overlapping area in between the field of Powder Mechanics and Numerical Simulation is on a microscopic level. Therefore the personnel who are expert in dealing with the experimental characterisation and analytical representation of the constitutive behaviour of the powders do not generally have a thorough knowledge in modelling, such as geometry set-up, boundary conditions, mesh techniques, discretisation techniques, numerical coding etc. On the other hand, those who are expert in numerical simulation generally do not deal with powder handling or have a deep understanding in complex powder characteristics, such as powder flowability, critical state of the powders, shear failure, Jenike's analytical method for hoppers, experimental testings and so on.

The difficulty for the author was that the two fields do not even share the same vocabulary. The author had to acquire complete understandings and thorough knowledge of both fields, related to the problem, and to integrate and interpret them in such a way that can be understood by both fields.

After the author was equipped with the knowledge from both sides, another huge difficulty lies in the implementation of the knowledge. The mathematical approaches used by both fields are not truly compatible. For example, in traditional Structure Engineering, the strength of the material is determined by its Young's Modulus. However Young's Modulus is not a parameter in Powder Mechanics, instead, the strength of the material is determined by its stress history and cohesion. Other example is the failure condition. In traditional Structure Mechanics, the yield stress determines whether the material behaves elastically or plastically. However, the yield surface determines

whether a powder behaves elastically or plastically.

The numerical simulations of Powder Mechanics has been "borrowing" existing numerical models from other similar engineering disciplines. These parameters from powder characteristics are almost never mentioned in the history of powder simulation.

Therefore in this project, the author had to introduce a wide range of new components to the codes in PHYSICA to accommodate the discrepancy between the two fields, introducing concepts and terminology not previously known to the FEA field.

8.1.3 Challenges Solved

Numerical Representation of Failure Criteria from Analytical Model As mentioned in the previous section, the characteristics in Powder Behaviour are often unheard of in numerical simulations; one of the many issues addressed in the project is the numerical representation of failure criteria derived from the Jenike model, Equations 5.26 and conducted the calculation in the numerical solver PHYISICA.

Implementation of Stress History in simulation

The stress history affects both the strength and failure condition of the powder, it is very important to introduce and implement it in PHYSICA. Without it the Failure Criterion will not withstand.

The stress from previous time step is stored as a new variable. Equation 5.26 indicates that the cohesion, c, and the gradient of the loci, m, are the numerical contributors in the model to predict the failure of each element. The cohesion changes with various pre-consolidation stresses but the gradient of the loci remains constant at the value of 0.6 for flour.

The changes in the cohesion are accounted for in the code developments in PHYISICA.

Implementation of Complex Material Properties   During the process module, the author has also introduced the material strength relationship between the current stress, which is represented in terms of Young's Modulus. The switch between different material properties is also built in.

In powder machines, it is known that wall friction is one of the main factors to hold the arch in place. The wall friction with sliding mechanism is also introduced into PHYSICA and implemented.

8.1.3.1   New Challenges Discovered

Numerical singularity errors that have affected the calculation in the corner.

The wall friction with the sliding mechanism is newly introduced in PHYSICA, it is limited to accommodates a sliding inclination of 45°.

8.1.3.2   Challenges that Remain Unsolved

The implementation of the orthotropic material property still remains unsolved. Powder is a very complex material, stress history is only one of the contributor to its strength.

8.2 Future Work

8.2.1 Expansion curve of E

One of the most significant contributions has been to allow the change in Young's modulus according to the stress conditions. Stress conditions include compaction and expansion.

During outlet opening stage, the elements under failure condition are in tensile stress.

The author conducted the drained tri-axial test described in Cam-Clay model in the Civil Engineering Laboratory with the attempt to obtain the expansion curve of "E".

Figure 8.1: Empirical apparatus of Tri-axial test

The dry powder is filled in a rubber sleeve and submerged in water. However, the apparatus was originally designed to test clay and soil specimens, the pressure range applied to the water is extensively large, in the range of $200kPa$ and beyond, compared to the pressure range of the test on typical powder between $15 - 80kPa$ [77; 115], in order to observe the recovery behaviour. The high pressure range of the traditional tri-axial tester for clay loses the ability to to record any recovery in dry powder when the powder is under relaxation. Hence most adoptions of Cam-Clay model in powder

136

mechanics simulations have been on compression and compaction only.

Therefore the author is proposing the sophisticated apparatus to conduct compression on dry powder with low stress, previously introduced by Tripodi and Puri [77; 115].
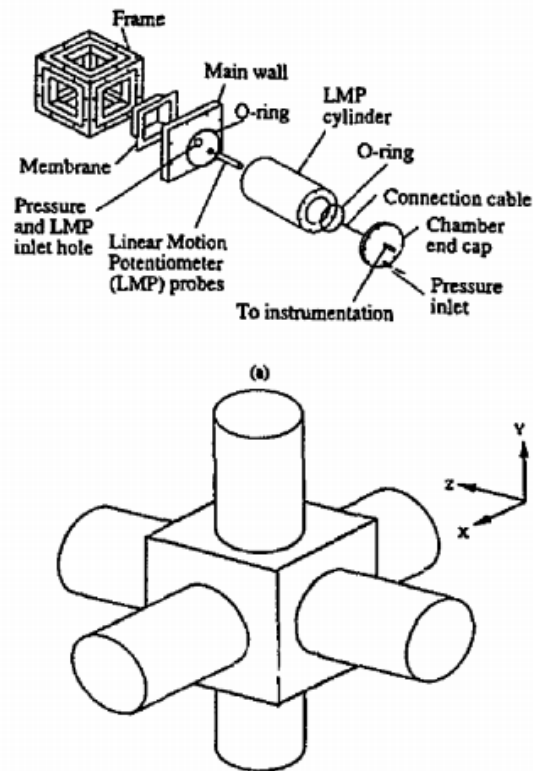
Figure 8.2: Empirical apparatus of Tri-axial test for dry powder

The powder specimen is now filled in a cubical frame instead of a cylinder to allow different compacting stress in different directions. This apparatus ensures that the applied stress can be anisotropic.

8.2.2 Orthortopic Non-linear Elasticity in 3D

FEA equations in PHYSICA is coded in-line with Hooke's law:

$$\sigma = D\epsilon \tag{8.1}$$

where the stress σ and the strain ϵ are stored in arrays with six components for three-dimension, which is demonstrated as following:

and D is the compliance matrix.

In this research, the properties were programmed to be non-linear isotropic "elastic".

The 3D compliance matrix of isotropic material is a symmetric matrix, by engineering definition [116; 117] it is shown as below:

$$D = \frac{E(1-\nu)}{(1+\nu)(1-2\nu)} \begin{bmatrix} 1 & \frac{\nu}{1-\nu} & \frac{\nu}{1-\nu} & 0 & 0 & 0 \\ \frac{\nu}{1-\nu} & 1 & \frac{\nu}{1-\nu} & 0 & 0 & 0 \\ \frac{\nu}{1-\nu} & \frac{\nu}{1-\nu} & 1 & 0 & 0 & 0 \\ 0 & 0 & 0 & \frac{1-2\nu}{2(1-\nu)} & 0 & 0 \\ 0 & 0 & 0 & 0 & \frac{1-2\nu}{2(1-\nu)} & 0 \\ 0 & 0 & 0 & 0 & 0 & \frac{1-2\nu}{2(1-\nu)} \end{bmatrix} \tag{8.2}$$

where E and ν are Young's modulus and Poisson's ratio respectively. They are both one single variable, which are coded and stored as below:

```
Young's  modulus  =  [E]
Poisson  ratio    =  [V]
```

and the compliance matrix D 8.2 [1] is coded as following:

```
        SUBROUTINE  elasticity_matrix
    @               ( Idee , Dee , E, V, Approx )

        INTEGER      Idee
        REAL         E,      V
        REAL         Dee( Idee , Idee )
        CHARACTER    Approx*6

C   Local variables.
        INTEGER      i
        REAL         vv

        CALL set_null_matrix (Idee , Idee , Dee)

        IF ( Approx .EQ. 'THREED' ) THEN
            vv           =    E * (1 - V) /((1 + V) * (1 - 2*V))
            Dee(1,1)     =    1
            Dee(2,2)     =    1
            Dee(3,3)     =    1
            Dee(1,2)     =    V / (1 - V)
            Dee(2,1)     =    V / (1 - V)
            Dee(1,3)     =    V / (1 - V)
            Dee(3,1)     =    V / (1 - V)
            Dee(2,3)     =    V / (1 - V)
            Dee(3,2)     =    V / (1 - V)
            Dee(4,4)     =    (1 - 2*V) / (2 * (1 - V))
            Dee(5,5)     =    (1 - 2*V) / (2 * (1 - V))
            Dee(6,6)     =    (1 - 2*V) / (2 * (1 - V))
        END IF

        CALL multiply_matrix_by_scalar
    @       (Idee , Idee , vv , Dee)

        END
```

where vv is introduced as a co-efficient of the matrix with respective of E and ν.

---

[1]The terminology, the compliance matrix D, used in literature is the equivalent to the terminology, the elasticity matrix Dee, used in Physica coding

However, the 3D compliance matrix of orthotropic material is not a symmetric matrix, by engineering definition [118; 119] it is shown as below :

$$
\begin{bmatrix}
\frac{1}{E_x} & -\frac{v_{yx}}{E_y} & -\frac{v_{zx}}{E_z} & 0 & 0 & 0 \\
-\frac{v_{xy}}{E_x} & \frac{1}{E_y} & -\frac{v_{zy}}{E_z} & 0 & 0 & 0 \\
-\frac{v_{xz}}{E_x} & -\frac{v_{yz}}{E_y} & \frac{1}{E_z} & 0 & 0 & 0 \\
0 & 0 & 0 & \frac{1}{2G_{yz}} & 0 & 0 \\
0 & 0 & 0 & 0 & \frac{1}{2G_{zx}} & 0 \\
0 & 0 & 0 & 0 & 0 & \frac{1}{2G_{xy}}
\end{bmatrix}
\tag{8.3}
$$

where bot Young's modulus and Poisson's ratio are different is different direction. They should be re-introduced and stored in two different arrays. e.g:

Young's modulus = [E_x, E_y, E_z, G_yz, G_zx, G_xy]

Poisson's ratio = [V_xy, V_yx, V_xz, V_zx, V_yz, V_zy]

However, the change in variable type (change from a number to an array) will largely affect the calculation across the equation system. At the same time, all Young's modulus and Poisson's ratio are non-linear according to the stress history. The challenge of implementation of a non-linear orthotropic materials lies in the re-configuration of the compliance matrix. The codes in PHYSICA are extremely nested, each PHYSICA module interacts and exchanges information with other modules. In order to change the compliance matrix, `SUBROUTINE elasticity_matrix` requires well-thought planning, heavy re-coding and careful debugging.

This is the reason for the author to choose Physica as the primary numerical solver package. Physica is the sole numerical solver which allows both non-linear and orthotropic happening at the same time, whereas ANASYS and Comsol only has the ability to simulate either situation separately.

In addition to coding the matrix, The author would also suggest future work to include

establishing an empirical method to measure the Young's modulus and the Poisson's ratio in different direction in respective of the stress, which has been suggested by Mann [120].

8.2.3   Refined mesh at corner

There is a stress singularity point at the corner of the hopper, where the parallel section meets the converging section. The singularity point is believed to be caused by the numerical limitation of solving a nodal point in a structured mesh: a mesh which is made of rectangular elements. The techniques to remove the singularity point in Finite Element Analysis include substituting the elements at corner with: a) refined unstructured elements or b) the round-edged elements [121; 122]. These techniques were not considered in this model, because changing from structured mesh to unstructured mesh would not be compatible with the codes for the material filling process. The codes are built in the manner that each uniform layer of element changes its material properties in accordance with the time step. Unstructured mesh would not provide uniform layers, and disturb the model. Therefore the author decided to keep the mesh structured. That singularity point is far away from the hopper outlet, it is considered to have minimal effect on predicting the arching condition at the outlet.
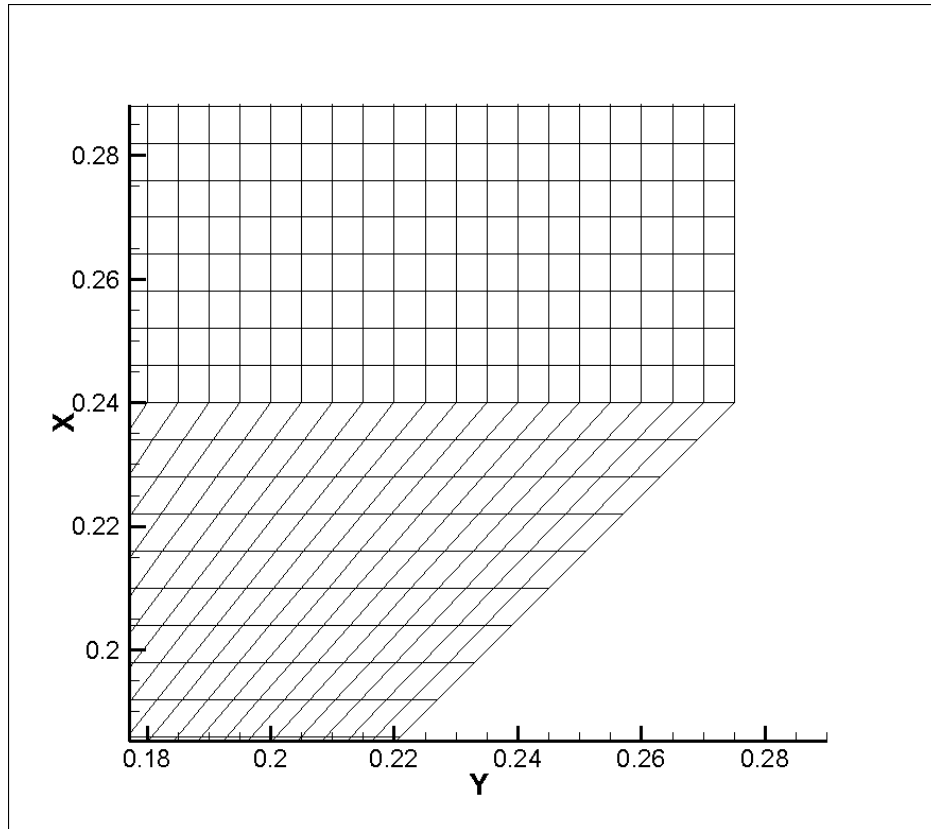
Figure 8.3: A structured mesh zoom-in at the corner.

This mesh structure prevent from having sharp corner of the mesh at the switch point in the hopper. The author would suggest an unstructured mesh at the corner to minimise the effect of

REFERENCES

[1] P Chapelle, N Christakis, J Wang, N Strusevich, MK Patel, M Cross, H Abou-Chakra, J Baxter, and U Tuzun. Application of simulation technologies in the analysis of granular material behaviour during transport and storage. *Proceedings of the Institution of Mechanical Engineers, Part E: Journal of Process Mechanical Engineering*, 219(1):43–52, 2005. 3

[2] H Abou-Chakra, U Tüzün, I Bridle, M Leaper, MSA Bradley, and AR Reed. An investigation of particle degradation by impact within a centrifugal accelerator type degradation tester. *Proceedings of the Institution of Mechanical Engineers, Part E: Journal of Process Mechanical Engineering*, 217(3):257–266, 2003. 3

[3] Nicholas Christakis, Pierre Chapelle, Nadezhda Strusevich, Ian Bridle, John Baxter, Mayur K Patel, Mark Cross, Ugur Tüzün, Alan R Reed, and Michael SA Bradley. A hybrid numerical model for predicting segregation during core flow discharge. *Advanced Powder Technology*, 17(6):641–662, 2006. 3

[4] RJ Berry and MSA Bradley. Investigation of the effect of test procedure factors on the failure loci and derived failure functions obtained from annular shear cells. *Powder technology*, 174(1):60–63, 2007. 3

[5] Tong Deng, Richard J Farnish, and Michael SA Bradley. Evaluation of particle degradation due to high-speed impacts in a pneumatic handling system. *Particulate Science and Technology*, 26(5):438–450, 2008. 3

[6] Tariq Hussain, Waseem Kaialy, Tong Deng, Mike SA Bradley, Ali Nokhodchi, and David Armour-Chélu. A novel sensing technique for measurement of magnitude and polarity of electrostatic charge distribution across individual particles. *International journal of pharmaceutics*, 441(1):781–789, 2013. 3

[7] Mark Cross. Computational issues in the modelling of materials-based manufacturing processes. *Journal of Computer-Aided Materials Design*, 3(1-3):100–116, 1996. 3

[8] N Christakis, MK Patel, M Cross, J Baxter, H Abou-Chakra, U Tüzün, et al. Continuum modelling of granular flows using physica, a 3-d unstructured, finite-volume code. 2001. 3

[9] M Bradley and R Farnish. Overview of particulate handling technology. 2016. 3

[10] John J Fitzpatrick and Lilia Ahrné. Food powder handling and processing: Industry problems, knowledge barriers and research opportunities. *Chemical Engineering and Processing: Process Intensification*, 44(2):209–214, 2005. 3

[11] Joseph Marius DallaValle. Micromeritics: the technology of fine particles. 1900. 7

[12] Joseph Marius DallaValle et al. Micromeritics. 1948. 7

[13] Dale E Fonner, Gilbert S Banker, and James Swarbrick. Micromeritics of granular pharmaceutical solids i: Physical properties of particles prepared by five different granulation methods. *Journal of pharmaceutical sciences*, 55(2):181–186, 1966. 7

[14] Joseph Marius Dallavalle. Micromeritics. *Soil Science*, 56(2):151, 1943. 7

[15] Andrew W Jenike. Storage and flow of solids, bulletin no. 123. *Bulletin of the University of Utah*, 53(26), 1964. 7, 20, 115

[16] AW Jenike. Gravity flow of bulk solids. university of utah engineering experiment station. *Bulletin*, 108, 1961. 7, 118

[17] Edward W Merrow, Kenneth E Phillips, and Christopher W Myers. Understanding cost growth and performance shortfalls in pioneer process plants. 1981. 8

[18] J Baxter, H Abou-Chakra, U Tüzün, and B Mills Lamptey. A dem simulation and experimental strategy for solving fine powder flow problems. *Chemical Engineering Research and Design*, 78(7):1019–1025, 2000. 8

[19] Jayant Khambekar and Roger A Barnum. Prb coal- material handling challenges and solutions. *Power Engineering*, 117(3):48–54, 2013. 9

[20] R Farnish and R Berry. Storage and discharge of powders and bulk solids. 2012. 9

[21] Dietmar Schulze. Flow properties of powders and bulk solids. *Braunschweig/-Wolfenbu ttel, Germany: University of Applied Sciences*, 2006. 14, 20, 22

[22] JoT Jenkins and SB Savage. A theory for the rapid flow of identical, smooth, nearly elastic, spherical particles. *Journal of Fluid Mechanics*, 130:187–202, 1983. 16, 32

[23] JF Carr and DM Walker. An annular shear cell for granular materials. *Powder Technology*, 1(6):369–373, 1968. 22

[24] J Schwedes and D Schulze. Measurement of flow properties of bulk solids. *Powder technology*, 61(1):59–68, 1990. 22

[25] Jörg Schwedes. Measurement of flow properties of bulk solids. *Powder Technology*, 88(3):285–290, 1996. 22

[26] Dietmar Schulze. Powders and bulk solids. *Behaviour, Characterization, Storage and Flow. Springer*, 2008. 22

[27] Jiayuan Zhang, Ziguo Hu, Wei Ge, Yongjie Zhang, Tinghua Li, and Jinghai Li. Application of the discrete approach to the simulation of size segregation in granular chute flow. *Industrial & engineering chemistry research*, 43(18):5521–5528, 2004. 24

[28] Stefan Luding. Introduction to discrete element methods: basic of contact force models and how to perform the micro-macro transition to continuum theory. *European Journal of Environmental and Civil Engineering*, 12(7-8):785–826, 2008. 24

[29] Peter A Cundall and Otto DL Strack. A discrete numerical model for granular assemblies. *Geotechnique*, 29(1):47–65, 1979. 24

[30] RJ Godwin and G Spoor. Soil failure with narrow tines. *Journal of Agricultural Engineering Research*, 22(3):213–228, 1977. 24

[31] KZY Yen and TK Chaki. A dynamic simulation of particle rearrangement in powder packings with realistic interactions. *Journal of Applied Physics*, 71(7): 3164–3173, 1992. 24

[32] Consuelo Margarita Kong and John J Lannutti. Effect of agglomerate size distribution on loose packing fraction. *Journal of the American Ceramic Society*, 83(9):2183–2188, 2000. 25

[33] Carl Wassgren and Jennifer Sinclair Curtis. The application of computational modeling to pharmaceutical materials science. *MRS bulletin*, 31(11):900–904, 2006. 25

[34] A Samimi, A Hassanpour, and M Ghadiri. Single and bulk compressions of soft granules: experimental study and dem evaluation. *Chemical Engineering Science*, 60(14):3993–4004, 2005. 25

[35] Yong Xu, KD Kafui, C Thornton, and Guoping Lian. Effects of material properties on granular flow in a silo using dem simulation. *Particulate Science and Technology*, 20(2):109–124, 2002. 25

[36] Kurt Liffman, Myhuong Nguyen, Guy Metcalfe, and Paul Cleary. Forces in piles of granular material: an analytic and 3d dem study. *Granular matter*, 3(3): 165–176, 2001. 25

[37] BK Mishra. A review of computer simulation of tumbling mills by the discrete element method: part icontact mechanics. *International journal of mineral processing*, 71(1):73–93, 2003. 26

[38] RJ Bathurst and Leo Rothenburg. Micromechanical aspects of isotropic granular assemblies with linear contact interactions. *Journal of Applied Mechanics*, 55(1): 17–23, 1988. 26

[39] Helio A Navarro and Meire P de Souza Braun. Linear and nonlinear hertizian contact models for materials in multibody dynamics. 2013. 27

[40] H Kruggel-Emden, S Wirtz, and V Scherer. A study on tangential force laws applicable to the discrete element method (dem) for materials with viscoelastic or plastic behavior. *Chemical Engineering Science*, 63(6):1523–1541, 2008. 27

[41] CM Wensrich and A Katterfeld. Rolling friction as a technique for modelling particle shape in dem. *Powder Technology*, 217:409–417, 2012. 28

[42] YC Zhou, BD Wright, RY Yang, BH Xu, and AB Yu. Rolling friction in the dynamic simulation of sandpile formation. *Physica A: Statistical Mechanics and its Applications*, 269(2):536–553, 1999. 28

[43] NL Johnson. The effect of tangential contact force upon the rolling motion of an elastic. *TRANS. ASME*, 80:339, 1958. 28

[44] Alberto Di Renzo and Francesco Paolo Di Maio. Comparison of contact-force models for the simulation of collisions in dem-based granular flow codes. *Chemical Engineering Science*, 59(3):525–541, 2004. 29

[45] Goro Kuwabara and Kimitoshi Kono. Restitution coefficient in a collision between two spheres. *Japanese journal of applied physics*, 26(8R):1230, 1987. 29

[46] Jérg Theuerkauf, Shrikant Dhodapkar, Karl Jacob, et al. Modeling granular flow. *Chemical Engineering*, 114(4):39–46, 2007. 29

[47] Thorsten Pöschel and Patric Müller. Event-driven dem of soft spheres. 1542: 149–152, 2013. 29

[48] Marcus N Bannerman, Severin Strobl, Arno Formella, and Thorsten Pöschel. Stable algorithm for event detection in event-driven particle dynamics. *Computational Particle Mechanics*, 1(2):191–198, 2014. 29

[49] C Spandonidis and J Spyrou. Use of granular material dynamics simulation for the study of cargo shift of ships. pages 497–507, 2012. 29

[50] Tomohiko G Sano and Hisao Hayakawa. Simulation of granular jets: Is granular flow really a perfect fluid? *Physical Review E*, 86(4):041308, 2012. 29, 43

[51] Anton Manoylov, Valdis Bojarevics, and Koulis Pericleous. Modeling the break-up of nano-particle clusters in aluminum-and magnesium-based metal matrix nano-composites. *Metallurgical and Materials Transactions A*, 46(7):2893–2907, 2015. 29

[52] Qicheng Sun, Guangqian Wang, and Yong Xu. Dem applications to aeolian sediment transport and impact process in saltation. *Particulate science and technology*, 19(4):339–353, 2001. 29

[53] Limin Wang, Guofeng Zhou, Xiaowei Wang, Qingang Xiong, and Wei Ge. Direct numerical simulation of particle–fluid systems by combining time-driven hard-sphere model and lattice boltzmann method. *Particuology*, 8(4):379–382, 2010. 29

[54] JE Hilton, LR Mason, and PW Cleary. Dynamics of gas–solid fluidised beds with non-spherical particle geometry. *Chemical Engineering Science*, 65(5):1584–1596, 2010. 29

[55] Paul W Cleary. Large scale industrial dem modelling. *Engineering Computations*, 21(2/3/4):169–204, 2004. 29

[56] Anil W Date. Introduction to computational fluid dynamics. 2005. 30

[57] Chuen-Yen Chow. An introduction to computational fluid mechanics. 1979. 30

[58] John David Anderson and J Wendt. Computational fluid dynamics. 206, 1995. 30

[59] Alan R Abrahamsen and D Geldart. Behaviour of gas-fluidized beds of fine powders part i. homogeneous expansion. *Powder technology*, 26(1):35–46, 1980. 30

[60] D‿ Sathiyamoorthy and Ch Sridhar Rao. Gas distributor in fluidised beds. *Powder Technology*, 20(1):47–52, 1978. 30

[61] R‿ J Wakeman and BW Stopp. Fluidisation and segregation of binary particle mixtures. *Powder Technology*, 13(2):261–268, 1976. 30

[62] N Chepurniy. Kinetic theories for granular flow: inelastic particles in couette flow and slightly inelastic particles in a general flow field. *Journal of fluid mechanics*, 140(223-222):256, 1984. 32

[63] Lu Huilin, Dimitri Gidaspow, Jacques Bouillard, and Liu Wentie. Hydrodynamic simulation of gas–solid flow in a riser using kinetic theory of granular flow. *Chemical Engineering Journal*, 95(1):1–13, 2003. 32

[64] Renzo Di Felice. The pseudo-fluid model applied to three-phase fluidisation. *Chemical engineering science*, 55(18):3899–3906, 2000. 32

[65] Lu Huilin, He Yurong, Dimitri Gidaspow, Yang Lidan, and Qin Yukun. Size segregation of binary mixture of solids in bubbling fluidized beds. *Powder Technology*, 134(1):86–97, 2003. 32

[66] Yonghao Zhang and Jason M Reese. The influence of the drag force due to the interstitial gas on granular flows down a chute. *International journal of multiphase flow*, 26(12):2049–2072, 2000. 32

[67] BH Ng, YL Ding, and M Ghadiri. Modelling of dense and complex granular flow in high shear mixer granulatora cfd approach. *Chemical engineering science*, 64 (16):3622–3632, 2009. 32

[68] Alex Skvortsov, Brigitta Suendermann, Grant Gamble, Michael Roberts, Omar Ilaya, and Dinesh Pitaliadda. Scaling laws of tracer dispersion in a multicompartment structure. *Experimental Thermal and Fluid Science*, 45:110–116, 2013. 32

[69] Ramesh Pankajakshan, Brent J Mitchell, and Lafayette K Taylor. Simulation of unsteady two-phase flows using a parallel eulerian–lagrangian approach. *Computers & Fluids*, 41(1):20–26, 2011. 32

[70] BA Wols, JAMH Hofman, WSJ Uijttewaal, LC Rietveld, and JC van Dijk. Evaluation of different disinfection calculation methods using cfd. *Environmental Modelling & Software*, 25(4):573–582, 2010. 32

[71] Per Strålin. Lagrangian cfd modeling of impinging diesel sprays for di hcci. 2007. 32

[72] Riccardo Artoni, Alberto Zugliano, Alessandra Primavera, Paolo Canu, and Andrea Santomaso. Simulation of dense granular flows: Comparison with experiments. *Chemical Engineering Science*, 66(3):548–557, 2011. 33

[73] Riccardo Artoni, Andrea Santomaso, and Paolo Canu. Simulation of dense granular flows: Dynamics of wall stress in silos. *Chemical Engineering Science*, 64 (18):4040–4050, 2009. 33

[74] Andrew Schofield. Original cam-clay. 1993. 33

[75] Andrew Schofield and Peter Wroth. Critical state soil mechanics. 1968. 33

[76] Jacob Lubliner. Plasticity theory. 2008. 33

[77] MA Tripodi, VM Puri, HB Manbeck, and GL Messing. Triaxial testing of dry, cohesive powder and its application to a modified cam-clay constitutive model. *Powder technology*, 80(1):35–43, 1994. 34, 136, 137

[78] David Muir Wood. Soil behaviour and critical state soil mechanics. 1990. 38

[79] NA Fleck, GM Muller, MF Ashby, and JW Hutchinson. Strain gradient plasticity: theory and experiment. *Acta Metallurgica et Materialia*, 42(2):475–487, 1994. 41

[80] K H Roscoe and JB Burland. On the generalized stress-strain behaviour of wet clay. 1968. 41

[81] T Schanz, PA Vermeer, and PG Bonnier. The hardening soil model: formulation and verification. *Beyond 2000 in computational geotechnics*, pages 281–296, 1999. 42, 126

[82] Hector Alarcon, Jean-Christophe Géminard, and Francisco Melo. Effect of cohesion and shear modulus on the stability of a stretched granular layer. *Physical Review E*, 86(6):061303, 2012. 42, 126

[83] Simon B Ross-Murphy. Rheological methods. pages 343–392, 1994. 43

[84] James Freeman Steffe. Rheological methods in food process engineering. 1996. 43

[85] PFG Banfill. Rheological methods for assessing the flow properties of mortar and related materials. *Construction and Building materials*, 8(1):43–50, 1994. 43

[86] Eugene Cook Bingham. Fluidity and plasticity. 2, 1922. 43

[87] E C Bingham. An investigation of the laws of plastic flow. *US Bureau of Standards Bulletin*, 13:309–353, 1916. 43

[88] Falah Alobaid, Jochen Ströhle, and Bernd Epple. Extended cfd/dem model for the simulation of circulating fluidized bed. *Advanced Powder Technology*, 24(1): 403–415, 2013. 45

[89] Tingwen Li, Pradeep Gopalakrishnan, Rahul Garg, and Mehrdad Shahnam. Cfd–dem study of effect of bed thickness for bubbling fluidized beds. *Particuology*, 10(5):532–541, 2012. 45

[90] KW Chu, B Wang, AB Yu, A Vince, GD Barnett, and PJ Barnett. Cfd–dem study of the effect of particle density distribution on the multiphase flow and performance of dense medium cyclone. *Minerals Engineering*, 22(11):893–909, 2009. 45

[91] M Ranjbar-Far, Joseph Absi, and Gilles Mariaux. Finite element modeling of the different failure mechanisms of a plasma sprayed thermal barrier coatings system. *Journal of thermal spray technology*, 21(6):1234–1244, 2012. 51

[92] Ares J Rosakis and G Ravichandran. Dynamic failure mechanics. *International journal of solids and structures*, 37(1):331–348, 2000. 51

[93] George Ellwood Dieter and David Bacon. Mechanical metallurgy. 3, 1986. 56

[94] William F Hosford and Robert M Caddell. Metal forming: mechanics and metallurgy. 2011. 70

[95] Robert M Jones. Mechanics of composite materials. 1998. 72

[96] Luigi Bruno, Giuseppina Felice, Leonardo Pagnotta, Andrea Poggialini, and Giambattista Stigliano. Elastic characterization of orthotropic plates of any shape via static testing. *International Journal of Solids and Structures*, 45(3): 908–920, 2008. 72

[97] Simon Salager, Bertrand François, Mathieu Nuth, and Lyesse Laloui. Constitutive analysis of the mechanical anisotropy of opalinus clay. *Acta Geotechnica*, 8 (2):137–154, 2013. 72

[98] HS Shin and GN Pande. Identification of elastic constants for orthotropic materials from a structural test. *Computers and Geotechnics*, 30(7):571–577, 2003. 73

[99] Marco Alfano and Leonardo Pagnotta. Determining the elastic constants of isotropic materials by modal vibration testing of rectangular thin plates. *Journal of Sound and Vibration*, 293(1):426–439, 2006. 73

[100] Shun-Fa Hwang and Chao-Shui Chang. Determination of elastic constants of materials by vibration testing. *Composite Structures*, 49(2):183–190, 2000. 73

[101] Arthur Peter Boresi, Richard Joseph Schmidt, and Omar M Sidebottom. Advanced mechanics of materials. 1993. 73

[102] Kalyan Kumar Phani and Dipayan Sanyal. A new approach for estimation of poissons ratio of porous powder compacts. *Journal of materials science*, 42(19): 8120–8125, 2007. 75

[103] S Parthasarathi, T Prucher, CJ Yu, J Jo, and RJ Henry. Determination of dynamic elastic properties of powder metallurgy components. pages 1631–1638, 1993. 75

[104] Lawrence E Kinsler, Austin R Frey, Alan B Coppens, and James V Sanders. Fundamentals of acoustics. *Fundamentals of Acoustics, 4th Edition, by Lawrence E. Kinsler, Austin R. Frey, Alan B. Coppens, James V. Sanders, pp. 560. ISBN 0-471-84789-5. Wiley-VCH, December 1999.*, 1, 1999. 93, 106

[105] Robert James Berry. The measurement of cohesive arches in silos using the technique of laser ranging. 2003. 106

[106] KS Manjunath and AW Roberts. Wall pressure-feeder load interactions in mass-flow hopper/feeder combinations. *Bulk Solids Handling*, 6(4), 1986. 109

[107] M Guaita, A Couto, and F Ayuga. Numerical simulation of wall pressure during discharge of granular material from cylindrical silos with eccentric hoppers. *Biosystems engineering*, 85(1):101–109, 2003. 109

[108] JM Rotter, CJ Brown, and EH Lahlouh. Patterns of wall pressure on filling a square planform steel silo. *Engineering structures*, 24(2):135–150, 2002. 109

[109] R Holdich. Fundamentals of particle technology. 2012. 111

[110] Józef Horabik and Marek Molenda. Properties of grain for silo strength calculation. pages 195–217, 2002. 111

[111] DF Bagster. A note on the pressure ratio in the janssen equation. *Powder Technology*, 4(4):235–237, 1971. 111

[112] JK Walters. A theoretical analysis of stresses in silos with vertical walls. *Chemical Engineering Science*, 28(1):13–21, 1973. 111

[113] AO Atewologun and GL Riskowski. Experimental determination of janssen's stress ratio by four methods for soybeans under static conditions. *Transactions of the ASAE*, 1991. 111

[114] P Brahma and S Mukherjee. A realistic way to obtain equivalent youngs modulus of layered soil. pages 305–308, 2010. 126

[115] S Kamath and VM Puri. Measurement of powder flow constitutive model parameters using a cubical triaxial tester. *Powder Technology*, 90(1):59–70, 1997. 136, 137

[116] RT Fenner. Engineering elasticity: application of numerical and analytical techniques. 1986. 138

[117] OC Zienkiewicz and RL Taylor. The finite element method, volume 1-basic formulation and linear problems-1994. 138

[118] OC Zienkiewicz and RL Taylor. The finite element method. volume 1: Basic formulation and linear problems. volume 2: Solid and uid mechanics and non-linearity. 1991. 140

[119] Olek C Zienkiewicz and Robert L Taylor. The finite element method for solid and structural mechanics. 2005. 140

[120] Ronald W Mann, Gary A Baum, and Charles C Habeger Jr. Determination of all nine orthotropic elastic constants for machine-made paper. 1979. 141

[121] GN Pande and J Middleton. Numerical techniques for engineering analysis and design: Proceedings of the international conference on numerical methods in engineering: Theory and applications, numeta87, swansea, 6–10 july 1987. 1, 2012. 141

[122] GB Sinclair. Stress singularities in classical elasticity–i: Removal, interpretation, and analysis. *Applied Mechanics Reviews*, 57(4):251–298, 2004. 141

Appendix A

Code development

A.1 Material Properties during Filling

A.1.1 inform file

```
MATERIAL_PROPERTY_MODULE
  DENSITY
    MATERIAL   1   USER_ROUTINE   layered   1   484.3
    SAVE_PROPERTY  TRANSIENT
  END
  YOUNGS_MODULUS
    MATERIAL   1   USER_ROUTINE    powderE   1   855.6E+3
    SAVE_PROPERTY  TRANSIENT
  END
  POISSONS_RATIO
    MATERIAL   1   CONSTANT   0.3
  END
  YIELD_STRESS
    MATERIAL   1   CONSTANT   1.0E+10
```

```
    END
END


```

A.1.2   casecode.f

```fortran
      subroutine case_mat_prop ( Ia , Ra, La, Cha,   Handld )
      dimension                  Ia(*), Ra(*)
      logical                    La(*), Handld, found
      character        Cha(1)*(*)

      real, parameter :: m=0.6 !angle of internal friction

      include  '../inc/generic.fh'
      include  '../inc/mprop.fh'

      save  nx, iStr , iCohe, Einit , RhoInit , iTheta , iTanTheta
      save  iRyl, iRg, iFail
      data      iStr   / -1 /        , RhoInit  / 0. /
      data  nx    / 0 /
      if ( nx .eq. 0 )  then
        io = 31
        open( io ,  File='divisions ', Status='old ')
         read(io , *)  nx
        close(io)
        write( * ,  '(A, I4)') 'nx =', nx
      endif

      iele  = PRP_ELE_ID - 1
      layer = 1 + MOD( iele , nx )

      if  ( PRP_EQN_NAM(1:7) .EQ.  'layered ' )   then
        Handld = .TRUE.
        if ( RhoInit .eq. 0. )  RhoInit = Ra( PRPDAT_ID )
        ! if  ( layer .eq. 1 )  write(*,'(A, I4)') '@',  PRP_
          ELE_ID
        dens = 1.2
        if  ( layer .EQ. TIME_STEP_NUMBER )  dens = Ra( PRPDAT
          _ID )
        Ra( PRPVAR_ID + iele ) = dens
```

```
      endif

      if  ( PRP_EQN_NAM(1:7) .EQ. 'powderE' )  then
        Handld = .TRUE.
        itime  =  TIME_STEP_NUMBER
        if  ( layer > itime )  then
          Ra( PRPVAR_ID + iele ) = 1.01e5  ! bulk modulus of
              air
        elseif  ( layer .EQ. itime )  then
          Ra( PRPVAR_ID + iele ) = Ra( PRPDAT_ID )  ! initial
              value
        else
!     compacted material:
      if  ( iStr .eq. -1 )  then
        call get_variable_info ('STRESS', iStr , isz ,itp ,iwd,
          msh, found)
        if  ( .not. found )  Stop 1
        call mem_real_ele ( 'Cohe', 1, iCohe )
        Einit = Ra( PRPDAT_ID )
        call mem_real_ele ( 'Theta', 1, iTheta )
        call mem_real_ele ( 'TanTheta', 1, iTanTheta )

        call mem_real_ele ( 'Ryl', 1,  iRyl )
        call mem_real_ele ( 'Rg' , 1,  iRg  )
        call mem_real_ele ( 'Failure', 1,  iFail )

      endif

        Str_xx = Ra( iStr + 6*iele )
        Str_yy = Ra( iStr + 6*iele + 1 )
        Str_xy = Ra( iStr + 6*iele + 3 )
        str1 = Max( 1.e-9, -Str_xx )
        str2 = Max( 1.e-9, -Str_yy )
        str3 = ABS( Str_xy )
        strM = (str1+str2)/2.

        Dens = 61.266*Log( strM ) + 114.54
        Etan = 692.5 *Exp(0.0147*Dens)

        Ra( DENSIT_P  + iele ) = Max( Dens, RhoInit )
        Ra( PRPVAR_ID + iele ) = Max( Etan, Einit )
```

```
    Ra( iCohe + iele ) = 0.1732*str1
    Ra(iTheta+iele)=0.5*abs(atan((2.*str3)/(abs(str1−str
        2)))*180./3.14)

    sin2Theta = (2*str3)/sqrt((2*str3)**2+(str1−str2)
        **2)
    cos2Theta = (2*str3)/(str1−str2)
    Ra(iTanTheta+iele)=sin2Theta/(1+cos2Theta)
    write (*,*)  istr
    var1 = (StrM−Ra(iCohe + iele)*m)*m/(m**2+1.)
    Ra(iRyl + iele) = ( var1 + Ra(iCohe+iele) )/(sin(
        atan(1./m)))
    Ra( iRg + iele ) = Sqrt( (0.5*(str1 − str2))**2 +
        str3**2 )
    Ra( iFail + iele ) = Ra( iRg + iele ) − Ra( iRyl +
        iele )
  end if
endif

end
```

A.2 Wall Friction

A.2.1 inform

```
DISCRETISATION_METHOD FINITE_ELEMENT

BOUNDARY_CONDITIONS
  P_PATCH  3   DISPLACEMENT   VALUE   0.0
  P_PATCH  4   DISPLACEMENT   VALUE   0.0
  P_PATCH  5   DISPLACEMENT   VALUE   0.0
  P_PATCH  6   DISPLACEMENT   VALUE   0.0

  F_PATCH  4   PRESSURE   VALUE   0.176
     .
     .
     .
```

.
.

A.2.2   casecode.f

```fortran
subroutine  tangnor ( itensor , s , un ,  st , valtang ,
    valnor )
dimension                s (*) , un (*) ,   st (*)
parameter   ( n = 3 )
dimension  SV(n)   !  stress  vector :

if  ( itensor > 0 )   then
  SV(1) = un(1)*s(1) + un(2)*s(4) + un(3)*s(6)
  SV(2) = un(1)*s(4) + un(2)*s(2) + un(3)*s(5)
  SV(3) = un(1)*s(6) + un(2)*s(5) + un(3)*s(3)
else
  SV(1:3) = s(1:3)
endif

dotp = 0.
do  i = 1, n ;   dotp = dotp + SV(i)*un(i) ;   enddo
t = 0.
do  i = 1, n
  st(i) = SV(i) - dotp*un(i)
  t = t + st(i)**2
enddo
valtang = Sqrt( t )
valnor  = dotp

end

subroutine  case_struct_pre_solution ( Ia , Ra , La , Cha )
dimension                 Ia (*) , Ra (*)
logical                   La (*)
character                 Cha(1) *(*)

include '../ inc/generic.fh'
include '../ inc/geom.fh'
logical   found
```

```
      dimension    et(3) , s6(3)

      itim = TIME_STEP_NUMBER
      write (* , '()')
      write (* , '(A, I6)') 'pre_solution : timestep ', itim

      call get_variable_info ( 'VBPRES', ipr , isz ,itp ,iwd ,msh,
          found)
      if ( .not. found ) stop 1

      do i = 0, TOTGPT-1 ; do ix = 0, 2
        Ra( ipr + 3*i + ix ) = 0.
      enddo ;  enddo

      call get_variable_info ('DelDisp', iep , isz ,itp ,iwd ,msh,
          found)

      if ( (.not. found) .or. (itim < 2) )  then
         ! Before 1st structure call :
         RETURN
      else

      write (* , 1)  ( 1000.*Ra( iep + i ), i=0, 5 )
 1    format ( 6F12.5 )

      call get_variable_info ('STRESS', iSt , isz ,itp ,iwd ,msh,
          found)
      if ( .not. found ) stop 2

      do ifac = 0, TOTFAC-1
        ipat = Ia( FPATCH_P + ifac )
        iele = Ia( FTCIND_P + ifac*NFTCFD + FACE_LOW_ELE-1 ) -
            1
        A = Ra( AREA_P + ifac )

        call get_pressure_load ( Ia, Ra, ipat , ipres , value )

        if ( ipres .eq. 1 ) then   !   vtxb.fh : PARAMETER
           (PRESLD = 1)
          iface = ifac + 1
          nor = normal_face ( iface )
```

```
          ix   = iSt + 6*iele

!         i1 = CENTRE_P + 3*iele ;   x = Ra(i1); y = Ra(i1+1); z =
    Ra(i1+2)
!         write(*,'()')
!         write(*, '(A, I4, 3F9.5)') 'Ele:', 1+iele, x,y,z
!         write(*, 1)  (Ra(ix+i), i=0,5)

!!!!          call tangnor ( 0, Ra(ix), Ra(nor),  et, st3, sn3 )
              call tangnor ( 1, Ra(ix), Ra(nor),  s6, st6, sn6 )

!         call face_centre ( Ia, Ra, iface,  x, y, z )
!         write(*, 1 ) x, z, sn6, st6   !!!  sn3, st3

              fricmax = Max( -sn6, 0. ) * value
!!!!          fricmax = Min( fricmax, 0.5*(st3 + st6) )   !  Max(
    st3, st6 ) )

              npif = Ia( NOPINF_P + ifac ) ;   val = A*fricmax/(1.*
                npif)
              do  ipif = 0, npif-1
                inod = Ia( FACPTS_P + ifac*TOTPIF + ipif ) - 1

!            Latest displacement tangential component:
                ix = iep + 3*inod
                call tangnor ( 0, Ra(ix), Ra(nor),  et, etlen, en
                  )

                do   i = 1, 3
                  i1 = ipr + 3*inod + i-1

                  if  ( etlen > 0. )  then
!                 Apply friction force opposite to tangential
    displacement:
                    Ra( i1 ) = Ra( i1 ) - et(i)/etlen * val
                  elseif  ( st6 > 0. )  then
!                 Apply friction force opposite to latest
    tangential stress:
                    Ra( i1 ) = Ra( i1 ) - s6(i)/st6 * val
                  else
                    write(*,'(A, 2I8)') 'No fric.', 1+inod, i
```

161

```
            Ra( i1 ) = 0.
          endif  !  etlen
       enddo
     enddo  !  ipif
   endif  !  'pressure' patch
 enddo  !  faces loop

! Reset of stresses to 0 must be after the friction
   calculation :

    call get_variable_info ('STRAIN', iEps, isz ,itp ,iwd ,msh,
        found)
    do  i = 0, TOTELE–1 ;  do  j = 0, 5
      ioff = 6*i + j
      Ra( iSt + ioff ) = 0. ;  Ra( iEps + ioff ) = 0.
    enddo ;  enddo

    call get_variable_info ('DISP', idis, isz ,itp ,iwd ,msh,
        found)
    if  ( .not. found )  stop 3
    do  i = 0, TOTGPT–1 ;  do  j = 0, 2
      Ra( idis + 3*i + j ) = 0.
    enddo ;  enddo

    endif  !  'DelDisp' found
    end
```

A.3   Storing Stress History

A.3.1   inform

```
DATABASE_MODULE
   INPUT_DATABASE  hopperStr
#                   name = filename without extension of
   PRINT_READ_VARIABLES  ON

   OUTPUT_DATABASE  hopper_open
```

```
#                         nam1 − change  database  filename  to  prevent
    overwriting
END
```

A.3.2 casecode.f

```
save   nx ,  iStr ,
 .
 .
 .
 .
 .
  call  get_variable_info  ( 'STRESS' ,  iStr ,  isz , itp , iwd ,
    msh ,  found )
  if   ( .not.  found )   Stop 1
 .
 .
 .
 .
 .
```

A.4   Initial Flow at outlet opening

A.4.1   Fortran code to adjust geo file in PHYSICA

```
C      Make changes  to  the  .geo  data  in  memory :


       do   i  =  1 ,  np

         if  (  ixp ( i )  .EQ.  1  )   then
           iyp ( i )  =  1
         endif

       enddo
```

A.4.2 Geo file

```
0.00000E+00   0.00000E+00   0.00000E+00   1   1   5
6.00000E−03   0.00000E+00   0.00000E+00   0   3   5
1.20000E−02   0.00000E+00   0.00000E+00   0   3   5
         .
         .
         .
         .
         .
1.65000E+00   2.75000E−01   0.00000E+00   2   4   5
0.00000E+00   0.00000E+00   1.00000E−02   1   1   6
6.00000E−03   0.00000E+00   1.00000E−02   0   3   6
1.20000E−02   0.00000E+00   1.00000E−02   0   3   6
         .
         .
         .
         .
         .
```

A.4.3 inform

BOUNDARY_CONDITIONS

```
!    P_PATCH   1   DISPLACEMENT   VALUE   0.0
     P_PATCH   3   DISPLACEMENT   VALUE   0.0
     P_PATCH   4   DISPLACEMENT   VALUE   0.0
     P_PATCH   5   DISPLACEMENT   VALUE   0.0
     P_PATCH   6   DISPLACEMENT   VALUE   0.0

     F_PATCH   4   PRESSURE   VALUE   0.3

     P_PATCH   7    CONSTRAINT   VALUE   45544
     P_PATCH   8    CONSTRAINT   VALUE   45547
     P_PATCH   9    CONSTRAINT   VALUE   45550
     P_PATCH   10   CONSTRAINT   VALUE   45553
     P_PATCH   11   CONSTRAINT   VALUE   45556
     P_PATCH   12   CONSTRAINT   VALUE   45559
         .
```

.
.
.
.
.

```
P_PATCH   84   CONSTRAINT     VALUE   92023
P_PATCH   85   CONSTRAINT     VALUE   92026
P_PATCH   86   CONSTRAINT     VALUE   92029
```

END

A.5   Failure Criteria

A.5.1   casecode.f

```
subroutine case_output_results ( Ia, Ra, La, Cha )
dimension                       Ia(*), Ra(*)
logical                         La(*), found, failed
character           Cha(1)*(*)

real, parameter :: m=0.6   ! angle of ?

include '../inc/geom.fh'

call get_variable_info ('STRESS', iStr, isz,itp,iwd,msh,
    found )
if ( .not. found )  stop 1
call mem_real_ele ( 'Ryl', 1,  iRyl )
call mem_real_ele ( 'Rg' , 1,  iRg  )
call mem_real_ele ( 'Failure', 1,  iFail )

call get_variable_info      ('Cohe', iCohe, isz,itp,iwd,
    msh, found )
if ( .not. found )  stop 2
failed = .false.
call save_restart_variable ( 'Cohe',  ierr, failed )
```

```
do   iele = 0, TOTELE-1
    Str_xx = Ra( iStr + 6*iele )       !   Vertical
    Str_yy = Ra( iStr + 6*iele + 1 ) !   Horizontal
    Str_xy = Ra( iStr + 6*iele + 3 ) !   Shear

    str1 = Max( 1.e-9, -Str_xx )
    str2 = Max( 1.e-9, -Str_yy )
    str3 = ABS( Str_xy )
    StrM  =(str1+str2)/2

    Var1 = (strM-m*Ra(iCohe + iele))/(m**2+1.)
    Ra(iRyl + iele )=sqrt((Var1-strM)**2+(m*Var1+Ra(iCohe
        +iele))**2)
    Ra( iRg + iele ) = Sqrt( (0.5*(str1 - str2))**2 +
        str3**2 )
    Ra( iFail + iele ) = Ra( iRg + iele ) - Ra( iRyl +
        iele )

enddo
end
```

A.6   Removal of Elements in casecode.f

A.6.1   inform

```
MATERIAL_PROPERTY_MODULE
  DENSITY
    MATERIAL  1   USER_ROUTINE   dummy   0
    SAVE_PROPERTY   TRANSIENT
  END

  YOUNGS_MODULUS
    MATERIAL  1   USER_ROUTINE   remove   1   1.E5
    SAVE_PROPERTY   TRANSIENT
  END
```

```
  POISSONS_RATIO
    MATERIAL  1  CONSTANT    0.3
  END

  YIELD_STRESS
    MATERIAL  1  CONSTANT    1.0E+10
  END
END
```

A.6.2   casecode.f

```
      subroutine  case_mat_prop ( Ia , Ra, La, Cha,   Handld )
      dimension                   Ia (∗) ,  Ra(∗)
      logical                     La(∗) , Handld , found , failed
      character          Cha(1) ∗(∗)

      include  '../ inc/mprop.fh '
      include  '../ inc/geom.fh '

      if   ( PRP_EQN_NAM(1:5)  .EQ.  'dummy'  )   then
        Handld = .TRUE.   !   Density

        call mem_real_ele ( 'Failure ', 1,   iFail )
        iele = PRP_ELE_ID − 1
        x = Ra( CENTRE_P + 3∗ iele )
        if ( (Ra( iFail + iele ) .GE.  0.0) .AND. (x .LT.  0.1)
          ) then
          Ra( PRPVAR_ID + iele  ) = 0.0
        endif
      endif

      if   ( PRP_EQN_NAM(1:6)  .EQ.  'remove'  )   then
        Handld = .TRUE.   !   Young's

        call mem_real_ele ( 'Failure ', 1,   iFail )
        iele = PRP_ELE_ID − 1
        x = Ra( CENTRE_P + 3∗ iele )
        if ( (Ra( iFail + iele ) .GE.  0.0) .AND. (x .LT.  0.1))
            then
```

```
        Ra( PRPVAR_ID + iele ) = Ra( PRPDAT_ID )  !  value
           from inform
        write (*,'(I8, 2F9.3)') 1+iele , x, Ra( CENTRE_P + 3*
           iele+1 )
      endif
    endif

    end
```

A.7   Calculation of Structure Modules

The use of compliance (elasticity) matrix in stress-strain calculation:

```
C Initialise element stiffness matrix.
C
        CALL set_null_matrix (dofine , dofine , elestf)
C
C Arrange element topology to working topology.
C
        CALL vb_get_element_nodes
    @        (eleno , Ia(ELEPTS_P) , TOTPIE, TOTEL2, nodiel ,
    @         Ia(NODINX_P))
C
C Set the X,Y of the nodes in the element to WKCORD.
C
        CALL vb_get_node_coords
    @        (nodiel , Ia(NODINX_P) , VBDIMS, TOTGP2, Ra(XYZCRD
      _P) ,
    @         Ra(WKCORD_P))

        CALL vb_get_node_dof
    @        (VBDIMS, nodiel , dofine , IA(NODINX_P) , dofinx)
C
C Obtain material properties for this element.
C
        youngg = Ra(MSHYNG_P+eleno −1)
        poissn = Ra(POISSONS_P+eleno −1)
C
```

```
C Calculate the elasticity matrix dee.
C
          CALL elasticity_matrix
     @          (nostrs, dee, youngg, poissn, APPROX)
C
C Calculate contributions from sub-control volumes at internal
    faces.
C
          DO 350 face = 1, ningpt
C
C Obtain local S,T,U coordinates of the integration point.
C
            CALL vb_local_coords
     @           (TOTEL2, eleno, Ia(ELETYP_P), Ra(IPS_P), IIPS,
     @            JIPS, KIPS, face, scoord, tcoord, ucoord)
C
C Obtain derivatives of shape functions LDER at the
   integration point.
C
            CALL vb_local_derivatives
     @           (scoord, tcoord, ucoord, Ra(LDER_P), Ia(locate
     ),
     @            nodiel, eldims)
C
C Calculate the Jacobian matrix JACMAT.
C
            CALL calc_matrix_product
     @           (eldims, nodiel, VBDIMS, Ra(LDER_P), Ra(WKCORD
     _P),
     @            Ra(JACMAT_P))
C
C Obtain the inverse of the matrix JACMAT.
C
            IF (eldims .EQ. VBDIMS ) THEN
              CALL find_matrix_inverse
     @         (VBDIMS, Ra(JACMAT_P), Ra(INVJAC_P), det, Errinf
     , Failed)
              IF (Failed) GOTO 9000
            ELSE
              CALL vector_inverse
```

```
      @              (VBDIMS, Ra(JACMAT_P), Ra(INVJAC_P), det, Errinf
         , Failed)
                 IF (Failed) GOTO 9000
            END IF
C
C Obtain the global derivatives GDER of the shape funtions
C with respect to the global coordinates X,Y.
C
            CALL calc_matrix_product
      @              (VBDIMS, eldims, nodiel, Ra(INVJAC_P), Ra(LDER
         _P),
      @               RA(GDER_P))
C
C Calculate the strain−displacement matrix bee.
C
            CALL set_null_matrix (nostrs, dofine, bee)
            CALL strain_matrix
      @              (nostrs, dofine, VBDIMS, nodiel, Ra(GDER_P),
      @               Ra(SFUN_P), Ra(WKCORD_P), APPROX, bee)
C
C Calculate dbee = dee * bee
C
             CALL calc_matrix_product
      @              (nostrs, nostrs, dofine, dee, bee, dbee)
C
C Calculate the transpose of bee
C
               CALL transpose_matrix (nostrs, dofine, bee, bt)
C
C Calculate the btdbee = bt* dbee
C
               CALL calc_matrix_product
      @              (dofine, nostrs, dofine, bt, dbee, btdbee)

               CALL calculate_quotient
      @              (nodiel, VBDIMS, ningpt, Ia(locate), IIPS,
         JIPS, KIPS,
      @               det, Ra(SFUN_P), Ra(WKCORD_P), Ra(IPS_P),
         quot)

               CALL multiply_matrix_by_scalar
```

```
      @                         ( dofine , dofine , quot , btdbee )
C
C Subtract btdbee from element stiffness matrix .
C
               CALL subtract_matrix
      @                         ( dofine , dofine , elestf , btdbee ,
          elestf )
```

Appendix B

Analytical method

B.1 Slide method
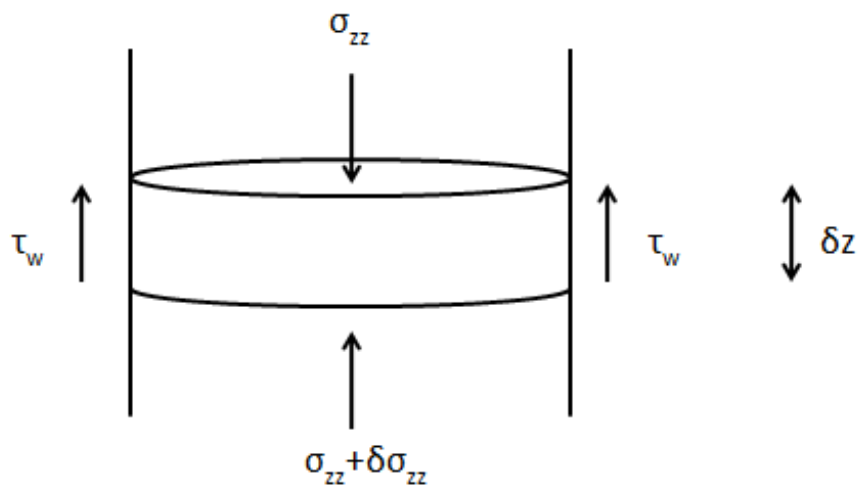
Figure B.1: Stresses acting on a differential slice of cylindrical element.

Force balance vertically on the element is:

$$(g\rho\delta z + \sigma_{zz})(\frac{\pi}{4}D^2) = (\sigma_{zz} + \delta\sigma_{zz})(\frac{\pi}{4}D^2) + \tau_w(\pi D\delta\sigma_{zz}) \tag{B.1}$$

In simokied form, by dividing Equation B.1 by $D\delta\sigma_{zz}$

$$g\rho - \frac{\delta\sigma_{zz}}{\sigma_{zz}} + \frac{4\tau_w}{D} \tag{B.2}$$

For a cohesionless material in an active (filling) case:

$$\tau_w = \nu_w\sigma_{rr} \tag{B.3}$$

From assumption of making both the normal vertical stress and the normal horizontal stress are the principal stresses:

$$\sigma_{zz} = \sigma_1\sigma_{rr} = \sigma_3 \tag{B.4}$$

From the Mohr's circle

$$K = \frac{\sigma_{rr}}{\sigma_{zz}} = \frac{\sigma_3}{\sigma_1} = \frac{1 - \sin varphi}{1 + \sin varphi} \tag{B.5}$$

where K is the Janssen's ratio, a ratio between the vertical applied stress and the horizontal stress exerted from the wall to the material.

Substitute Equation B.3 and B.5 into Equation B.2, Equation B.2 becomes a first order ODE:

$$g\rho = \frac{d\sigma_{zz}}{dz} + \frac{4\nu_w Kz}{D} \tag{B.6}$$

solving the ODE, it becomes:

$$\sigma_{zz} = \frac{rhogD}{4\tau_w K} + C \exp \frac{-4\nu_w Kz}{D} \tag{B.7}$$

A general solution with the boundary condition, $\sigma_{zz} = Q_0 at z = 0$, is

$$\sigma_{zz} = \frac{\rho gD}{4\tau_w K} + [1 - \exp \frac{-4\nu_w Kz}{D}] + Q_0 \exp \frac{4\nu_w Kz}{D} \tag{B.8}$$